Design and Analysis of LH2 tank structures for aircraft retrofit applications

Master of Science Thesis

Anna Biancotto

Delft University of Technology

Design and Analysis of LH2 tank structures for aircraft retrofit applications

by

Anna Biancotto

to obtain the degree of Master of Science
at the Delft University of Technology,
to be defended publicly on Friday October 4, 2024 at 9:30 AM.

Student number:	5861543
Project duration:	15/01/2024 - 04/10/2024
Thesis committee:	Dr. C.D. Rans (chair)
	Dr.ir. M.F.M. Hoogreef (external evaluator)
	Dr.Ing. S.G.P. Castro, TU Delft (supervisor)
	Dr.ir. J.A. Pascoe, TU Delft (supervisor)

Cover: Clouds over Flying Airplane - Mike González (Modified)
https://www.pexels.com/photo/clouds-over-flying-airplane-16418551/
Style: TU Delft Report Style, with modifications by Daan Zwaneveld

Acknowledgements

This research is conducted within the research and innovation programme Luchtvaart in Transitie, which is co-funded by the Netherlands National Growth Fund and in part by the European Union. It is part of the ”Hydrogen Aircraft Powertrain and Storage Systems (HAPSS)” project, and part of The CrashProof Knowledge Centre (CrashProofLab) [21].

As I near the completion of my Master of Science in Aerospace Engineering, it feels important to take a moment to reflect and express my gratitude to the many people who have helped make this journey possible.

I would like to begin by thanking the people I left behind in Italy when I moved to Delft two years ago. First and foremost, my deepest thanks go to my parents Franca and Mario, and my sister Alice, who have been a constant source of motivation, support, and inspiration throughout this journey. I am also incredibly grateful to the rest of my large family, who have always made my visits home so special, giving me the strength to leave again and pursue my ambitions abroad.

I extend my heartfelt thanks to my closest friends. Even though distance has separated us, our bonds have remained unshakable, and your friendship has been a constant source of strength and comfort. I am deeply thankful for your continued support, for always being there to listen, and for reminding me of home, even from afar.

A special thank you goes to Simone, who has been a solid and unwavering point of reference throughout this entire experience. Despite the physical distance between us, you have been my steady source of support and, for this, I am profoundly grateful.

I would also like to acknowledge the wonderful people I have met here in the Netherlands, with whom I have forged friendships that I know will last a lifetime. Thank you for being there, for sharing these past two years with me, and for making me feel at home in this new, sometimes grey, land far from my own. I could not have done it without you.

A special thank you goes then to my thesis supervisors, Saullo and John-Alan. I am incredibly grateful for your guidance and support throughout the past nine months. Your expertise and insightful advice were invaluable, and I also greatly valued the freedom you gave me to explore ideas independently and take ownership of my work. You were always available when I needed assistance, and our brainstorming sessions were particularly helpful in shaping the direction of the project. Your approach allowed me to grow both as a researcher and as a problem-solver, and for that, I am truly thankful.

I would also like to express my gratitude to all my colleagues at NLR. Your support and insights were incredibly valuable during my graduation internship, and I deeply appreciate the collaborative spirit and shared knowledge that contributed to the success of my project.

Finally, to everyone who has been part of this journey, both near and far, thank you. This achievement would not have been possible without the collective encouragement, guidance, and support I have received along the way.

Anna Biancotto
Delft, September 2024

Summary

This thesis investigates the design and analysis of *cryogenic liquid hydrogen storage tanks in the context of aircraft retrofit*. Hydrogen propulsion offers significant potential for achieving zero emissions in aviation, but its adoption introduces challenges related to safe and efficient storage.

The research focuses on comparing single-wall and double-wall tank architectures, assessing their ability to meet stringent operational, thermal, and structural performance requirements. In the preliminary assessment of a tank design's viability, two key performance requirements are cruise time and dormancy time. A minimum cruise time of 20 minutes ensures the tank can support basic flight operations, while a dormancy time of 1 day ensures no hydrogen loss occurs if the aircraft remains stationary for an extended period, accounting for potential delays.

The methodology to calculate *cruise time* involves determining the maximum time the aircraft can remain in the cruise phase based on the inner tank dimensions, fill ratio, and mission profile. The *dormancy time* is the time required for the tank pressure to reach the venting pressure, at which point hydrogen must be released, and is calculated by implementing a thermodynamic model that simulates the tank's dynamic behavior over time, accounting for heat inflow from the external environment.

The evaluation of the *single-wall tank* reveals its simplicity and potential cost-effectiveness, but also exposes considerable limitations in terms of thermal insulation for the specific retrofit case study. This design approach is a viable option for larger-scale applications, where a lower surface area-to-volume ratio reduces heat transfer and, consequently, hydrogen boil-off. However, the compact dimensions of the tanks required for aircraft retrofitting present a significant challenge due to the inherently higher surface area-to-volume ratio, which leads to increased thermal losses and prevents the single-wall architecture from meeting the performance requirements imposed by this specific case study.

In contrast, the *double-wall tank*, equipped with a vacuum layer and multi-layer insulation (MLI), offers improved thermal performance. The heat transfer from the external environment is significantly reduced, allowing to preserve the cryogenic temperature of the hydrogen fuel. However, the added complexity introduces new challenges, particularly regarding the design of the inner vessel support system which must maintain the inner vessel's position while accommodating thermal displacements and managing structural loads. Assessing the heat leakage budget for the support structure is the final critical step, as it determines the maximum allowable heat inflow through the support system, ensuring the tank meets its dormancy time requirements while allowing for design optimization.

The thesis develops a design methodology for the *inner vessel support system*, balancing the need for flexibility (to accommodate thermal contraction experienced during the first filling of the tank) with sufficient stiffness (to withstand operational loads, including emergency landing conditions). This approach involves selecting suitable materials and geometries that meet thermal requirements, while accurately determining the support structure's stiffness properties. Different loading scenarios, such as normal operations and emergency landing conditions, are evaluated to analyze stresses and displacements in both the tank and support system. Adjustments to the design are made if stress or displacement exceed safe limits. The analysis reveals that optimizing the support structure is critical for the double-wall tank's overall feasibility. While the double-wall design is technically viable and meets the thermal performance requirements, its success depends on further refinement of the support system to minimize heat leakage and ensure structural integrity.

The results of this study suggest that, although single-wall tanks are not suitable for this application, double-wall tanks offer a promising solution for retrofitting aircraft with cryogenic liquid hydrogen storage. Nonetheless, significant challenges remain, particularly in designing efficient support structures that can handle the operational demands without compromising thermal performance. Future work should focus on optimizing the support system design, exploring flexible materials, and considering additional factors such as sloshing loads to further improve tank reliability and performance.

In general, this thesis contributes to the *development of a robust methodology for the preliminary design of cryogenic hydrogen storage tanks*, providing a foundation for further advancements in hydrogen-powered aviation.

Contents

List of Figures

List of Tables

Nomenclature

Abbreviations

Abbreviation	Definition
AIC	Aviation Induced Cloudiness
AMC	Acceptable Means of Compliance
API	American Petroleum Institute
$APDL$	ANSYS Parametric Design Language
APU	Auxiliary Power Unit
$ASME$	American Society of Mechanical Engineers
$ATAG$	Air Transportation Action Group
CGH_2	Pressurised Hydrogen
CO	Carbon Monoxide
CO_2	Carbon Dioxide
CS-25	EASA's "Certification Specifications and Acceptable Means of Compliance for Large Aeroplanes"
CTE	Coefficient of Thermal Expansion
CFR	Code of Federal Regulations
DRI	Dynamic Response Index
EAC	Energy Accommodation Coefficient
$EASA$	European Union Aviation Safety Agency
$ESDARC$	Energy Supply Device Aviation Rulemaking Committee
EU	European Union
FAA	Federal Aviation Administration
FAR-25	FAA's "Federal Aviation Regulation Part 25 - Airworthiness Standards: Transport Category Airplanes"
FEA	Finite Element Analysis
FR	Fill Rate
GH_2	Gaseous Hydrogen
HC	Hydrocarbons
H_2	Hydrogen
HCI	Head Injury Criterion
$HDPE$	High-density Polyethylene
HV	High Vacuum
HV-MLI	High Vacuum Multi-Layered Insulation
$IATA$	International Air Transport Association
LCP	Longitudinal Circle Packing
LH_2	Liquid Hydrogen
LHP	Lateral Hexagonal Packing
LNG	Liquefied Natural Gas
LSP	Lateral Square Packing
$MEOP$	Maximum Expected Operating Pressure
MLI	Multi-Layer Insulation
$MTOW$	Maximum Take-Off Weight
$NASA$	National Aeronautics and Space Administration
$NFPA$	National Fire Protection Association
NO_x	Oxides of Nitrogen
OEM	Original Equipment Manufacturer
$PEEK$	Polyetheretherketone

Abbreviation	Definition
$PEEQ$	Plastic Strain Equivalent
PEM	Proton-Exchange Membrane
$VDMLI$	Variable Density Multi-Layer Insulation
VCS	Vapor-Cooled Shield
UAV	Unmanned Aerial Vehicles

Symbols

Symbol	Definition	Unit
A	Area	[m^2]
A_{ij}	Terms of the extensional stiffness matrix A	[-]
A_{pipe}	Cross-sectional area of a pipe	[m^2]
$A_{support}$, A_s	Cross-sectional area of a support	[m^2]
C_2	Empirical constant for thermal conductivity expression	[W/m·K]
c	Damping coefficient of the support system	[Ns/m]
c_c	Critical damping coefficient	[Ns/m]
C_s	Specific heat of the tank structure	[J/kg·K]
D_{ij}	Terms of the bending stiffness matrix D	[-]
E	Young's modulus	[Pa]
E_j	Joint efficiency	[-]
E_s	Young's modulus of the material selected for the supports	[Pa]
F_{ax}, F_{flex}	Axial and Flexural components of the force	[N]
F_{u_s}, F_{v_s}, F_{w_s}	Forces applied at the free end of the support (beam)	[N]
F_j	Force applied to the free end of the support in direction j	[N]
f	Relative density of the spacer to the solid material	[-]
g	Acceleration of gravity	[m/s^2]
h	Impulse response function of the system	[1/s]
H	Heaviside step function	[-]
h_g	Enthalpy of the gaseous hydrogen	[J/kg]
h_l	Enthalpy of the liquid hydrogen	[J/kg]
I_s	Moment of inertia about the neutral axis of the support	[kgm^2]
I_x, I_y	Moments of inertia of the beam's cross-section	[kgm^2]
k	Stiffness value of the spring that represents the support system	[N/m]
k_{G10-CR}	Thermal conductivity of G10-CR glass fiber composite	[W/m·K]
k_{al}	Thermal conductivity of aluminum alloy AL5083-O	[W/m·K]
k_{ax}	Axial stiffness of the support	[N/m]
k_{eq}	Equivalent stiffness	[N/m]
k_{flex}	Flexural stiffness of the support	[N/m]
k_{ij}	Mid-surface curvature term in the ij direction ($i, j = x, y, z$)	[-]
k_{ins}	Thermal conductivity of the insulation material	[W/m·K]
$K_{rad,i}$	Radiation heat transfer coefficient of the i-th MLI layer	[W/m^2·K]
$K_{rg,i}$	Residual gas heat transfer coefficient of the i-th MLI layer	[W/m^2·K]
$K_{s,i}$	Solid heat transfer coefficient of the i-th MLI layer	[W/m^2·K]
$L_{bridge,c}$	Length of the support through the insulation layer	[m]
$L_{bridge,m}$	Length of the pipe through the insulation layer	[m]
L_s	Length of the support	[m]
N	Axial force applied to the support	[m]
N_{MLI}	Number of MLI layers	[-]
N_{pipes}	Total number of pipes in one tank	[-]
$N_{supports}$	Total number of supports in one tank	[-]
$N_{s,max}$	Maximum allowed number of supports	[-]
M	Molecular weight of the residual gas	[kg/mol]

Symbol	Definition	Unit
m_g	Mass of the gaseous hydrogen	[kg]
m_i	Mass of the inner vessel	[kg]
m_l	Mass of the liquid hydrogen	[kg]
m_s	Mass of the tank structure	[kg]
M_x, M_y	Bending moments in the support (beam)	[Nm]
P	Pressure	[Pa]
$P_{burst-disc}$	Burst-Disc pressure	[Pa]
P_{design}	Design pressure	[Pa]
P_{in}	Internal design pressure	[Pa]
P_{vent}	Venting pressure	[Pa]
P_s	Saturation pressure	[Pa]
P_{vacuum}	Residual gas pressure	[Pa]
p_0	Assumed acceleration impulse that happens at the respective time t	[m/s^2]
$\dot{Q}_{in}$	Heat transfer rate from the outside to the inside of the tank	[W]
$\dot{Q}_{pipes}$	Heat flow through the pipes	[W]
$\dot{Q}_{supports}$	Heat flow through the supports	[W]
$\dot{Q}_{supports,max}$	Budget for the heat leakage through the support structure	[W]
$\dot{Q}_{tank-wall}$	Heat flow through the tank walls	[W]
$\dot{Q}_{total}$	Total heat flow into the storage vessel	[W]
R	Universal gas constant	[J/mol·K]
R_{HV-MLI}	Thermal resistance of the HV-MLI insulation layer	[K/W]
R_{in}	Inside radius of the shell considered	[m]
$R_{rg,i}$	Thermal resistance of residual gas	[K/W]
R_{pipe}	Thermal resistance of one pipe	[K/W]
r_s	Local radius for a specific section of the sphere	[m]
R_s	Radius of the support's cross-section	[m]
$R_{support}$	Thermal resistance of one support	[K/W]
$R_{tank-wall}$	Thermal resistance of the walls of the tank	[K/W]
$R_{s,i}$	Thermal resistance of solid conduction through the spacer	[K/W]
$R_{rad,i}$	Thermal resistance of radiation heat transfer between two adjacent reflection shields	[K/W]
$R_{eq,i}$	Thermal resistance of the i-th MLI layer	[K/W]
S_a	Stress amplitude of the load cycle	[Pa]
S_{al}	Thermal shape factor of the aluminum layer (tank wall)	[m]
S_{ins}	Thermal shape factor of the insulation material	[m]
S_m	Mean stress of the load cycle	[Pa]
S_{ma}	Maximum allowable stress value	[Pa]
S_N	Fatigue strength at N cycles	[Pa]
$(S_N)_{S_m=0}$	Fatigue strength at N cycles for the case of completely reversed loading	[Pa]
S_u	Ultimate strength of the material	[Pa]
T	Temperature	[K]
$T_{avg,i}$	Average temperature of the i-th MLI layer	[K]
T_{ext}	Temperature of the environment surrounding the tank	[K]
T_{i1}	Temperature of the outer boundary surface of the i-th MLI layer	[K]
T_{i2}	Temperature of the inner boundary surface of the i-th MLI layer	[K]
T_{int}	Temperature inside the tank	[K]
t_n	Threshold time after which the system response begins	[s]
t_s	Thickness of the support's cross-section	[m]
t_{vacuum}	Thickness of the vacuum insulation layer	[m]
U	Strain energy	[J]
U_d	Strain energy density	[J/m^3]
u	Displacement function in x direction	[m]

Symbol	Definition	Unit
u_s	u displacement of the vessel at the contact point with the support	[m]
V	Volume	[m^2]
v	Displacement function in y direction	[m]
v_s	v displacement of the vessel at the contact point with the support	[m]
w	Displacement function in z direction	[m]
w_s	w displacement of the vessel at the contact point with the support	[m]
W_f	Work performed by the external forces	[J]
W_p	Work done by the internal pressure difference acting on the inner walls of the vessel	[J]
W_s	Work done by the supports	[J]
x	Coordinate tangential to the shell surface, related to angle θ	[m]
x_g	Global x coordinate	[m]
x_s	x coordinate of the support (beam)	[m]
y	Coordinate tangential to the shell surface, related to angle ϕ	[m]
y_g	Global y coordinate	[m]
y_s	y coordinate of the support (beam)	[m]
z	Coordinate perpendicular to the shell surface	[m]
z_g	Global z coordinate	[m]
z_s	z coordinate of the support (beam)	[m]
$z_1(t)$	Displacement of the outer vessel over time due to impact	[m]
$z_2(t)$	Displacement of the inner vessel over time due to impact	[m]
α	CTE	[m/mK]
α_m	Material coefficient to approximate the fatigue limit	[-]
$\beta_{i,j}$	Angle defined between the axial direction of the i^{th} support $z_{s,i}$ and the direction j	[rad]
Δp	Pressure difference	[Pa]
$\delta(t)$	Displacement imposed on the support system over time	[m]
ΔT	Temperature difference between the interior and exterior of the tank	[K]
ϵ_1, ϵ_2	Emissivities of the outer and inner boundary surfaces	[-]
$\epsilon_{i+1}, \epsilon_i$	Emissivities of the outer and inner boundary surfaces of the i^{th} layer	[-]
ϵ_{ij}	Strain in the ij direction ($i, j = x, y, z$)	[m/m]
ϵ_{ij0}	Mid-surface strain in the ij direction ($i, j = x, y, z$)	[m/m]
ζ	Damping factor	[-]
θ	Angle of interest for the shell coordinate system	[rad]
λ	Thermal conductivity of the spacer material	[W/m·K]
ν	Poisson's ratio	[-]
ν_s	Poisson's ratio of the material selected for the supports	[-]
Π_t	Total potential energy	[J]
ρ_l	Density of liquid hydrogen	[kg/m^3]
ρ_g	Density of gaseous hydrogen	[kg/m^3]
σ	Stefan-Boltzmann coefficient	[W/m^2·K^4]
σ_{cr}	Critical axial compressive stress for local buckling	[Pa]
σ_{ij}	Stress in the ij direction ($i, j = x, y, z$)	[Pa]
$\sigma_{z,s}$	Normal stress in the support	[Pa]
ϕ	Angle of interest for the shell coordinate system	[rad]
ω_d	Damped natural frequency of the system	[Hz]
ω_n	Natural frequency of the system	[Hz]

1 Introduction

The aviation industry is undergoing a major transformation as it strives to meet increasingly stringent environmental regulations and reduce carbon emissions. The shift towards alternative propulsion systems, presents a unique opportunity to achieve sustainable, zero-emission aviation. Hydrogen-powered aircraft have emerged as a promising solution, but their adoption faces significant technical challenges, particularly in designing efficient and safe hydrogen storage systems suitable for aviation. Among various storage options, cryogenic liquid hydrogen tanks present a particularly promising avenue for hydrogen-powered aircraft. However, these tanks introduce significant design challenges, requiring specialized solutions to ensure safe, efficient, and reliable storage.

1.1. Purpose of this thesis

The purpose of this thesis is to develop a comprehensive methodology for modeling and designing single-wall and double-wall cryogenic hydrogen storage tanks to meet the thermal and structural performance requirements for retrofit aircraft, addressing challenges like thermal efficiency, accomodation of thermal displacements, crashworthiness requirements, and support structure design.

The study explores the two key tank architectures (single-wall and double-wall tanks) evaluating their performance under various operational and safety-critical conditions. The importance of this evaluation lies in the fact that, while the literature provides general considerations on the advantages and disadvantages of each architecture and presents solutions for individual case studies, there is no clear definition of the specific conditions under which each design is best suited. Therefore, a major aim of this thesis is to define the areas of applicability for single-wall and double-wall tanks, identifying the specific scenarios in which each design performs optimally. This analysis serves as a framework for determining the most suitable tank architecture based on the operational demands and safety requirements of various contexts. Ultimately, the study provides the necessary insights to assess which design is most appropriate for the specific retrofit case study considered.

Furthermore, this thesis aims to develop a comprehensive approach for designing the inner vessel support structure in double-wall tank systems. The support structure is crucial for maintaining the correct positioning of the inner vessel, accommodating thermal expansion and contraction, and withstanding the structural loads experienced during flight. Since the support system must connect the inner and outer vessels, which operate at significantly different temperatures, it presents a major challenge also in terms of minimizing heat leakage while ensuring structural integrity. This thesis seeks to address this challenge by developing a design methodology able to effectively evaluate a broad spectrum of preliminary design options, allowing for approximate assessments of the thermal and structural performance of numerous design alternatives quickly, identifying promising options before committing to more detailed and computationally expensive analyses.

By addressing both the technical and practical aspects of hydrogen storage systems, this research aims to expand the understanding of hydrogen propulsion in aviation while offering guidance on design requirements for future aircraft retrofits.

1.2. Structure of the report

This report is organized into five content chapters starting from an overview of sustainable aviation and leading to the detailed technical analysis of hydrogen storage systems for retrofitting aircraft.

Chapter 2 introduces the context of the research through a literature study. The chapter discusses the potential of hydrogen as an alternative to traditional aviation fuels, outlining its environmental benefits and technical challenges, and introduces the specific case study considered throughout the thesis, which involves the retrofit of a regional airliner with a cryogenic liquid hydrogen storage system.

Chapter 3 presents the single-wall tank model and the methodology to investigate the ability of the tank to meet the performance requirements. The main question that this chapter aims to answer is whether there is a single wall tank design suitable for the selected case study in which the material insulation layer is able to reduce the heat flow to such an extent that the dormancy time requirement is met and, at the same time, is not too thick so as to allow the storage of sufficient liquid hydrogen to guarantee the minimum required cruise time.

Chapter 4 shifts focus to the double-wall tank architecture, which offers a more robust thermal performance due to the combination of vacuum and multi-layer insulation (MLI) systems. The double-wall tank model is described, and the methodology for evaluating its feasibility is outlined. The analysis investigates how varying factors such as vacuum pressure, properties of MLI components, and MLI layer density influence the tank's ability to meet dormancy and cruise time requirements. The chapter presents key considerations regarding the support structure of the double-wall tank and the additional complexity it introduces.

Chapter 5 focuses on the design and analysis of the inner vessel support structure for the double-wall architecture. The requirements for the support system are outlined and the design methodology is presented, as well as the challenges of designing a support structure able to withstand dynamic forces, accommodate thermal expansion, and minimize heat transfer.

Chapter 6 summarizes the key findings of the research, discusses the limitations of the single-wall tank architecture and the potential feasibility of the double-wall tank, and highlights the importance of the support structure design for the inner vessel, as well as the challenges it presents. Finally, Chapter 7 provides recommendations for further research.

2
Literature Study

The main topics that will be presented in this chapter and their interconnections are summarised in the mind map in Figure 2.1. The aim is to help the reader follow the progression of the discussion, starting from the broad topic of sustainable aviation and narrowing down to the specific retrofit case study. It aims to clarify the steps taken to move from the general context to the specific topic, highlighting which topics will be explored in more detail and which will not.

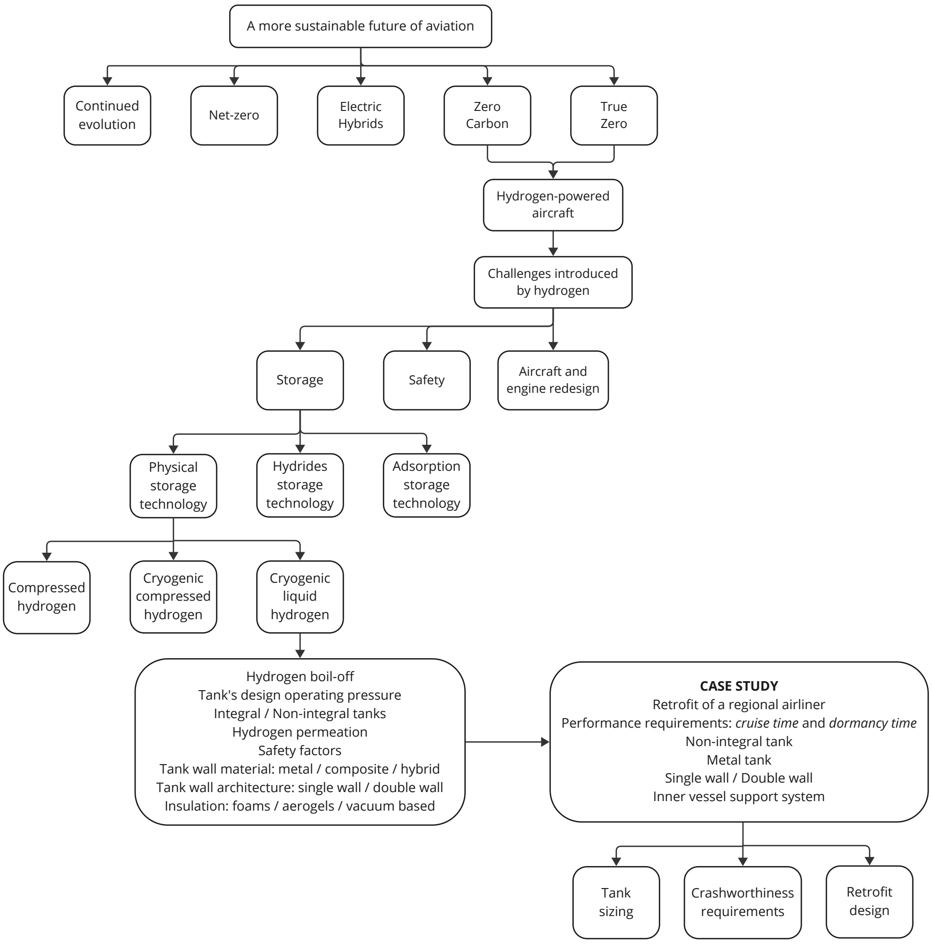

Figure 2.1: Mindmap of the literature study

2.1. Future of aviation

As global economies, cultures, and populations become increasingly interconnected, the aviation sector assumes a vital function in facilitating connections between individuals and economies.

The COVID-19 pandemic brought about unprecedented challenges including a significant decline in passenger demand and extensive financial losses for airlines and airports, but the industry is now on a path to recovery. The insights from Boeing's Commercial Market Outlook report for 2023-2042 [17] highlight the industry's remarkable resilience and ability to adapt to changing market conditions. As of 2023, the global aviation sector is steadily regaining its pre-pandemic traffic levels, with domestic and regional markets leading the rebound, followed closely by a resurgence in international travel. The forecast for air traffic is that it will double over the next 20 years, at a growth rate of 3.7% from pre-pandemic levels. To accommodate future growth, airlines will receive over 42,000 new airplanes.

Similar conclusions can be drawn from the Global Outlook for Air Transport reports published by IATA in June 2023 [3] and December 2023 [2]. The long-term outlook for air travel growth remains robust, with expectations that demand will double by 2040, driven by a 3.4% average annual growth rate. In this time frame, origin-destination passengers are expected to increase from around 4 billion in 2019 to just over 8 billion by 2040.

Taking into account the growth forecasts in the aviation industry, the environmental impact of traditional kerosene-based aviation in the future becomes even more concerning. Specific matters are engine exhaust emissions' effects on global warming, the ozone layer, and human health.

In 2009, the aviation sector developed an ambitious climate action plan at a global level with the aim to reduce aviation CO_2 emissions by 50% by 2050, as compared to the levels in 2005 [1]. This target was aligned with the 'well below 2ºC' goal set by the Paris Agreement. However, scientific evidence on the difference between the 2ºC goal and a 1.5ºC trajectory made it clear that achieving net-zero emissions by mid-century across all sectors is a crucial step in mitigating the effects of climate change.

In December 2019, the European Commission launched the Green Deal strategy [30] to address climate change and promote sustainability. The aim is to achieve climate neutrality within the EU by 2050 through a significant reduction of greenhouse gas emissions by at least 55% by 2030 compared to 1990 levels. This strategy involves initiatives such as improving data collection and dissemination, utilizing nature-based solutions, and integrating climate adaptation considerations into macro-fiscal policies. The target of making all sectors and EU member states carbon-neutral by 2050 is even more ambitious than those set by the Air Transport Action Group (ATAG) in 2009.

These targets testify how the aviation sector is being pushed towards decarbonization with increasing pressure.

Over the past 30 years, aviation managed to improve its carbon efficiency: increased seat density, operational and technological improvements have resulted in a 50% increase in fuel efficiency for revenue passenger kilometer (number of kilometers traveled by paying passengers) [23]. This trend is expected to continue with further flight optimization, airport taxiing, and flight routing.

Despite the advancements in energy efficiency for new commercial aircraft and engines, the projected growth in global air travel is expected to outweigh their effect. While fuel burn is decreasing at a rate of approximately 1% per year, aircraft fleet sizes are increasing at a rate of approximately 4% per year [73]. By 2050, the aviation industry could be responsible for as much as 24% of global CO_2 emissions, compared to the current 3%. Even if aircraft efficiency could increase twice as fast as today's pace, the prediction is that aviation would still be contributing to 19% of global emissions by 2050. Radical changes seem then necessary to meet decarbonization goals, including the exploration of new sustainable aviation fuels and new propulsion technologies [23].

Different strategies for reducing the aviation industry's emissions can be explored and these could be categorized into five different approaches [73], each with varying degrees of impact on carbon dioxide, and non-carbon greenhouse effects:

- **Continued evolution**: these solutions allow a partial reduction of greenhouse emissions by further improving the existing technology. This category includes efficiency and operational improvements as well as more electric aircraft.
- **Net-zero**: these solutions are not able to produce a reduction in gross emissions but aim to reduce the net emissions acting on the carbon sinks attributed to that entity. Offsets and sustainable

aviation fuels are possible strategies in this direction.

- **Electric Hybrids**: these solutions offer a partial reduction in all greenhouse gas emissions by enhancing electrification and obtaining hybrid-electric aircraft.
- **Zero Carbon**: these solutions allow to reduce carbon gross emissions to zero, but may emit other greenhouse gases, as happens with hydrogen combustion.
- **True Zero**: these solutions zero the release of greenhouse gases during operation. Both hydrogen fuel cell and battery electric aircraft are in this category.

As has already been pointed out, to meet the decarbonization goals, it seems necessary to assume a radical change from the current technology: the ”true zero” strategies, having the greatest potential to reduce emissions drastically, are the way to go even if they require fundamental re-designs of aircraft architecture and systems.

2.2. Hydrogen-powered aircraft

Hydrogen stands out as a promising fuel for aviation due to its versatility, energy efficiency, low pollution, and renewable status [60]. The two hydrogen propulsion systems under consideration are:

- **Hydrogen combustion aircraft**: thrust is generated through the combustion of hydrogen in a modified gas-turbine engine [8]. The only difference between this technique and conventional internal combustion is the use of hydrogen in place of fossil fuels.
- **Hydrogen fuel cell aircraft**: a fuel cell is a device that converts energy stored in molecules into electricity through an electrochemical reaction [9]. It is composed of two electrodes - an anode and a cathode - separated by an electrolyte membrane. Hydrogen enters the anode and reacts with a catalyst, splitting into electrons and protons. Oxygen from the ambient air enters the cathode. The protons move through the membrane to the cathode, while the electrons flow out of the cell, creating an electrical current which can be used to power things like electric or hybrid-electric propulsion systems. At the cathode, the protons and oxygen combine to form water. Most advanced and suitable for aviation today are low-temperature proton-exchange membrane (PEM) fuel cells [23].

Compared to hydrogen combustion aircraft, hydrogen fuel cell aircraft could offer increased efficiency requiring 20-40% less fuel. Fuel cell propulsion has in fact higher energy conversion rates with efficiencies of around 45-50% due to the combination of fuel cell efficiency (55%) and electric powertrain efficiency (90%), which is better than the roughly 40% efficiency of hydrogen combustion [73]. Furthermore, there are many similarities to electric aircraft (including high-voltage/high-power cabling, power electronics, and electric motors) which allow for compatibility with the ever-evolving electric powertrain supply chain, as well as design considerations for maximizing the benefits of distributed propulsion.

Using hydrogen can significantly reduce greenhouse gas emissions, especially when used in fuel cell propulsion: emissions are almost entirely limited to water vapor, eliminating CO_2,NO_x, CO, HC, and soot emissions. Even though water vapor is also a greenhouse gas that could cause contrails and Aviation Induced Cloudiness (AIC), research suggests that this is not a main concern since the pure nature of hydrogen and oxygen electrolysis reaction in the fuel cell implies that any impurities are likely to be minimal [73]. Further precautions can also be implemented as flying at lower altitudes to further lessen the impact of water vapor on global radiative forcing and innovative design approaches could allow for the storage and controlled release of water vapor.

Another advantage of utilizing hydrogen over liquid hydrocarbon fuels lies in its production process, which involves electrolysis of water. This method can be implemented in any region with access to water and an electrical supply, offering a versatile and potentially widespread means of production. Unlike traditional fossil fuels, which are concentrated in specific geographical regions and require extraction processes that are often environmentally damaging, hydrogen production through electrolysis is relatively clean and can be decentralized. This decentralization of production reduces dependency on a limited number of countries possessing carbon fossil reserves, thereby enhancing energy security and promoting global sustainability efforts.

Hydrogen has potential beyond aviation and can be used in various industries, which may accelerate fuel cell and storage system development, infrastructure expansion, and cost reduction. This broader adoption could also help reduce research and development burdens for the aviation sector.

2.2.1. Challenges introduced by hydrogen

While hydrogen offers numerous advantages as a fuel for aerospace applications, its adoption presents major challenges: the need to develop hydrogen storage solutions that are both effective and weight-efficient, safety challenges, and the requirement for extensive aircraft and engine redesigns.

High gravimetric energy density of hydrogen VS low volumetric energy density

One of the biggest obstacles to the development of effective and weight-efficient hydrogen storage solutions is balancing the high gravimetric energy density of hydrogen with its low volumetric energy density [73]. In terms of energy density on a mass basis, hydrogen has an energy content of 143 MJ/kg, which is up to three times higher than that of liquid hydrocarbon fuels [54]. However, this advantage is partially offset by the weight and complexity of the required fuel system. In terms of energy density on a volume basis, hydrogen is significantly disadvantaged due to its low density: at standard temperature and pressure, the density of gaseous hydrogen is only 0.0899 g/L, whereas air has a density of 1.225 g/L and kerosene has a density of approximately 800 g/L under the same conditions. Since uncompressed gas state hydrogen has a very low density and energy content, the most conventional way to store it is as compressed or liquefied gas in tanks.

At present, liquid hydrogen storage provides a higher volumetric energy density compared to gaseous storage. However, even considering liquid hydrogen state and best storage conditions, hydrogen would require around **four times** more storage volume than kerosene in order to store the same amount of energy [44]. Furthermore, hydrogen liquefies at temperatures below -250 °C: this implies the need for cryogenic cooling, which consumes a significant amount of the stored energy, complicates tank design with insulation and cooling systems, and adds to the complexity of lightweight yet robust storage tanks capable of withstanding cryogenic temperatures [44].

Safety challenges

Choosing hydrogen as fuel brings also safety challenges which require special attention due to hydrogen's distinctive properties in comparison to regular hydrocarbon fuels [14]. The hazards associated with hydrogen use include physiological, physical, and chemical risks [60]. In addition to the ease of leaking, hydrogen is more buoyant and prone to dispersion, necessitating specialized systems for both liquid hydrogen (LH_2) and gaseous hydrogen (GH_2). These systems must address the rapid vaporization and upward dispersion of hydrogen in the event of a leak. Furthermore, hydrogen is characterised by a wide flammability range and low ignition energy, making it highly combustible. At 1 atm and 298 K, the flammability range extends from 4$\%$ to 75$\%$ of hydrogen-to-air volumetric ratios, requiring only 7.2$\%$ of the ignition energy needed for gasoline at the same pressure and temperature conditions [28]. Unlike kerosene, which requires a specific temperature range to form a flammable atmosphere, any release of hydrogen can potentially lead to an explosive atmosphere at much lower concentrations. However, this risk can be reduced by the rapid ascent and dispersion of hydrogen before ignition occurs. Unless the leak happens in an enclosed and poorly ventilated space, the danger is typically less severe. On the other hand, the flames produced by hydrogen combustion are often hard to detect, which can make firefighting more difficult. Catastrophic accidents could arise from explosives and the fire hazard caused by the violent exothermic reactions that ignite when oxygen is present or from the sudden depressurization of the tank due to structural failure.

The fatigue life of an LH_2 fuel tank can be significantly affected by fueling cycles. Low temperatures associated with cryogenic storage can lead to embrittlement of materials, increasing their yield strength but reducing ductility and toughness. This trade-off ultimately limits the number of cycles a material can withstand before failure. Moreover, continuous exposure to hydrogen gas can induce hydrogen diffusion into the material that could cause hydrogen embrittlement and hydrogen-induced cracking, further compromising material integrity [63]. These factors pose a risk of catastrophic failure in storage tanks and related components.

As can be deduced from the above, advancements in storage technology are essential for unlocking hydrogen's full potential as a clean and efficient energy carrier.

Aircraft and engine redesigns

Hydrogen fuel cell propulsion necessitates a comprehensive overhaul of current aviation systems, including the integration of distributed electrical propulsion systems with high voltage/high power requirements [73]. This transformation will require significant modifications to both the architecture and functionality of aircraft to fully exploit the potential of hydrogen and fuel cells. For liquid hydrogen storage, tank designs must minimize heat leaks by favoring shapes with low surface area-to-volume ratios. Furthermore, given hydrogen's low volumetric energy density, it is crucial to limit the weight and drag penalties associated with integrating hydrogen tanks into aircraft configurations.

Typically, the wings of hydrogen-powered aircraft are "dry," meaning they do not contain fuel. This design choice arises because wings, with their high surface area-to-volume ratios, are not ideal for minimizing heat transfer [31]. However, the absence of fuel in the wings eliminates the load alleviation typically provided by the weight of conventional fuel, likely leading to a heavier wing structure. The most common configuration for hydrogen storage involves integrating tanks into the fuselage of a traditional tube-and-wing aircraft [31]. Some designs allocate an entire section of the fuselage's cross-section for one or more hydrogen tanks. This approach offers the highest tank volume relative to surface area and enables integral tank designs, where the tank's outer surface conforms to the fuselage's shape. Alternatively, some designs position the tank above the fuselage along its length [31]. While this configuration requires more insulation and incurs a weight penalty due to its longer, thinner tank shape, it provides safety advantages. Tanks placed higher are in fact less vulnerable to debris damage during landing and takeoff and are safer in the event of a belly landing. Moreover, positioning the tanks above the cabin and outside the pressure vessel reduces the risk of leaks affecting the passenger area, as any leakage is more likely to vent upward and away from the cabin.

During the transition phase from traditional fossil fuel-based propulsion systems to hydrogen-based propulsion systems, retrofitting existing aircraft presents a viable alternative to a complete redesign. By preserving the baseline aircraft's shape and primary structure, retrofitting ensures consistency in mass distribution and structural integrity and allows for the continued use of established aerodynamics, flight mechanics, and structural characteristics. Nonetheless, given the long lifecycle of commercial aircraft, retrofitting serves as an effective strategy to gradually integrate hydrogen technology into the existing fleet without necessitating immediate, large-scale redesigns.

2.3. Hydrogen storage technologies

There are several ways to store hydrogen for future use and Table 2.1 presents an overview of the main storage solutions currently available.

Hydrogen is usually found in its gaseous form under standard atmospheric conditions and is commonly stored in this form at different pressure levels, with established standards of 350 bar and 700 bar for various applications. High-pressure levels are in fact needed to achieve feasible storage volume, but, at the same time, face constraints related to construction, cost, maintenance, and safety [54]. Alternative methods such as cryogenic compression and liquid storage, as well as the use of adsorption materials and metal hybrids, are also available. Another option is to convert hydrogen into different chemical compounds, such as methane or ammonia, for easier storage and transportation.

The presented methods are used in various industries, but the aviation sector primarily focuses on physically storing hydrogen in vessels due to its simplicity and widespread use.

Table 2.1: Differentiation of storage conditions for hydrogen [26]

Type to store	Form of storage	Temperature	Pressure	Medium	H_2 density (kg/m³)	Storage density (mass%)	Comments
Physical storage technology	Pressurized	293 K/20 °C	350 or 700 bar	Gaseous	25–42	~4	Low quantities, serial standard
	Cryo compressed	50 K/−223 °C	350 bar	Gaseous	~80	~9	High storage volume, heavy and expensive
	Cryo liquid	37 K/−236 °C	3–5 bar	Liquid	~65	~10	High quantities, low pressure, standby, boil off
Hydrides storage technology	Metal hybrid	Ambient	Ambient	Metal alloy powder	~45–150	~2	Heavy, expensive, complex, safe
	Chemical	>373 K/>100 °C	Ambient	Solid or powder	~49–105	1–18	Complex
	Organic	Ambient	Ambient	Liquid	~1	~6	Safe handling heat to release
Adsorption storage technology	Carbon	<77 K (best)/<−196 °C	>100 bar (best)	Solid	~18	1–2	Storing needs high energy
	MOFS	<253 K/<0 °C (best)	>100 bar (best)	Solid or powder	~5–45?	1–5	Experimental expensive
	Zeolite	<77 K (best)/< −196 °C	>100 bar (best)	Solid or powder	~11–122	1–2	Safe storage heavy

2.3.1. Physical storage technology

The conventional method of storing hydrogen physically is the basic technology used in the aviation industry due to its simplicity and cost-effectiveness compared to the other options [26]. Some of the alternatives are in fact still in the research phase and can be expensive and risky to implement.

As already mentioned in the previous section, in order to achieve a feasible storage volume for aviation applications, hydrogen must be subjected to high pressures or cryogenic temperatures. The storage state of hydrogen is a crucial aspect of discussion, as it affects both the hydrogen density and the structural design of the tank. The primary options are the three blue areas highlighted in Figure 2.2: pressurised storage (CGH_2), transcritical storage (cryo-compressed), and liquid storage (LH_2).

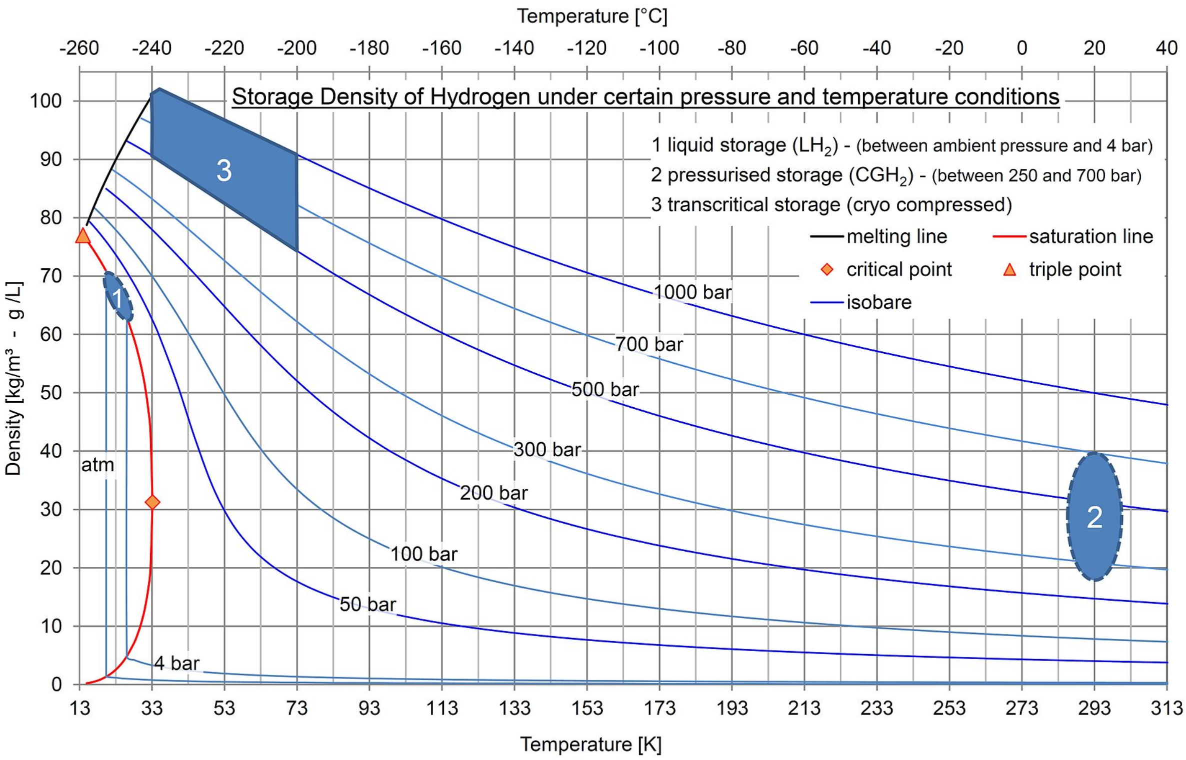

Figure 2.2: Storage density of hydrogen for different pressure and temperature conditions [6]

- **Compressed hydrogen**: region 2. Hydrogen gas is stored at pressure that are higher than the standard atmospheric pressure. In aviation applications, higher pressures are utilized to accommodate larger masses of hydrogen which allow for an extended aircraft range. However, while higher-pressure storage allow for an increase in gravimetric and volumetric hydrogen storage densities, it also requires stricter safety measures [37]. Two main pressure levels are commonly employed: 350 bar and 700 bar.
- **Cryogenic compressed hydrogen**: region 3. Hydrogen is stored at extremely low temperatures in a pressurized vessel (nominally at 350 bar). Even if this method allows for higher densities than traditional liquid hydrogen storage, there are various challenges related to insulation and precautions for high-pressure accumulation that usually result in thicker vessel walls and increased weight. The significant weight associated with these systems is in fact a notable disadvantage for aviation applications, making them less suitable for use in aircraft.
- **Cryogenic liquid hydrogen**: region 1. Hydrogen is stored at cryogenic temperatures (below -250 °C) and low pressure (around 3 bar). This method offers the highest storage density enabling to minimize the storage size of the vessel. The risks associated with high-pressure storage systems are mostly avoided but the main challenge is the need for reliable insulation to keep the vaporizing due to heating low. The main disadvantages include higher energy requirements for liquefaction and liquid hydrogen boil-off, where external heat leaks into the fuel tank and vaporizes the liquid hydrogen due to its low boiling point.

Since aircraft applications requires high volumetric and gravimetric storage densities, cryogenic liquid hydrogen seems to be the best alternative [20]. Cryogenic liquid hydrogen tanks require only half the volume of gaseous hydrogen tanks, which results in lighter storage systems. This is particularly important for flights that range from short to long-haul since the airplane needs to transport several tons of hydrogen on each trip [23]. Furthermore, the low pressures involved limit the risk of leakage and explosions, making cryogenic liquid hydrogen also safer and significantly lighter than highly compressed hydrogen [12].

2.4. Cryogenic liquid hydrogen storage tanks

The cryogenic liquid hydrogen state is defined in a range of pressure between 0.1 and 0.4 MPa and at temperatures below 20 K, where hydrogen exists in a saturated liquid form [25]: in a biphasic saturated state, both liquid and gaseous phases are present, which means that LH_2 cannot fill the total internal volume of the tank. The liquid and gaseous phases are in equilibrium and show the same temperature and pressure, forming a saturated liquid-gas mixture. In this state, pressure and temperature of the mixture are bijectively related, independent of other variables.

This chapter explores the essential aspects of cryogenic liquid hydrogen storage tank design. It begins by discussing hydrogen boil-off, a significant issue resulting from heat inflow that leads to pressure buildup in the tank and, eventually, fuel loss. Following this, considerations on the tank's design operating pressure are presented, focusing on maintaining structural integrity and safety. The chapter then compares integral and non-integral tanks, analyzing their impact on aircraft structure and performance potential. The topic of hydrogen permeation is also covered, highlighting material selection challenges. Finally, the role of safety factors in ensuring reliability and durability in tank design is addressed.

Hydrogen boil-off

The normal boiling point of liquid hydrogen is -252 °C and it is crucial to keep the temperature below this level to prevent fuel loss and pressure buildup inside the tank. During ground operations, significant temperature differences between the the tank's interior and exterior (ΔT) can reach up to ΔT = 300 °C. Heat transfer from the external environment causes a rise in the internal temperature of the tank, which in turn causes liquid hydrogen to gasify (hydrogen boil-off) and rise to the gaseous upper region of the LH_2 tank, known as the ullage [31]. This process results in an increase in pressure inside the tank. Since cryogenic tanks are typically designed to withstand relatively low pressures, any pressure build-up beyond the tank's design limit must be avoided to ensure safety. Venting valves are thus crucial for releasing excess pressure. However, this necessary venting entails the release of hydrogen boil-off, resulting in fuel loss and reduction of the flight range.

To limit hydrogen boil-off caused by heat leakage from the external environment, the tank should be designed with a low surface area-to-volume ratio to minimize the heat transfer into the fuel. Spherical tanks offer the most optimal geometry for achieving this ratio, as they inherently have a lower surface area relative to their volume. Additionally, increasing the tank's size further improves the surface area-to-volume ratio.

On top of this, insulation systems should be implemented to minimize heat exchange and prevent pressure escalation [58]. An efficient and lightweight insulation system is essential for reducing LH_2 boil-off while contributing minimally to the overall tank mass. The selection of insulation materials should focus on achieving the lowest possible thermal conductivity, as this reduces steady-state heat flux and minimizes the amount of heat that reaches the cryogenic fluid. Additionally, for long-term storage, insulation materials with low thermal diffusivity, characterized by high specific heat, are preferred. This ensures that thermal energy takes longer to penetrate the insulation and reach the cryogenic hydrogen, thereby extending the time before any significant temperature rise occurs.

It is however important to consider that insulation systems impact the overall tank weight. While additional insulation reduces heat leak and consequently lowers hydrogen boil-off, this comes at the cost of increased insulation mass. Conversely, reducing the amount of insulation decreases the insulation mass, but this is offset by the need for additional hydrogen propellant and a larger tank to manage boil-off losses. Furthermore, the weight penalty of excessive insulation can adversely affect the autogenous tank pressurization.

Other mechanisms that can cause hydrogen boil-off are ortho-para conversion and sloshing [70]. The *ortho-para conversion of hydrogen* refers to the transformation from ortho-protium hydrogen, where the nuclear spins of atoms within the molecule align in the same direction, to para-protium hydrogen, where the nuclear spins point in opposite directions. At temperatures close to the hydrogen normal boiling point, this conversion occurs spontaneously, and when normal hydrogen is converted into liquid para-hydrogen, a significant amount of energy is released (exothermic reaction) [19]. Catalysts are employed at the industrial level to accelerate the conversion of ortho-hydrogen to para-hydrogen, preventing boil-off losses during the liquefaction of hydrogen [59]. While the use of catalysts does impose an efficiency penalty due to the increased cooling load required to remove the heat generated, it is essential for optimizing the liquefaction process. Common catalysts include diamagnetic solids like germanium or silver, copper, various oxides such as Fe_2O_3 and Cr_2O_3, alumina-supported perovskites, and gold nanoparticles [59].

Sloshing occurs when liquid within a tank gathers on one side and strikes the tank wall, resulting in a hydraulic jump. This phenomenon converts the kinetic energy of the impact into thermal energy. To prevent or reduce the effects of sloshing in aircraft fuel tanks, designers often incorporate specialized features such as baffles and sponge-like mesh structures [56]. Baffles are internal partitions that disrupt the fluid's movement, dampening the oscillations and minimizing the impact of sloshing on the tank walls. Additionally, sponge-like mesh materials are used to absorb and dissipate the energy of the moving liquid.

Tank's design operating pressure

The tank design operating pressure is the maximum expected operating pressure (MEOP) or venting pressure [31]. The tank walls must withstand the pressure differential between the design pressure and the minimum atmospheric pressure experienced during aircraft flight. While lower design pressures lead to lighter tank walls due to structural sizing considerations, there are two relevant factors that demand higher design pressures. Firstly, maintaining the tank pressure above atmospheric and cabin pressure is necessary to prevent air leakage and the formation of combustible mixtures. Additionally, a higher venting pressure allows for more LH_2 to boil off before venting becomes necessary. Consequently, typical minimum operating pressures are around 1.2 bar, with venting pressures typically ranging between 2 and 5 bar.

Integral or non-integral tanks

When designing a new hydrogen-powered aircraft architecture, tanks can be integral or non-integral to the aircraft's structure: while integral tanks provide fuel containment, support fuselage loads, and act as aircraft's structural support, non-integral tanks function solely as fuel containers, installed inside and supported by a conventional airframe [20]. Integral tanks must conform to the shape of the aircraft, often necessitating quite complex architecture, whereas non-integral tanks are not constrained by the aircraft's contours, allowing for a simpler architecture that is easier to manufacture. Theoretically, non-integral tanks could be positioned anywhere in the aircraft and are easier to design since they do not have to support aircraft structural loads. At the same time, integral tanks occupy the whole fuselage cross-section, allowing for larger dimensions of the tank and, consequently, lower surface-to-volume ratios [31]. The potential of integral tanks is superior to that of the non-integral tanks [77]: they enable weight saving for the aircraft, achieved by using the tank wall to serve multiple load-carrying purposes. Additionally, integral tank designs make it easier to inspect and repair both the tank/fuselage structure and insulation. In contrast, repairing non-integral tanks would necessitate their removal from the aircraft.

In retrofit scenarios, where the baseline aircraft's shape and primary structure need to be preserved, integral tanks are not a viable option due to the constraints of the existing aircraft structure. Instead, retrofitting efforts must focus on non-integral tanks, which can be installed within the existing airframe without significant structural alterations. These non-integral tanks are designed to pass through the aircraft's doors and can be more easily adapted to fit within the existing space constraints, making them the preferred option for retrofitting scenarios.

Hydrogen permeation

Hydrogen can penetrate materials in either aqueous or gaseous states and propagate through various pathways, ultimately leading to material degradation and eventually failure [63]. The material selection is crucial to limit the unwanted effects of this phenomenon [58]. In general, hydrogen permeates metals at a slower rate than through non-metallic materials. Still, the higher density of metallic materials is a disadvantage as it can limit aircraft payload and range. Combining composite materials and metallic liners could help address permeability concerns but, at the same time, it may still face potential problems due to differences in thermal expansion coefficients between the composite wall and metallic liner. In fact, when layering different materials, their thermal expansion coefficients should be compatible so that induced stresses during cooling and heating do not rupture the tank. Recent efforts have explored the use of polymeric films and coatings to act as barriers against hydrogen permeation in composite tanks.

Safety factors

The use of safety factors ranging from 1.4 to 2.0, along with conservative material strength estimates, poses challenges to design lightweight structures, especially when using new and advanced materials [58]. Although aircraft designers have successfully managed these challenges for decades, the complexity of characterizing materials under cryogenic conditions and the variability introduced during manufacturing still demand careful consideration. This variability in the material characterisation creates a wide range of material properties, requiring a significant margin between the average measured and allowable values. To address these challenges, innovative tank designs that incorporate integrated health-monitoring techniques and reduce reliance on explicit and implicit safety factors will be necessary. Finding the right balance between minimizing weight, enduring repeated mission cycles, and ensuring manufacturability, inspection, and confidence in usage presents a significant challenge.

In conclusion, the design of efficient hydrogen storage tanks is a complex process that involves various challenges such as insulation, geometry, material permeation, embrittlement, and safety issues. To address these challenges, various studies have been conducted aiming to develop lightweight, durable, and reliable tank structures. However, designing a hydrogen storage tank depends on the specific application and mission requirements, making it difficult to establish universal guidelines.

In the following section, advancements, methodologies, and insights gained from previous research efforts in the field of hydrogen tank design are presented in order to provide valuable insights into the current state-of-the-art technologies and approaches.

2.4.1. Potential design solutions

The following parameters are crucial during the tank system design phase: mass density, thermal conductivity, strength and toughness, coefficient of thermal expansion, stiffness, and thermal diffusivity [58]. Each of these parameters directly influences how well the tank meets its functional requirements, which encompass factors such as structural integrity, thermal management, and overall reliability. The performance of the tank can be expressed as a function of these functional requirements, the geometry of the tank, and the properties of the material from which it is constructed.

The *mass density* of the tank determines its weight, which affects fuel efficiency, payload capacity, and maneuverability of the vehicle or aircraft that carries it. *Thermal conductivity* plays a crucial role in dissipating or retaining heat, which is essential for maintaining the temperature of the stored contents within acceptable limits. Additionally, insulation systems can face mechanical compression (which might be caused by various factors like weight, pressure differentials, shock, vibration, dimensional changes, or a combination of them) which can pose a threat to its effectiveness. A low-contact resistance insulation system is characterised by a thermal conductivity that is sensitive to compression loads applied to it and this is an unwanted feature in this kind of application [58]. This characteristic is commonly found in insulation materials that achieve low thermal conductivity through the presence of internal voids or porous structures: while these are effective in reducing thermal conductivity by impeding heat transfer, can compress under mechanical stress, altering the material's thermal performance. The *strength and toughness* of the tank material are fundamental for ensuring that it can withstand mechanical stresses, such as pressure fluctuations or external impacts, without failing. The *coefficient of thermal expansion* impacts how much the tank material expands or contracts with temperature changes, which is critical for preventing structural deformation or leakage. *Stiffness* contributes to the tank's rigidity, enabling it to resist deformation under load and maintain its shape. Lastly, *thermal diffusivity* governs how quickly heat can propagate through the tank material, impacting its thermal response time and ability to mitigate temperature gradients.

Cryogenic hydrogen tank insulation design is complex and influenced by various factors [81]. This complexity can lead to over-sizing of insulation systems, resulting in increased system mass and potential penalties for tank wall weight. Excessive insulation thickness may even require the addition of heat to the tank to maintain pressure above the minimum specified level and prevent air leakage [77]. Defining a specific design mission is essential to effectively address both mechanical and thermal design aspects. Pressure fluctuations within the tank depend on several mission-dependent parameters, including heat input through insulation, initial pressure at each flight phase, remaining fuel quantity, and engine fuel consumption rates. Thus, understanding of these factors is crucial to optimize the design of cryogenic hydrogen tanks for their intended applications and missions.

This section addresses the key considerations in the design of storage solutions for hydrogen-powered aircraft, specifically focusing on the selection of tank wall materials, tank wall architecture, and insulation systems. Each of these elements plays a crucial role in ensuring the efficiency, safety, and performance of the storage tanks used to contain liquid hydrogen.

Tank wall material

High strength, fracture toughness, stiffness, low density, and impermeability to LH_2 and GH_2 are required for tank walls. No single material is able to provide all these qualities simultaneously [77]. Furthermore, the storage of liquid hydrogen requires consideration of cryogenic temperature, hydrogen permeation, and embrittlement issues.

Fracture toughness is critical especially in cryogenic environments where the propagation of cracks within insulation can create a leakage path, compromise thermal properties and accelerate boil-off of fuel, which can jeopardize the success of the mission. Adopting a damage tolerant design criterion is important to ensure that flight safety can be maintained even in the event of structural damage of reasonable magnitude which may be caused by accidental impact, fatigue or other sources [20]. In order to achieve that, a fracture control plan should be implemented. Minimum requirements on material fracture properties, such as fracture toughness, resistance to stress corrosion cracking, and fatigue crack growth, should be set as well as the maximum allowable size of flaws that may be missed during inspection and still be able to sustain the combination of operating pressure and limit loads due to maneuvers or gusts. Undetected flaws should in fact remain sub-critical under normal service condition to prevent catastrophic failure.

Moreover, two fracture toughness-related performance indices, namely yield-before-break and leak-before-break, must be considered: the first index ensures that the material deforms stably before reaching critical flaw propagation, facilitating early detection (the stress required to propagate a critical flaw has to be greater than that to yield the material), while the second criterion focuses on detecting leaks before catastrophic failure (maximum pressure carried would result in the stable growth of a crack just large enough to penetrate both the inner and outer surface) [77].

Possible candidates are sought within metallic and composite materials, as these categories of materials can provide sufficient strength, acceptable low density and decent fracture properties. Table 2.2 briefly summarizes the advantages and disadvantages of various options for tank wall materials.

When it comes to choosing materials for tank walls, metals are usually preferred over composites. While composites have the potential to significantly reduce weight, they introduce uncertainties regarding hydrogen permeation and fatigue properties, especially at cryogenic temperatures. These uncertainties pose risks and can result in high variability in material behavior. On the other hand, metals are better understood and offer a higher degree of predictability. Using composite materials requires the need for extensive preliminary studies on material characteristics before practical application, which may not be feasible for projects that has to be delivered within a few years. Although composite technology is promising, the lack of necessary information makes it difficult to use without resorting to high safety factors, ultimately leading to increased weight and negating the advantage these materials offer.

Metals that have acceptable properties from ambient to cryogenic temperatures include austenitic stainless steels, monels, and aluminum alloys.

In previous studies [81], [25], [36], [66], [10], [48], particular attention has been directed towards aluminum alloys. Certain aluminum alloys demonstrate ductility at cryogenic temperatures, along with weldability, stress corrosion resistance, high fracture toughness, and resistance to flaw growth. These attributes make aluminum alloy a common choice for cryogenic storage tanks, especially considering its superior strength-to-weight ratio compared to other materials compatible with cryogenic conditions [57]. Additionally, aluminum is known to exhibit minimal susceptibility to hydrogen embrittlement.

Table 2.2: Advantages and disadvantages of various LH_2 tank wall materials [58]

Discriminators	
	Metallic
Advantages	Well established, currently in use Relatively low cost, easy to fabricate Insignificant permeation, alleviating need for permeation barrier
Disadvantages	Higher mass High thermal conductivity
	Composite[a]
Advantages	Low mass High specific strength and stiffness Tailorable properties
Disadvantages	Higher cost Prone to permeation by hydrogen Prone to microcracking due to constituent CTE mismatch Potential need for barrier or liner, resulting in component CTE mismatch issues Fabrication, processing, and joining issues
	Hybrid construction[a]
Advantages	Potential optimum design for lowest mass
Disadvantages	Fabrication complexity Higher cost CTE mismatch issues

[a]CTE is coefficient of thermal expansion.

Tank wall architecture

The allowable shapes of hydrogen tanks are heavily dependent on their intended application, whether they are integral or non-integral to the aircraft's structure. Integral tanks serve multiple functions, acting as both fuel containment units and structural supports for the fuselage. In contrast, non-integral tanks are solely tasked with fuel storage, installed within the conventional airframe and supported independently. This distinction in function dictates varying shape requirements and limitations.

The design of integral tanks must integrate with the aircraft's architecture, demanding complex engineering solutions tailored to the specific airframe geometry and loads. Non-integral tanks afford greater flexibility in shape design, with options such as spherical or cylindrical configurations [58]. Spherical-shaped tanks offer minimum surface area-to-volume ratio, effectively minimizing passive heat transfer into the tank. However, given that the fuselage is essentially cylindrical, spherical tanks may not optimize the use of the available space, potentially leaving gaps or requiring inefficient arrangements. In contrast, cylindrical tanks, while having a higher surface area-to-volume ratio and thus greater passive heat loads, are better suited for integration within the fuselage.

The study by Winnefeld et al. [81] proposes a mathematical approach to express the options for tank geometries, utilizing the description of an ellipsoid as presented in Figure 2.3. This method ensures a highly flexible geometric design, considering both ellipsoidal heads and elliptical shells.

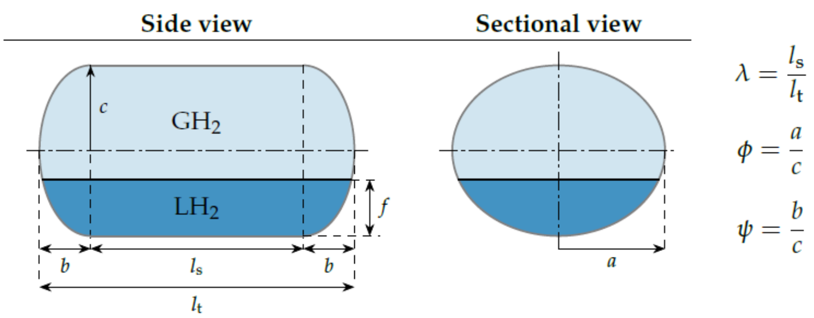

Figure 2.3: Nomenclature describing the geometric tank design [81]

The shape of the tank is characterized by three dimensionless parameters: ϕ and ψ, which define the ratios between the ellipsoidal axes, and λ, which represents the ratio of the shell length l_s to the overall tank length $l_t = l_s + 2b$. Parameter ϕ determines the shape of the shell (circular tank shell for ϕ = 1), while parameter ψ dictates the shape of the tank heads (hemispheres for ψ = 1). In order to avoid having an under-constrained system, the parameter λ is limited to values below 1. This parameterized description facilitates the assessment of multiple potential shapes and enables optimization of the shape based on the particular case study at hand.

Two general categories for tank wall construction are single-wall and double-wall architecture [58]. The advantages and disadvantages of these two architectures are summarised in Table 2.3.

Table 2.3: Advantages and disadvantages of various liquid hydrogen storage tank wall construction architecture [58]

Discriminators	
	Single wall
Advantages	Simple construction
	Low cost
Disadvantages	Limited insulation schemes
	Not optimum for low weight
	Not practical for longer term application
	Double wall
Advantages	Optimum for low weight
	Allows for more insulation schemes
Disadvantages	Higher cost
	Complex fabrication

Single-wall architecture offers relatively simple and cost-effective solutions, but their compatibility is limited to foam-based or similar insulation systems. Double-wall architecture presents a more versatile approach. It may employ two structural walls with minimal physical contact, housing a high-vacuum-based insulation system or a different kind of insulation material. Within the double-wall architecture, the presence of both an outer and inner vessel necessitates a support system for the inner vessel to maintain its proper positioning. This is crucial to prevent contact with the walls of the outer shell while accommodating thermal contraction and expected G-forces in the x, y, and z directions [18].

Insulation

The primary objective is to develop an insulating system that is both highly effective and lightweight, ensuring minimal LH_2 boil-off while contributing the least possible mass to the overall tank structure.

In accordance with Brewer's specifications [20], a thermal protection system needs to fulfill certain criteria to be effective. First, the insulation materials used should be impervious to air or have the capacity to be made impermeable as this would eliminate the need for active purging to prevent cryopumping. Additionally, these materials should be resilient against aging or cracking when subjected to repeated thermal or mechanical stresses. They should also be able to withstand extreme exterior temperatures and allow for easy repair or replacement as and when needed.

For an insulation system to be efficient, it needs to be characterised by low thermal conductivity, a low thermal diffusivity and a low density [58]. Reducing thermal conductivity minimizes the steady-state heat flux, thereby decreasing the rate of heat flow through the insulation. Similarly, minimizing thermal diffusivity reduces the temperature increase per unit of time, effectively prolonging the time taken for thermal energy to reach the fuel. Additionally, minimizing material density yields a lightweight solution.

Various investigations conducted on material selection for insulation in cryogenic liquid hydrogen tanks have led to the identification of foams, aerogels, and vacuum based insulation combined with Multi-Layer Insulation (MLI) as possessing the most desirable material properties for aerospace applications [77], [20], [58]. These materials are characterised by small thermal distortions due to their low thermal conductivity and low thermal expansion coefficient. This characteristic is particularly desirable as high thermal distortion may lead to a comparatively large relative displacement, inducing stress within the insulating material that can exceed the material strength. In the event of mechanical failure, the thermal properties of the insulating system would be degraded leading to serious problems for the storage system.

Advantages and disadvantages of the insulation methods considered are presented in Table 2.4, listed in order of increasing thermal performance.

Table 2.4: Advantages and disadvantages of various insulation methods [58]

Location		Discriminators
		Foam
Outside	Advantages	Currently in use, well established Low cost, easy to implement Light weight and low density
	Disadvantages	Limited to short duration missions because of excessive thermal conductivity Low resistance to thermal radiation Potential damage from environmental hazards
Inside	Advantages	Low cost Structural wall not exposed to cryogenic conditions Reduced CTE mismatch issues of composite constituents, resulting in reduced microcracking
	Disadvantages	Necessitates larger structural tank wall, resulting in increased mass Difficult to seal from cryogenic fluid • Fluid infiltration leads to increased thermal conductivity • Potential loss of structural wall integrity May interfere with fluid management upon failure
		Aerogel
Between walls	Advantages	Extremely low thermal conductivity[a]
	Disadvantages	New material, not well characterized Limited mechanical properties
		Vacuum
Between walls	Advantages	Near zero thermal conductivity Well established
	Disadvantages	Heavier tank walls required Costly to implement and maintain No resistance to radiation heat transfer Near catastrophic failure upon loss of vacuum
		MLI
Between walls	Advantages	Very low thermal conductivity and radiation heat transfer[b] Extremely low density Well established
	Disadvantages	High vacuum required Heavier tank walls required Costly to implement and maintain Near catastrophic failure upon loss of vacuum

[a]The balance between the structural and thermal properties can be altered to optimize for the application.
[b]MLI is available in graded form to improve thermal properties and to reduce the density, but at a higher cost.

Foams

Low density polymer foams constitute good candidates from the conductivity and mass point of view. Various types of open and closed-cell foams are considered [77]. Flexible open-cell thermo-formable polyimide foams are good for insulating complex shapes since they can easily adapt to complex geometries. However, they have an open-cell structure which can lead to cryo-pumping. Rigid polyurethane and polyisocyanurate foams are not thermo-formable hence delicate, but they are still great for insulation due to their properties. Rohacell closed-cell polymethacrylimide foam is both rigid and thermoformable, but the thermoforming process requires careful handling.

The foam insulation can be applied to the inside or to the exterior surface of the tank [77]. Applying insulation to the inside of the tank has the advantage of keeping the tank wall at a similar temperature as the surrounding environment, simplifying the problems of attachment and support for the tank. However, the internal insulation must be impermeable to GH_2 to prevent its diffusion to the tank wall, which could compromise its effectiveness. On the other hand, applying insulation to the exterior surface of the tanks presents significant challenges, such as the tank structure's significant expansion and contraction with LH_2 usage, attachment problems for structural support systems, and susceptibility to mechanical damage. External insulation must also be impermeable to air to prevent cryo-pumping, which would degrade its effectiveness.

Foam insulation has a successful track record in space applications, but presents some significant barriers for the application in the aviation field. Foams present difficulties in withstanding repeated thermal cycles and are prone to cracking or delaminating from the tank's structural wall under such thermal stress [31]. Transport aircraft are expected to fly multiple times per day and operate for extended periods between maintenance checks. This implies that the LH_2 tanks must cycle between cryogenic operating conditions and ambient temperature during maintenance or storage without being damaged. Although these insulation strategy presents lifetime and maintainability issues, foams are still taken into account in different studies due to their potential in offering higher tank gravimetric efficiencies.

Aerogels
Low-density aerogels in a flexible fibrous matrix provide maximum longevity, relatively low heat transfer, and great ease of usage. Silica aerogels excel in thermal performance as they are made up of highly porous and low-density materials, forming an open microstructure of interconnected particles. The combination of silica's low thermal conductivity and the nanometer-sized pore sizes results in exceptionally low thermal conductivity. However, the same properties that make them great insulators also make aerogels inherently fragile and brittle, making them unsuitable for load-bearing applications. Nonetheless, research work on enhancing the mechanical robustness of aerogels while maintaining their thermal insulation properties could make them a promising option for aircraft cryogenic insulation in the future.

An approach involves forming composites of fibers and aerogel by incorporating a small volume fraction (less than 5 percent) of short silica or silicon carbide fibers [58]. These fibers serve to decrease the transparency to thermal radiation at temperatures exceeding ambient, thereby enhancing the thermal performance of the material, and also contribute to strengthening the aerogel. However, this method is particularly effective when radiation serves as the main mode of heat transfer.

Vacuum based insulation
Insulation systems for cryogenic conditions which employ a vacuum environment are the most effective way to minimize heat transfer from the surroundings to the stored cryogenic substances [46]. Known as Dewar type tanks, the vacuum-insulated tanks feature a double-wall design with a vacuum layer in between. The vacuum jacked of this kind of tanks is evacuated in order to reduce convective heat transfer and residual gas conduction between LH_2 and external enrivonment [85].

Additional layers of reflective membranes, such as multi-layer insulation (MLI), further improve the thermal performance of the insulation system. The combination of multi-layer insulation and a vacuum jacket is comparable to low density foams in terms of range of densities, and can provide an apparent thermal conductivity that is roughly two orders of magnitude lower than the best low-conductivity foams. The MLI system employs multiple thermal radiation shields arranged perpendicular to the heat flow direction [77]. The shields consist of alternating layers of low-emissivity metal foil (such as aluminized or goldized Mylar or Kapton) and thin insulating spacers (which are made of materials like polyester, glass fiber paper, silk tissue, or Superfloc separators). This configuration prevents direct metal-to-metal contact, minimizes heat transfer through residual gas conduction by operating at vacuum levels, and features perforated metal foils to facilitate the evacuation of residual gases during vacuum setup. However, its performance is heavily influenced by pressure (which must remain below 13 mPa), type of residual gas present, and layer density. The thermal properties provided by this system are highly anisotropic and sensitive to mechanical compression.

Studies on traditional MLI have shown that heat transfer occurs mainly through solid conduction, gas conduction, and radiation [52]. Radiation is the primary factor on the high temperature side, while solid conduction between the radiation screens becomes significant on the cryogenic side. To address this issue, NASA developed the Variable Density Multi-Layer Insulation (VDMLI) technique, which involves modifying the density of the reflective and spacer layers within the MLI while maintaining the same number of layers. This adjustment aims to decrease the spacing between reflective layers near the hot boundary to block more heat radiation from the ambient environment and increase the spacing between reflective layers near the cold boundary to reduce heat flux at the walls of the inner vessel of the LH_2 storage tank [84].

High-vacuum insulation coupled with multi-layer insulation HV-MLI can be considered the most common vacuum based passive insulation system, given its wide use for storage of cryogenic liquids. The vacuum jacket is installed between the outer vessel (warm boundary) and the inner vessel (cold boundary), and the high vacuum (HV) function reduces the residual gas conduction and convective heat transfer between the external environment and cryogenic liquids. The performance of this kind of systems is influenced by multiple parameters:

- *Vacuum pressure*: the performance of HV-MLI insulation system is significantly influenced by the level of vacuum pressure. As can be deduced from Figure 2.4, when the vacuum pressure remains below 10^{-1} Pa, the apparent thermal conductivity of the MLI stays below 10^{-4} W/mK. However, as the vacuum pressure exceeds 10^{-1} Pa, there is a considerable rise in the apparent thermal conductivity [78]. This trend is confirmed by the behaviour of the temperature of outer surface of MLI (T_o). In fact, when the vacuum pressure remains below 10^{-1} Pa, the heat inflow stays almost constant implying that T_o remains steady since there is also no change in ambient temperature. However, as the vacuum pressure exceeds 10^{-1} Pa, the total heat inflow increases significantly causing the presence of a larger temperature difference between the outer surface of MLI and the ambient. The trend of the heat flux is perfectly consistent to that of the apparent thermal conductivity, as the heat load is directly proportional to the apparent thermal conductivity.

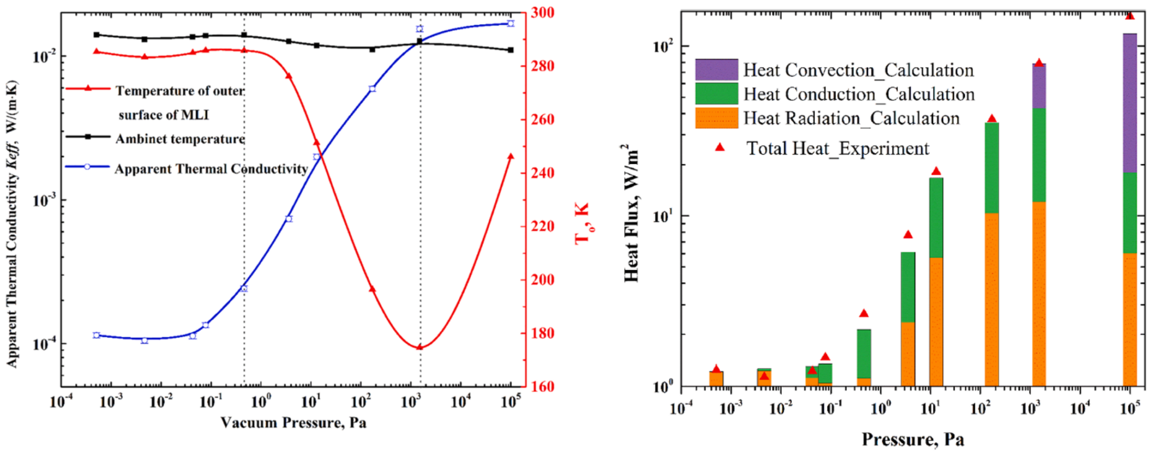

Figure 2.4: Apparent thermal conductivity, T_o and heat flux at different vacuum pressures [78]

- *Layer density*: the thermal performance of multilayer insulation systems is influenced by the density of layers of the system. Heat transfer by radiation can be reduced by increasing the number of shields, but heat transfer by solid conduction increases with increasing packing density since the thermal contact between the radiation shields and spacers gets better [80]. These opposing trends impose the need to evaluate what is the optimal value for the specific application.
- *Emissivity of the radiation shields*: heat transfer by radiation is directly influenced by the emissivity of the radiation shields. Emissivity is defined as the ratio between the energy radiated by the surface of a material and that radiated by a perfect emitter (black body) at the same temperature and wavelength and under the same viewing conditions. It is a dimensionless number between 0 (for a perfect reflector) and 1 (for a perfect emitter). In the current application, the energy coming from the external ambient in the form of heat has to be reflected, so the lower the emissivity, the higher the thermal performance of the insulation system. Usually the layers of low-emissivity metal foil are made of materials such as aluminized or goldized Mylar or Kapton.
- *Thermal conductivity of the spacer material*: the transmission of heat by solid conduction through the spacers of MLI structure is directly influenced by the thermal conductivity of the material used for the spacers. Since thermal conductivity is a measure of the material's ability to conduct heat, it is beneficial to select materials with low thermal conductivity values for this specific application.
- *Type of residual gas*: the way in which the type of residual gas influences the MLI thermal performance depends on the vacuum pressure and the respective rarefaction state of the gas. In

intermediate and molecular regime heat transfer (high rarefaction, low-pressures), gas energy accommodation coefficient (EAC) predominantly impacts MLI performance, whereas in continuum regime (dense gas, higher pressures), performance relies more on the thermal conductivity of the gas itself [72]. Based on the values presented in Figure 2.5 and on the results presented in reference [72], Argon emerged as a preferable choice among residual gases due to its low EAC and favorable apparent thermal conductivity across varied vacuum conditions. Throughout the transition from molecular to continuum regimes, MLI with residual Argon consistently maintained lower apparent thermal conductivity compared to other gases.

Gas	Air	He	Ne	Ar	Kr	Xe	H_2	D_2	N_2
EAC	0.85	0.0291	0.0729	0.3678	0.5016	0.7222	0.1392	0.2172	0.5098
K_{gas} (W/m K)	0.02412	0.1474	0.04551	0.01662	0.00888	0.00519	0.1742	0.00364	0.02428

Figure 2.5: Gas EAC and thermal conductivity [72]

The dependency of HV-MLI performance on these diverse parameters underscores the complexity inherent in designing and optimizing this type of insulation systems. Each factor interacts with others in intricate ways, making precise control and understanding of these variables essential for achieving optimal thermal insulation.

2.5. Case study: Non-integral metal LH_2 tank

The scenario in which this thesis project takes place is the retrofit of a regional airliner intended to be completed within a relatively short time frame (couple of years). This case study holds significant interest as it presents an opportunity to potentially accelerate the adoption of hydrogen propulsion technology. Retrofitting an existing aircraft entails less time and energy than designing an entirely new architecture. It involves maintaining the baseline aircraft's shape and main structure, ensuring consistency in mass distribution and structural integrity. While this approach simplifies the process, it may not offer optimal solutions due to limitations in modifying external shapes.

Several ongoing projects are currently focused on the idea of retrofitting, as this could be the fastest way to test the potential of this technology in aviation [15]. Partnerships between airlines, OEMs, and hydrogen-focused startups are increasing, with a focus on retrofitting regional jets and turboprops with hydrogen-electric propulsion systems. ZeroAvia is developing multiple hydrogen-electric powertrains tailored for various aircraft sizes, ranging from smaller 5-20-seat aircraft to larger 40-80-seat aircraft. Alaska Airlines is one of the operators supporting ZeroAvia: the airline is donating a Bombardier Q400 to ZeroAvia for retrofitting with a hydrogen-electric powertrain serving as a significant learning opportunity for future regional jet retrofits. Universal Hydrogen has secured agreements with numerous airlines and lessors, aiming to convert ATR 72s and Dash-8s to hydrogen power using fuel-cell technology. The development of modular hydrogen capsule technology by Universal Hydrogen addresses critical infrastructure challenges associated with hydrogen transportation. Companies like AeroTEC are providing essential engineering services and expertise. AeroTEC's Hydrogen Aviation Test and Service Center serves as a hub for retrofitting, flight testing, and certification of hydrogen-electric aircraft. Through collaboration with partners like ZeroAvia and Universal Hydrogen, AeroTEC aims to streamline the conversion process and accelerate the deployment of hydrogen-electric aviation solutions. Despite the challenges posed by regulatory certification and technological complexities, these projects represent a significant step towards realizing the vision of hydrogen-electric aviation. By leveraging existing airframes and infrastructure, retrofitting offers a pathway to reducing emissions and advancing sustainable air travel.

Performance requirements

In the design of LH_2 storage systems for this case study, two performance requirements are crucial benchmarks in the preliminary assessment of a design's viability: cruise time and dormancy time. Meeting both cruise time and dormancy time requirements is a strong indicator that a storage system design has the potential for further detailed analysis and optimization. Conversely, the design may not be viable, rendering the evaluation of more specific requirements unnecessary.

The **cruise time** represents the maximum time that can be spent in the cruise phase. The value of this parameter depends on the inner dimensions of the vessel, the fill ratio, and the mission profile including the hydrogen mass flow rates and time durations for the different phases of the mission. The average flight duration for a regional aircraft is approximately of 1 hour and the exact duration of each phase of the mission (take-off, climb, cruise, descent, and landing) depends on factors like the specific route, aircraft type, and overall mission requirements [79]. In the context of hydrogen storage systems, a cruise time requirement of 20 minutes is considered the minimum satisfactory duration for evaluating the viability of a design. This duration reflects the lower bound of typical cruise phases in regional aircraft operations, ensuring that the storage system is capable of handling at least the basic operational demands of such flights.

The **dormancy time** consists of the elapsed time after which the gas pressure inside the tank of a parked non-operating vehicle reaches the set point of the relief valve and some H_2 must be vented at a controlled rate. It is calculated as the time it takes to reach an internal tank pressure equal to the venting pressure and, hence, it is a function of the maximum allowable pressure and the pressure of stored H_2. The requirement for dormancy time of 1 day is established to ensure that no hydrogen loss occurs even if the aircraft remains stationary for an extended period. This condition is crucial to account for potential delays or postponements of flights due to various factors such as bad weather, air traffic, or other unforeseen circumstances.

Non-integral tank

The selection of this case study directly implies the adoption of a non-integral tank configuration. Integral tanks, which are structurally integrated into the airframe and support fuselage loads, present challenges when retrofitting existing aircraft due to the complexity of incorporating them into established structures. The integration of an integral tank would require extensive modifications to the aircraft's existing framework, potentially compromising its structural integrity and overall performance. Additionally, this would add to the certification effort, especially when altering primary loading structures. In contrast, non-integral tanks offer a more adaptable solution as they can be installed independently within the aircraft's existing structure without significant alterations to its external geometry. This flexibility makes non-integral tanks particularly suitable for retrofitting projects.

As previously discussed in section 2.2.1, hydrogen requires a significantly larger volume for storage compared to conventional hydrocarbon fuels. This requirement poses a challenge for integrating hydrogen storage systems into aircraft and the most viable location for hydrogen storage systems in an aircraft is typically within the fuselage. Due to the limited volume available within the fuselage, an aircraft retrofit would probably result in a reduction of the space available for passengers, potentially necessitating the replacement or rearrangement of passenger seating configurations.

Metal tank

Opting for a metal material is deemed the most viable option for a retrofit project aiming to be completed and operational within a relatively short time frame. As presented in Table 2.2, metals are typically preferred over composites when selecting materials for tank walls. While composites could offer substantial weight reduction, they introduce uncertainties regarding hydrogen permeation and fatigue properties, especially at cryogenic temperatures, which can result in significant variability in material behavior. Using composite materials requires extensive preliminary studies on material characteristics before practical application, which may not be feasible for projects with tight delivery schedules. The lack of essential information could ultimately results in high safety factors, implying increased weight and offsetting the advantages these materials offer.

In contrast, metals are better understood and offer a higher level of predictability. Previous studies have extensively examined various metal options, with particular attention given to aluminum alloys. These alloys exhibit favorable properties such as ductility at cryogenic temperatures, weldability, stress corrosion resistance, and high fracture toughness, making them suitable for cryogenic storage applications. Additionally, aluminum alloys are characterised by a superior strength-to-weight ratio compared to other materials compatible with cryogenic conditions, further reinforcing their suitability for LH_2 storage applications.

It's important to note the diverse range of material properties across different aluminium series, spanning from 1XXX to 7XXX. These properties, including weldability, strength, ductility, fracture toughness, and susceptibility to hydrogen-induced corrosion, are affected by factors such as temperature and hydrogen exposure. Although most aluminum alloys are weldable, the high-strength 2XXX and 7XXX series are generally considered non-weldable due to being precipitation hardened, with welding destroying the desired microstructure and reducing the material's strength compared to the base metal.

However, recent advancements in welding techniques have made it possible to weld 2XXX and 7XXX series alloys. Among the more readily weldable aluminum alloys, the 5XXX series is noted for its excellent weldability, while the 6XXX series also offers good weldability but may be sensitive to weld defects. Both the 5XXX and 6XXX series are distinguished by their favorable strength-to-weight ratios.

During cooling down to cryogenic temperatures, aluminum alloys typically exhibit increasing yield strength and could experience the ductile to brittle transition, which reduces their impact resistance and can lead to sudden vessel failure. Therefore, maximizing ductility and fracture toughness at the lowest operating temperature is crucial to mitigate such risks. Furthermore, hydrogen embrittlement poses a significant concern, particularly at room temperature, and needs to be evaluated for safe design practices.

Single-wall or double-wall tank?

In the current case study, both single-wall and double-wall (Dewar) tank architectures are considered as viable options. As presented in subsection 2.4.1, while single-wall designs are typically limited to foam-based or similar insulation systems which are not able to provide the same thermal efficiency as vacuum-based insulation systems. However, it is worth trying to understand whether this type of architecture could be a good fit for the selected case study, precisely because of its ease of implementation and lower cost. On the other hand, double-wall tanks with vacuum insulation offer superior thermal performance but come with increased complexity and cost.

Inner vessel support system

In the case of double-wall tank design, the presence of both an outer and inner vessel necessitates a support system for the inner vessel to maintain its proper positioning. This support system is essential to prevent contact between the inner vessel and the walls of the outer shell, while also accommodating thermal contraction and expected G-forces in all directions.

The main challenge is achieving a balance between structural integrity, thermal insulation, and weight. The support system must be robust enough to withstand static and dynamic loads experienced during flight maneuvers or potential impact scenarios, yet flexible enough to accommodate thermal expansion and contraction without compromising its effectiveness. Moreover, it should minimize heat transfer, thereby maintaining the cryogenic temperature of the fuel stored in the inner vessel while operating within the constraints of space and weight limitations imposed by the aircraft's design. The heat transfer rate from outer to inner vessel through the support structure is influenced by the dimensions of the supports, the thermal conductivity of the material they are made from, and the contact thermal conductivity between them and the walls. The temperature difference between the outer and inner vessel is around ΔT = 300 K so, even though the dimensions of the inner vessel supports are relatively small, the heat flux through them cannot be neglected [34].

The inner tank-supporting structure materials should then be characterised by a combination of high strength and low thermal conductivity [75]. Metals could offer high strength but also high thermal conductivity. Composites offer low weight, high specific strength, and tailorable properties, making them ideal for high-performance applications. On the downside, they are expensive, can have high permeation rates, and pose challenges with CTE mismatch and connection strength. Polymers are lightweight and have low conductivity, making them suitable for insulation purposes. However, they can be costly for high-strength applications, have high permeation rates, and generally exhibit poor mechanical properties compared to metals and composites.

In literature, a few design options concerning the design of support structures for double-wall tank configurations have been identified and are presented below. The proposed solutions are sparse and seem to be mainly defined for specific applications. There appears to be a lack of comparative study conducted among the different design options and their implications on tank performance for different case studies.

In the study conducted for the HYDRA-2 Drone [18], a double-wall metal LH_2 tank with vacuum based insulation has been developed. The support of the inner vessel is provided by the combination of structural supports and spring suspension placed longitudinally at both ends of the cylindrical inner vessel as presented in Figure 2.6. A glass fiber composite material known as G-10 CR is utilized for constructing rods due to its favorable thermal conductivity-to-strength ratio, specifically tailored for cryogenic applications. The spring suspensions are employed to counteract g-forces in the x direction, allowing limited displacement to prevent excessive piping deformation. The design ensures that any displacement of the inner vessel remains within the elastic deformation range of the hydrogen piping, while also maintaining the vessel's centered position during cooling.

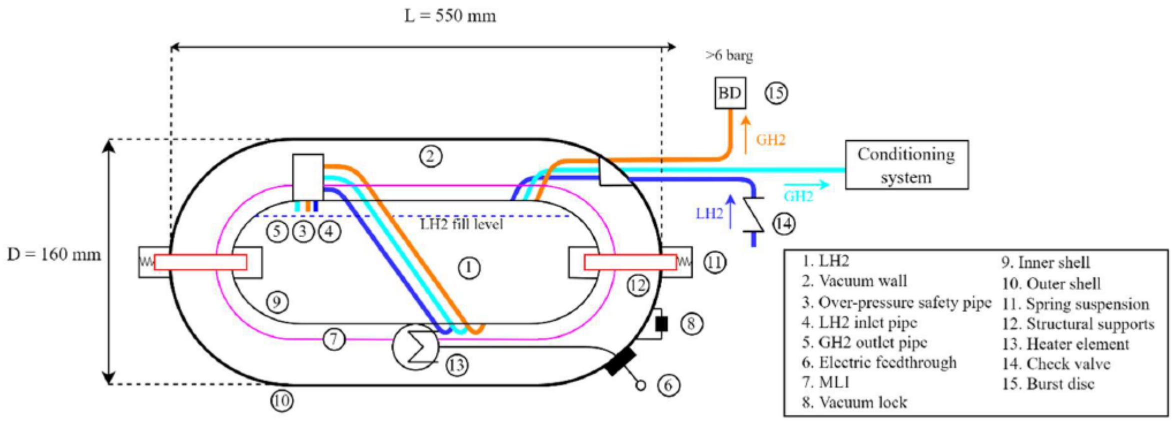

Figure 2.6: System schematic of the LH_2 storage vessel designed for the HYDRA-2 drone [18]

Similar solutions are provided in two other studies conducted for unmanned aerial vehicles (UAV).

The LH_2 storage system designed for the Genii UAV [4] features the cryogenic tank suspended within the vacuum tank using G-10 rods at each end to minimize conduction heat loads. One rod remains rigid, while the other consists of two nested sleeves containing a high compression spring. This spring applies a force to maintain the relative position between the two cylinders while accommodating thermal contraction and expansion.

The design of a 6 L LH_2 storage system [33] involves two concentric lightweight aluminum cylinders with high vacuum and multi-layer insulation in between. The inner vessel is suspended by two axial support G-10 CR pipes at each end of the cylinder, preventing contact with the outer shell.

The design proposed in reference [75] is a double-wall aluminum tank characterised by low density polyurethane foam as insulating material. The inner tank receives axial support from two continuous PEEK tubes and radial support from a staggered configuration of PEEK tubes mounted on a PEEK ring with an I-shaped cross-section as presented in Figure 2.7.

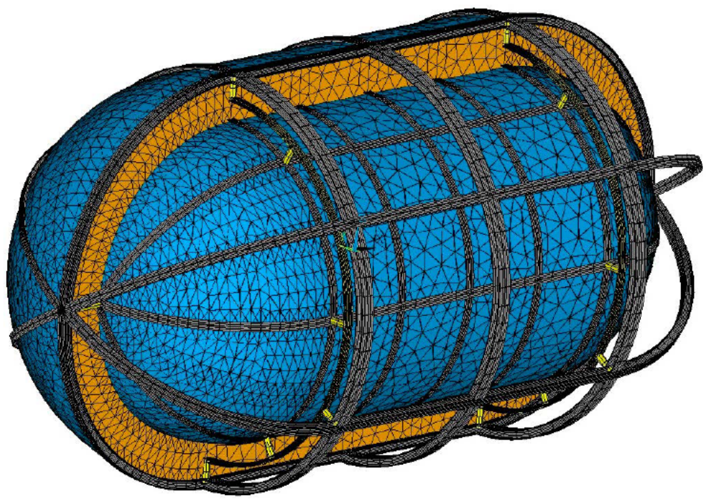

Figure 2.7: Diagram of the finalized tank: tank walls in blue, stiffening members in grey, inner tank supports in yellow and foam insulation in orange [75]

The design proposed in reference [83] is related to liquid hydrogen storage for high-altitude long-endurance remotely-operated aircraft. The spherical tank design incorporates a double vacuum jacket structure with the combined use of Multi Layer Insulation (MLI) and a spiral pipe acting as a Vapor-

Cooled Shield (VCS). The tank's inner tank is made of stainless steel, while stainless steel and composite materials are considered suitable for the outer tank. Zirconia ceramic pellets are chosen for their high strength, low thermal conductivity, and compatibility with metal bonding. The tank configuration comprises two concentric spherical tanks connected by eight point-contact insulating supports, with supporting components and coils made of stainless steel. Research results indicate that the insulating support can significantly reduce heat leakage, meeting both structural and thermal requirements for aerospace applications.

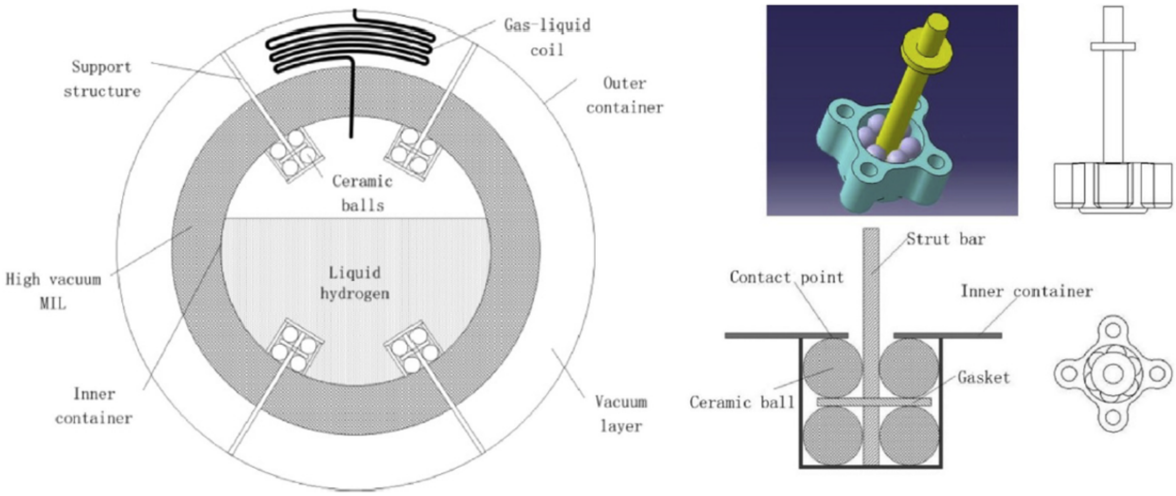

Figure 2.8: Schematic diagram of cryogenic liquid storage tank and details of the support structure [83]

The tank design presented in reference [48] is a double-walled aluminium vessel with capacity of about 100 kg of liquid hydrogen. The design pressure is 2 bar, the design over-pressure is 15 bar and the design temperature is 20 K. The insulation system consists in a spray on foam based on polyurethane materials. Each tank is supported by four longitudinal beams and, while the outer vessel has two rings for support, the inner vessel has seven due to the higher load of over-pressue. These beams present a I cross section and are made of aluminum 2219. The inner tank support structure consists of 10 PEEK tubes.

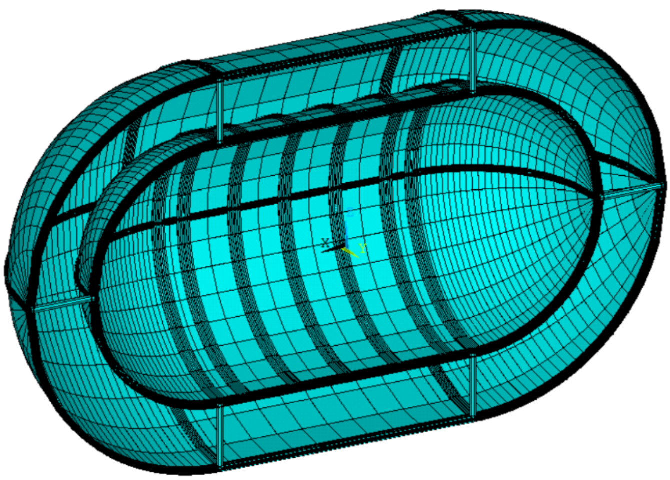

Figure 2.9: Section of the modeled tank showing the tank walls and the supporting structure [48]

While the specific focus of this study relates to cryogenic liquid hydrogen tanks, it is noteworthy to explore related literature on cryogenic tanks for liquefied natural gas (LNG) in mobile applications. Although LNG and liquid hydrogen serve different purposes, they share similar requirements for transport and storage in specialized double-walled cryogenic tanks. In LNG applications, maintaining the LNG in a liquid state necessitates a temperature inside the tank of approximately -160°C under a pressure of around 7 bar. Achieving and sustaining these conditions mandate the utilization of a vacuum insulation system and internal supports designed to minimize heat leakage into the tank. These internal supports must also withstand complex mechanical loads which are, however, smaller in magnitude than those related to the aerospace sector. While the case study of LNG tanks differs from that of liquid hydrogen, exploring design concepts from LNG applications can offer valuable insights for the design of inner vessel support structures in cryogenic liquid hydrogen tanks.

The work in reference [50] presents different design concepts for the inner vessel support structure for a double-walled metal LNG road tank. In general, the recommendation is to implement a combination of fixed and sliding supports: the fixed supports primarily block axial displacements of the inner tank relative to the outer jacket, while sliding supports limit radial displacements and accommodate thermal shrinkage. Heat transfer through supports mainly occurs via conduction, with a substantial temperature difference of approximately 180 K between the inner tank and the outer jacket. The three proposed design concepts are presented in Figure 2.10 and described below.

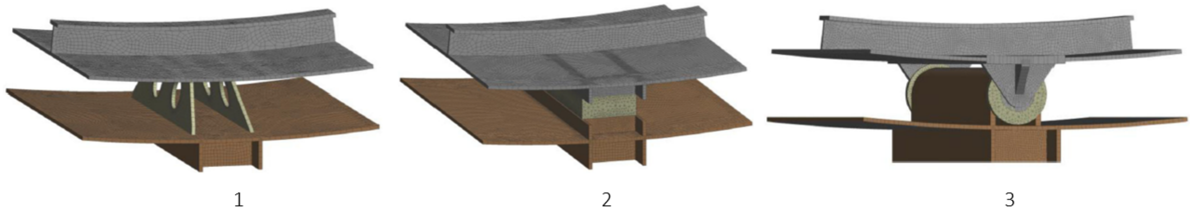

Figure 2.10: Design concepts for inner vessel support structure in LNG road tanker application [50]

- **Support 1**: the material is the same used for inner and outer tank, so stainless steel, and the connection to the rest of the structure is made by welded joints. The heat flow is limited by assuming a relatively small cross-section of the support plates with circular holes.
- **Support 2**: the support consists of a polyamide block placed in stainless steel brackets, offering low heat transfer coefficient but requiring a large cross-section for load transfer.
- **Support 3**: the design features a cylindrical joint which consists of stainless steel supports and a composite insert with high thermal resistance and mechanical strength. The insert is manufactured from synthetic resins in combination with high-strength glass reinforcements.

These design are evaluated by performing static mechanical analyses and transient thermal analyses. The results reveal that it is possible to achieve stress levels below the limit values of the materials for all the design concepts but further optimization is needed. Support 1 is characterised by the highest total heat transfer compared to the other two. A combination of composite insulating elements with steel elements welded to the tank and jacket holds promise for achieving both low heat leakage and adequate mechanical strength.

The study discussed in reference [49] focuses on minimizing heat leakage through the internal supports of a 20-feet mobile container equipped with a cryogenic tank designed for transporting liquefied gases with boiling temperatures as low as - 196°C. A dedicated test stand was built, consisting of a thermo-climatic chamber with ambient temperature controller and tanks equipped with measuring transducers. The tank design includes an inner shell, outer shell, inner shell supports, installation for loading and unloading, ferrules for leading conductors from transducers, and an eyehole. Computational simulations and experimental tests were conducted to evaluate heat transfer characteristics, with a focus on materials with low thermal conductivity. Results indicated that internal supports in contact with the cryogenic tank should be made of plastics with low thermal conductivity, with polycarbonate showing the most advantageous heat transfer characteristics.

2.6. Tank Sizing

The first step to size a LH_2 tank is to understand the specific aircraft related requirements, including the range, payload capacity, and duration of flights. This analysis helps determine the volume of liquid hydrogen needed to meet the mission objectives. Based on the aircraft's design and layout, as well as the available space and weight constraints, the most appropriate tank architecture has to be selected. Choosing the right materials and properly sizing the tank is crucial to minimize heat transfer, prevent liquid hydrogen boil-off, and ensure that the tank can withstand the loads and stresses experienced during flight.

Finite element methods are usually employed for analyzing complex structures and various digital solvers are available to handle structural, thermal, and fluid mechanics simulations. Towards the end of the 2010s, coinciding with the progression in the design of LH_2 aircrafts beyond the conceptual phase, there was a noticeable increase in the finite element analyses performed for LH_2 tanks alongside subsequent validations [75]. These offered insights into structural and damage tolerance behaviour. At the same time, other studies focused on the integration of LH_2 tanks within the aircraft fuselage sections utilizing finite element models that includes structural elements of the fuselage. These models were capable of predicting boil-off rates and assessing stress and displacement under diverse loading conditions such as pressure, thermal changes, and flight-related loads. Moving into the early 2020s, there was a focus on the development of computational tools tailored for exploring and comparing various design concepts and geometries.

Mantzaroudis and Theotokoglou [53] conducted a comprehensive study introducing a computational model capable of analyzing the structural and thermal aspects of independent-type double-walled LH_2 tanks. The tanks under investigation consist of an inner aluminum shell, insulating polyurethane foam, and an outer composite shell. This study evaluates key performance indicators such as gravimetric index and boil-off rate, and focuses on parametrically assessing the effect of LH_2 storage levels and tank geometrical configurations on thermal and structural performance. Finite element simulations are performed considering temperature-dependent material properties and various thermal and pressure loading conditions. The analyses takes into consideration multiple heat transfer mechanisms, including radiation, convection, and conduction, alongside mechanical stresses induced by temperature variations and internal pressure. The computational process involves iterative analyses to determine insulation thickness for achieving target boil-off rates, followed by structural analyses to ensure component integrity. The numerical models developed in ANSYS Parametric Design Language (APDL) facilitate the evaluation and selection of tank designs early in the aircraft design process, considering temperature-dependent non-linearities and various tank shapes.

A computational tool that could perform multi-physics analyses of several tank concepts would facilitate the design process of LH_2 tanks enabling to balance the competing demands. Trade-off studies could be conducted, leading to the eventual selection of an optimal solution for each case.

The work by Lampeas and Tzoumakis [48] focuses on the development of a comprehensive thermo-mechanical simulation model tailored for small-scale liquid hydrogen fuel tanks intended for aviation applications. The developed multi-parametric model is capable of accommodating various design geometries of the double-walled aluminum vessel and accounts both for the critical parameters regarding cryogenic metallic hydrogen tanks and for the temperature dependency of thermal and mechanical material properties. A three-dimensional finite element model has been implemented to simulate the operational environment of a liquid hydrogen tank, enabling accurate predictions of temperature and stress distributions across all tank components. The workflow consists in heat transfer analysis using finite element method followed by finite element thermo-mechanical stress analysis. The first one enables to obtain the temperature distribution of the tank and the supporting structure, while the second one involves stress analysis and strength evaluation. The verification of the model has been performed by comparing the calculated thermal and heat flux with theoretical estimates derived from an analytical model which considers thermal conduction, thermal convection, and thermal radiation. In the current approach, the heat losses due to conduction through the inner vessel support structure are neglected even though these could be significant. However, the multi-parametric nature of this model allows for trade-off studies between various design parameters as boil-off rate and weigth.

In the follow-up study conducted by Lampeas and Tzoumakis [47], the structural model has been added so to combine thermal and mechanical loads and conduct stress, strain and displacement calculations. The final result would be verifying the structural integrity of the tank.

Tzoumakis, Fotopoulos and Lampeas (work in reference [75]) proposed a comprehensive approach to address the challenges associated with the design and analysis of cryogenic tanks, particularly focusing on LH_2-powered aircraft applications. The study introduces a novel computational tool in the form of a multi-physics finite element digital simulation, designed to facilitate performing heat transfer and structural analysis in a fully parametric manner. A flowchart of the methodology is presented in Figure 2.11.

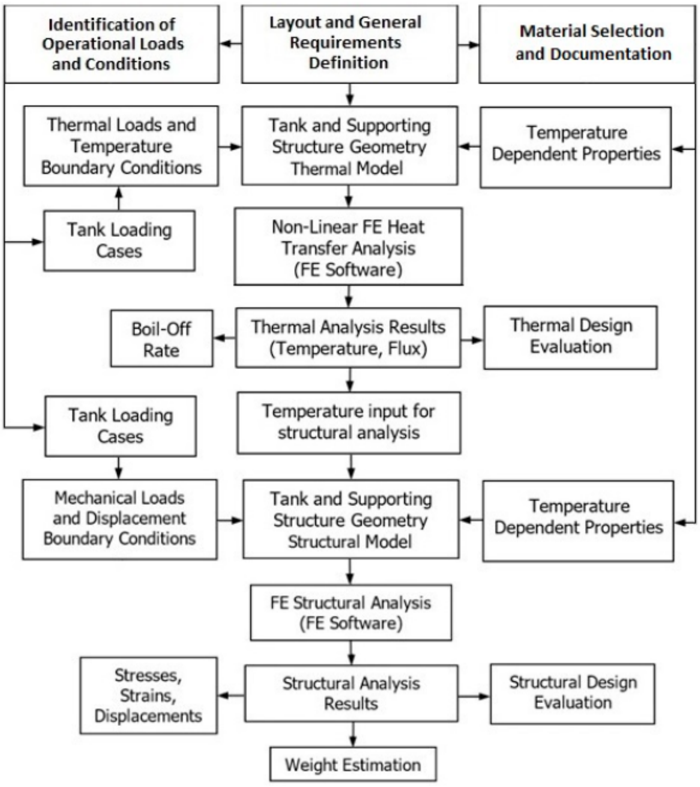

Figure 2.11: Flowchart of the methodology for LH_2 tank design and analysis used in the study [75]

The methodology presented by Tzoumakis, Fotopoulos and Lampeas [75] enables the exploration of different design variations, material choices, and geometric configurations to meet the conflicting demands of minimizing heat losses, ensuring structural integrity, while also optimizing for weight and cost efficiency. The simulations yield insights into both thermal performance and structural integrity, comprising non-linear finite element heat transfer analysis followed by structural analysis. The model includes thermal calculations for temperature distribution and heat flux, coupled with structural analysis considering the results of the thermal part and mechanical loads as inputs, including hydrostatic pressure from LH_2 and constant pressure from GH_2. Furthermore, the developed model features a flexible geometry creation module, enabling to generate axisymmetric double-walled tanks with adjustable dimensions and shapes, facilitating iterative design revisions. Material properties are also parametrically defined, allowing for the exploration of different material options. The computational tool is implemented using ANSYS parametric design language and the simulations are conducted within the ANSYS mechanical solver. Furthermore, Tzoumakis, Fotopoulos and Lampeas [75] outline a systematic methodology for the design process, from defining basic requirements to selecting materials and operational considerations, culminating in the development of the digital simulation. Through iterative iterations and parametric adjustments, the model aids in component sizing, understanding load effects, and predicting tank behavior, essential for integration into aircraft systems and predicting fatigue life.

In conclusion, the sizing of cryogenic LH_2 tanks for aircraft is a highly complex and multi-faceted process. The challenge is to balance mechanical and thermal requirements with the need to minimize weight and optimize structural integrity. As shown by the various research works, the existing design processes involve complex computational models and finite element analyses that account for material properties, geometric configurations, thermal loads, and structural stresses. The need to manage competing demands such as minimizing heat transfer while ensuring the tank can withstand the stresses of flight, underscores the complexity of this task. Ultimately, successful tank design hinges on the integration of advanced simulation tools and a deep understanding of the interplay between thermal and mechanical factors, which together drive the optimization of both performance and structural reliability.

2.7. Crashworthiness

Crashworthiness is the ability of an aircraft structure and its internal systems to protect occupants from severe injury during and after an event of controlled crash [69]. Especially in civil aircraft design, crashworthiness is considered a critical aspect that requires the same attention as strength and fatigue considerations. In a general crash scenario, the fuselage would undergo both elastic and plastic deformation, as well as fracture, in order to absorb the kinetic energy. This is crucial to ensure that occupants do not suffer severe injuries due to high deceleration forces, exposure to hazardous gases or elevated temperatures. Furthermore, the structure must deform in such a way that, during and after a crash, a survivable space is maintained, and evacuation routes remain unobstructed.

In assessing crashworthiness, one must address three primary sources of injury during aircraft crashes: excessive acceleration forces, direct trauma from contact with harmful surfaces, and exposure to environmental hazards such as fire, smoke, water, and chemicals, which can lead to burns, drowning, or asphyxiation. Effective crashworthiness designs aim to identify and mitigate these potential sources of injury within the constraints of a given design impact limit. This involves evaluating various aspects, including for example the strength of the cockpit and cabin, the adequacy of seats and restraint systems, the effectiveness of energy attenuation systems, the presence of injurious objects in the vicinity of the occupants, and considerations for post-crash factors such as fire prevention and providing adequate escape routes.

The European Union Aviation Safety Agency (EASA) and the Federal Aviation Administration (FAA) of the United States are two major aviation regulatory agencies that deal with establishing standards and regulations for aircraft certification. EASA's "Certification Specifications and Acceptable Means of Compliance for Large Aeroplanes (CS-25)" and FAA's "Federal Aviation Regulation Part 25 - Airworthiness Standards: Transport Category Airplanes (FAR-25)" provide guidelines and criteria for ensuring safety and airworthiness of aircraft. The crashworthiness of an aircraft fuselage is regulated by the emergency landing conditions, which are presented in the chapters 25.561 25.563 of CS-25 and chapter 25.561 25.563 of FAR-25.

Current requirements for the fuel tanks

CS 25.963 mandates that fuel tanks are able to withstand, without failure, the vibration, inertia, fluid and structural operational loads and are designed, located and installed to prevent fuel release in quantities sufficient to start a serious fire during otherwise survivable emergency landing conditions. Fuel tanks must resist rupture and retain fuel under ultimate hydrostatic design conditions. For each fuel tank and surrounding airframe structure, the effects of crushing and scraping actions with the ground should not cause the spillage of enough fuel, or generate temperatures that would constitute a fire hazard (under the conditions specified in CS 25.721(b)). Additionally, fuel tanks located in an area where experience or analysis indicates a strike is likely, must undergo analysis or tests to address penetration and deformation by tyre and wheel fragments, small debris from uncontained engine failure or APU failure, or other likely debris (such as runway debris). For pressurized fuel tanks, fail-safe mechanisms must be in place to prevent excessive pressure difference between the inside and the outside of the tank. Compliance with safety criteria is essential to mitigate risks associated with fuel release and potential fires in emergency landings.

The AMC 25.963 sets forth an acceptable means, but not the only means, of demonstrating compliance with the provisions of CS-25 related to the strength of fuel tanks in emergency landing conditions. The fuel tank should be able to sustain the inertia force of the emergency landing condition and apply a static ultimate load. Precautions should be taken so that the fuel tank, both in and near the fuselage, should not rupture under a survivable crash or, at least, should not be able to gather a sufficient hydrogen concentration to cause a serious fire. The fact that the strength of fuel tanks is subjected to the provisions of emergency landing conditions and should allow to survive the conditions of a survivable crash for humans implies that the fuel tanks are subjected to the same regulations as those concerned with the safety of humans.

Requirements for the hydrogen fuel cell system

The mere presence of hydrogen on board poses risks that imply the need for additional regulations. Its ability to permeate into materials, altering their properties, and the fact that it poses an additional risk to the operating personnel, points to the need to also consider the requirements for handling hazardous material under 29 CFR Part 1910 Subpart H Hazardous Materials and API Standard 620, "Design and Construction of Large, Welded Low-Pressure Storage Tanks". Its flammability poses a risk to the structure and entails the need to consider the requirements from NFPA 55 (National Fire Protection Association).

The Energy Supply Device Aviation Rulemaking Committee (ESD ARC) was established by the Federal Aviation Administration (FAA) on April 15, 2015, with the objective of providing recommendations for the development of appropriate airworthiness standards and guidance material for energy supply device installations on various aircraft, with a specific focus on hydrogen fuel cells. Several key decisions were made by the committee, including recommending the creation of a new regulation, referred to as the fuel cell system safety baseline regulation, proposing revisions to existing regulatory standards to accommodate fuel cell systems, and identifying operational regulations that could be directly applicable [27]. Among the various considerations presented in the report, the committee recommends that hydrogen tanks and fuel lines should be protected from unsafe temperatures and strategically positioned to minimize the likelihood and consequences of rupture during a crash landing. Furthermore, the fuel system in the fuselage should be designed and positioned to allow a reasonable level of deformation and stretching without the risk of leakage that could pose a hazard. The installation of hydrogen leakage detection systems in any area of the aircraft where hydrogen accumulation could potentially lead to hazardous conditions is also an important point.

Requirements for inner vessel support system

The support system positioned between the inner and outer vessel of a double-wall tank must effectively maintain the proper positioning of the inner tank and prevent any contact between the inner and outer vessels. This precaution is crucial due to the significant temperature differential between the two metallic vessels, as direct contact could lead to various critical issues. Primarily, such contact would compromise the insulation system, allowing a considerable influx of external heat into the tank containing liquid hydrogen. This would result in a rapid temperature increase, leading to boiling of the liquid hydrogen, a sudden rise in tank pressure, and potential overload of safety systems such as ventilation valve and burst disc. Moreover, the direct contact between surfaces at such different temperatures (up to 300 °C) could induce a thermal shock, potentially compromising the mechanical properties of the material. Additionally, it has to be considered that inlet, outlet, and over-pressure safety pipes are positioned between the inner and outer vessels. Therefore, the supports must also ensure sufficient space between the inner and outer vessels to accommodate these pipes, even during crash scenarios or emergency conditions. The thickness of these pipes also determines the necessary distance between the inner and outer vessels, as the vacuum and multi-layer insulation (MLI) system itself does not require significant installation space for proper functioning.

2.8. Retrofit design

The retrofit designs that will be considered in the following discussion come from the thesis project carried out by TU Delft master student Yi-Hsiu Wu [82]. The main goal of his work was to efficiently use the aircraft's interior space for installing hydrogen tanks. This could be a challenging task due to hydrogen's low density and the aircraft's exposure to various environmental conditions and potential crashes. Furthermore, the installation of the tanks must balance two primary factors: ease of installation and maximizing space utilization to extend the aircraft's range. However, achieving both factors simultaneously poses challenges, as increased space utilization leads to an increased installation complexity.

The research proposed installation methods based on packing solutions, arranging cylindrical tanks within specific volumes to maximize packing density. Assumptions regarding retrofitting methods and tank dimensions were outlined to guide the design process and mitigate complexity. All tanks have the same orientation, length, and diameter in order to simplify both the manufacturing process and the retrofitting process. Other design considerations include ensuring tanks fit through preexisting openings, maintaining structural integrity (the existing primary structure will not be altered or removed but reinforcement could be added to strengthen the loading-bearing capacity or energy-absorbing capability of the aircraft), and adhering to certification requirements. Only the horizontal orientation was considered in order to avoid the risks associated with choosing a vertical orientation (uncontrollable leaks originating at the lower end). The proposed tank model simulates an empty cylindrical container with tank heads on both ends, incorporating tank weight and liquid hydrogen weight. Retrofitting components were designed to fit through aircraft doors (cabin door and/or cargo door), with a focus on maintaining symmetry so to preserve the stability of the aircraft.

A validated numerical model is crucial for analyzing crashworthiness characteristics, with drop tests serving as a cost-effective and time-efficient validation method. The study focused on a Fokker F28 Fellowship model, adapted to simulate retrofit scenarios. Design methodologies include tank configuration and support designs, employing packing solutions to optimize space utilization. Supports were designed to secure tanks during flight and crash events, considering door limitations and crash survivability. The thesis emphasized safety and efficacy, validating designs against real-world crash tests to ensure compliance with safety regulations.

The available design space within the aircraft's fuselage is constrained by several parameters: permissible length (P_L = 2600 mm), floor width (F_W = 2880 mm), floor height (F_W = 980 mm), door width (D_W = 750 mm), door height (D_H = 1800 mm), and inner frame radius (r_{IF} = 1500 mm), along with a safety margin of 10mm to account for deformation during ground impact or significant acceleration loads ($spacing$ = 10 mm). These parameters ensure that the total design volume is limited, preventing tanks from directly impacting each other or compromising their integrity during drop tests or specific load cases.

The thesis project presented one longitudinal retrofit design (longitudinal circle packing LCP, Figure 2.12) and two lateral retrofit designs as optimal solutions (lateral hexagonal packing LHP in Figure 2.13 and lateral square packing LSP in Figure 2.14). The characteristics associated with the proposed retrofit design solutions are summarized in Table 2.5 (dimensions of the single tank and number of tanks).

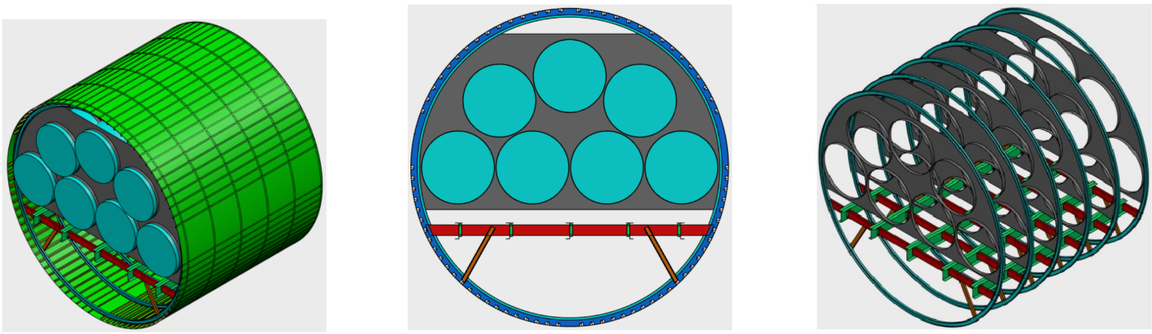

Figure 2.12: Longitudinal circle packing retrofit design [82]

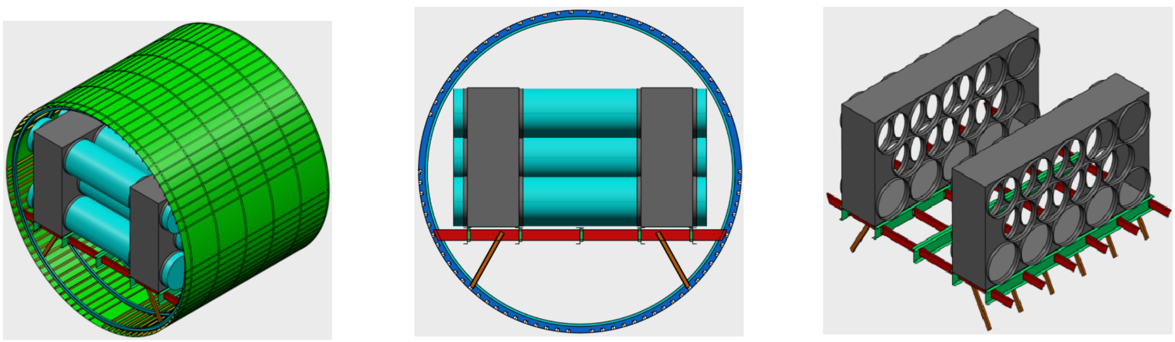

Figure 2.13: Lateral hexagonal packing retrofit design [82]

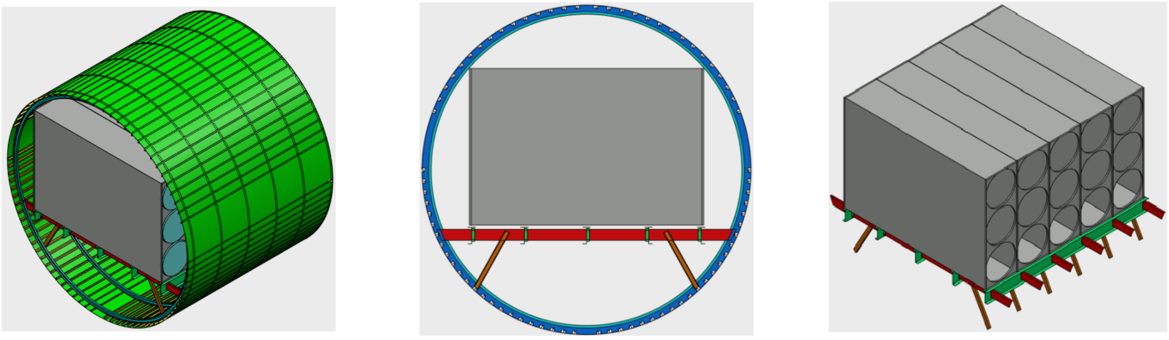

Figure 2.14: Lateral square packing retrofit design[82]

Table 2.5: Feasible design points considered in the analysis

Retrofit design	External diameter [mm]	External length [mm]	Number of tanks
LSP	498	2339	15
LHP	498	2570	14
LCP	750	2600	7

The proposed retrofit designs have then been analysed from the point of view of crashworthiness encompassing finite element analysis (FEA). Johnson-Cook material model was used to simulate the non-linear and plastic behavior of materials during drop tests. The fuselage, including supports, was modeled using AA 2024-T3 aluminum alloy, while the tanks were modeled with AA 2219-T87 aluminum alloy. Certification requirements, including fuel system certifications and crashworthiness certification, were addressed according to CS 25.963, CS 25.56, and AMC 25.963 guidelines.

Regarding inertia loading conditions, the thesis detailed the prescribed load factors for emergency landing conditions within the fuselage contour, as specified in JAR/CS 25.561. Dynamic crash conditions were also analyzed, considering vertical impact velocity based on maximum takeoff weight (MTOW), self-assessment of OEMs, accident studies, and underfloor structural depth. The thesis discussed the following crashworthiness criteria: plastic strain equivalent (PEEQ), visual inspection, energy dissipation (maximum strain energy through the impact history, stabilized plastic energy dissipation, and friction energy dissipation), acceleration-based injury criteria such as DRI and HIC, plastic energy dissipation distribution by component, kinetic and plastic energy time history.

The model was built using the 3DEXPERIENCE platform and analyses were performed using Abaqus/Explicit solver. Loading conditions include four quasi-static loading and one dynamic loading (forward 9.0g inertia loading, upward 3.0g inertia loading, sideward 3.0g inertia loading, downward 6.0g inertia loading, and drop test with an impact speed of 9.14 m/s), and boundary conditions were established to simulate the different loading scenarios. Interaction and contact properties were defined to prevent joint failure and ensure realistic simulation results.

All three packaging designs did meet the requirements of crashworthiness certification, with no plastic damage observed on the outer tank walls under any of the considered loading conditions. This indicates that the section carrying a typical fuselage could be certified across all three designs. Each design demonstrated different methods of energy dissipation in crash scenarios. The LCP design allows transverse cross beams to bend freely, dissipating significant energy through friction. The LHP design absorbs energy as strain energy but releases it as kinetic energy over a short time period, causing increased acceleration on the tanks. The LSP design exhibited the most plastic deformation in the lower fuselage, resulting in the highest level of plastic energy dissipation. Among the three, the LCP design showed the greatest potential for retrofitting baseline aircraft, offering advantages in both crashworthiness and operational range after retrofitting.

2.9. Research questions

The advancements of aerospace technology in a more environmentally friendly direction have led to the exploration of hydrogen as fuel. Among the various storage options, cryogenic liquid hydrogen (LH2) tanks seem to be particularly promising. However, they present unique challenges, requiring specialized solutions to ensure safe and efficient containment.

As presented in the previous sections, for the case study of an aircraft retrofit design, the choice converges towards a non-integral metal tank. Regarding the tank architecture, both single-wall tank and double-wall tank are considered as viable options. In literature, general considerations regarding the pros and cons of the two architectures have been found as well as solutions for individual case studies, but not a clear definition of the areas of applicability of the two design options. It is though very important to define the specific conditions under which a single-wall tank design is suitable and those scenarios where a double-wall tank design is more appropriate. This analysis will provide a framework for determining the optimal tank design based on the demands of various operational contexts. Subsequently, it can be assessed which design is most appropriate for the specific retrofit case study considered.

When evaluating the double-wall architecture, a critical aspect lies in the support system for the inner vessel, crucial for maintaining its precise positioning with respect to the outer vessel while accommodating thermal contraction and expansion and structural loads experienced during flight operations. These structures, having to connect inner and outer vessels which are at significantly different temperatures, risk being a major source of heat leakage if not designed efficiently. Despite the importance of this component, the literature reveals a conspicuous gap in comprehensive design methodologies and optimal material selection. While several studies have outlined specific support systems tailored for individual projects, a comprehensive methodology capable of giving general indications as to which of the infinite number of design directions to pursue remains notably absent. A crucial need exists for low-fidelity models that can effectively evaluate a broad spectrum of preliminary design options. While detailed finite element (FE) models excel in providing precise analyses of selected designs during the detailed design phase, they are often too resource-intensive and narrowly focused to be useful in the early stages of development. Such models would allow for approximate assessments of the thermal and structural performance of numerous design alternatives quickly, identifying promising options before committing to more detailed and computationally expensive analyses. This gap highlights the need for research efforts aimed at addressing the complexities related to inner vessel support configurations for double-wall tank designs.

Research objective: *To develop a suitable methodology for modeling and designing single-wall and double-wall cryogenic hydrogen storage tanks in order to meet the specific thermal and structural performance requirements for retrofit aircraft, while addressing challenges such as thermal efficiency, accomodation of thermal displacements, crashworthiness requirements, and support structure design.*

The research questions presented below aim to generate knowledge about the possibilities in designing single-wall and double-wall tanks.

1. In what scenarios do single-wall and double-wall cryogenic hydrogen tanks offer distinct advantages or limitations, and how should design choices be made based on these scenarios?
2. What are the performance capabilities and applicability limits of single-wall and double-wall architectures in the retrofit case study?
3. How to model the tank in order to evaluate the performance and behavior under the different loading and thermal conditions?
4. How do the performance requirements for cryogenic liquid hydrogen tanks influence the design of the internal support structure for double-wall tanks, and what are the best practices to ensure that the support structure meets these requirements without compromising the overall efficiency of the tank?
5. How to assess whether the design for the inner vessel support structure in a double-wall metal LH_2 tank is able to accommodate thermal expansion and contraction, minimize thermal conductivity, and ensure adequate stiffness and strength against external loads?

3

Single wall tank

In searching for the ideal design of a liquid hydrogen tank, the first step was to assess whether a double wall architecture was indeed necessary. The major benefits of the single wall tank concept are the relative simplicity of construction, the lower cost and the fact that it does not depend on maintaining vacuum for proper operation. It is then important to check whether a single-wall architecture would be able to meet the requirements regarding both time of flight and dormancy time. For the selected case study, a cruise time of at least 20 minutes and a dormancy time of at least 24 hours are required. The line of thought adopted involves first assessing the potential of the material insulation for a single wall architecture from a thermal point of view. The first question to be answered is therefore:

> *"Is there a single wall tank design suitable for the selected case study in which the material insulation layer is able to reduce the heat flow to such an extent that the dormancy time requirement is met and, at the same time, is not too thick so as to allow the storage of sufficient liquid hydrogen to guarantee the minimum required cruise time?"*

If so, a structural evaluation of the resulting architecture would be carried out.

3.1. Single wall tank model

The subject of this section is a cylindrical single-wall LH_2 vessel with hemispherical ends. The proposed design entails an aluminum tank shell, a layer of solid insulation, two composite structural supports, and three aluminum pipes. The single-wall tank model is presented schematically in Figure 3.1.

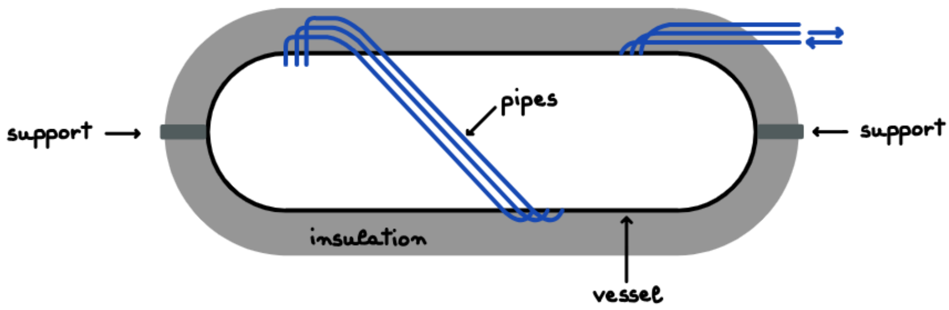

Figure 3.1: Single wall tank model

Shell

Choosing a cylindrical tank with hemispherical ends for storing liquid hydrogen offers a balanced solution that combines the advantages of both cylindrical and spherical designs. This design optimizes space utilization by offering a compromise between the efficient volume-to-surface-area ratio of spheres and the practicality of cylinders, especially in a cylinder-shaped environment such as the inside of the fuselage. The transition from the cylindrical body to the hemispherical ends creates a smooth, continuous surface, enhancing structural integrity and minimizing stress concentrations.

In section 2.5, it has been highlighted that the selection of materials for tank walls leans towards metals over composites due to the complexities that would be introduced by the latter, particularly regarding uncertainties related to hydrogen permeation and fatigue properties, especially under cryogenic conditions. Metals offer a higher level of predictability and understanding, making them a preferred choice despite the potential weight reduction benefits of composites. Particular attention is directed towards aluminum alloys, noted for their ductility at cryogenic temperatures, weldability, stress corrosion resistance, and high strength-to-weight ratio, which make them well-suited for cryogenic storage applications. With the considerations about the different aluminium series presented in section 2.5, the specific alloy that was selected for this case study is: AL5083-O.

The process of sizing the metal shell is based on defining the minimum required thickness of shell under internal pressure and checking whether that thickness value allows the external pressure to be withstood. The guidelines followed were taken from the ASME standards [13]: general requirement UG-27 ("thickness of shells under internal pressure") and the general requirement UG-28 ("thickness of shells and tubes under external pressure"). As defined in Equation 3.1, the minimum required thickness of cylindrical shells under internal pressure must not be less than that calculated by the following formulas: Equation 3.2 for circumferential stress, Equation 3.3 for longitudinal stress, and Equation 3.4 for stress in the spherical dome.

$$t_{shell} = max(t_{circumferential}, t_{long}, t_{spherical}) \tag{3.1}$$

$$t_{circumferential} = \frac{P_{in} R_{in}}{S_{ma} E_j - 0.6 P_{in}} \tag{3.2}$$

$$t_{long} = \frac{P_{in} R_{in}}{2 S_{ma} E_j + 0.4 P_{in}} \tag{3.3}$$

$$t_{spherical} = \frac{P_{in} R_{in}}{2 S_{ma} E_j - 0.2 P_{in}} \tag{3.4}$$

where P_{in} is the internal design pressure, R_{in} is the inside radius of the shell considered, S_{ma} is the maximum allowable stress value, and E_j is the joint efficiency (assumed equal to 0.9). This assumption follows the ASME standards [13], which allow the use a joint efficiency of 0.9 when the weld zone is thoroughly filled and the inspection can be performed either from both sides of the weld.

The external pressure applied to the shell corresponds to the cabin pressure which can range from a maximum of 101 kPa on the ground at sea level to a minimum of 75 kPa in flight [7]. The procedure to follow for evaluating the required minimum thickness of a cylindrical shell under external pressure is more complex as it requires consulting various tables and performing calculations which depends on the specific case. The various steps are comprehensively presented in passage UG-28 of the ASME standards [13].

Pipes

The three pipes serve the function of inlet, outlet and safety pipe. The safety pipe is connected to the burst disc which is used as a backup pressure relief mechanism and it is designed in order to ensure that the highest possible flow rate can be safely accommodated in order to avoid over-pressurization. The maximum flow rate corresponds to the maximum expected boil-off rate which occurs during a scenario where the liquid hydrogen storage vessel is immersed in an external fire. The sizing process for the pipes follows the guidelines provided by the international standard ISO 21013-3 "Cryogenic vessels - Pressure-relief accessories for cryogenic service".

With regard to the material selection for the pipes, it was decided to use the same material which has been selected for the vessel. This decision is mainly motivated by the desire to avoid problems arising from the mismatch between different coefficients of thermal expansions.

Vessel structural supports

At this early stage of evaluation of design concepts, the vessel structural supports design was simplified considerably. This is because the main aim at this stage is to obtain a realistic approximation of the amount of heat that can reach the inside of the vessel from the outside via the supports.

The structural supports are characterised by a cylindrical shape developing longitudinally through the thickness of the insulation layer. The support material is assumed to be G10-CR glass fiber composite. This material has excellent physical properties at cryogenic and operating temperatures and is characterised by a low thermal conductivity which makes it an efficient insulator [42].

Insulation

The main objective is to demonstrate whether the concept of a single wall tank with material insulation is feasible in the considered context, rather than to establish whether a specific type of material insulation can satisfy the requirements of the case study. Consequently, the emphasis is on the general characteristics of this category of materials, rather than on the specific properties of any one material. In particular, since the focus at this stage was directed towards the thermal performance of the insulation layer, the fundamental parameter is the thermal conductivity.

An analysis of the effective thermal conductivity of insulation materials for cryogenic LH_2 storage tanks was performed by Ratnakar et al. [65], providing a method for accurately estimating heat leak and boil-off rate from such tanks. The study encompasses a review of existing experimental data and various correlation models proposed for predicting effective conductivity across a spectrum of insulation systems, including powders, foams, fibrous materials, and multilayer configurations. The effective thermal conductivity may be influenced by factors such as the material composition, structural characteristics, temperature, pressure, and the composition of the gas present in the space between the components. In our specific case study, the temperature range is quite wide (from cryogenic temperatures of approximately 20K to worst-case ambient temperatures of approximately 300K) and the expected pressure conditions are in the order of 10^5-10^6 Pascal. Some general conclusions that can be drawn from the results presented in reference [65] are that at lower temperatures (moving towards cryogenic temperatures) and lower pressures (moving towards vacuum conditions), lower thermal conductivity values can be expected. In general, the magnitude of thermal conductivity for insulation materials employed in cryogenic LH_2 tank applications ranges approximately between 0.010 and 0.100 W/mK.

In Figure 3.2, the pressure dependence of thermal conductivity values of various materials (of which the most relevant for our study are shown in the legend) is presented. This confirms that the range that can be considered for further evaluating the potential of insulation materials is between 0.010 and 0.020 W/mK. In the following discussion, three thermal conductivity values are considered in order to represent the range. These values are the following: $k_{best} = 0.010$ W/mK (best value of the range), $k_{nominal} = 0.015$ W/mK (average value of the range), and $k_{worst} = 0.020$ W/mK (worst value of the range).

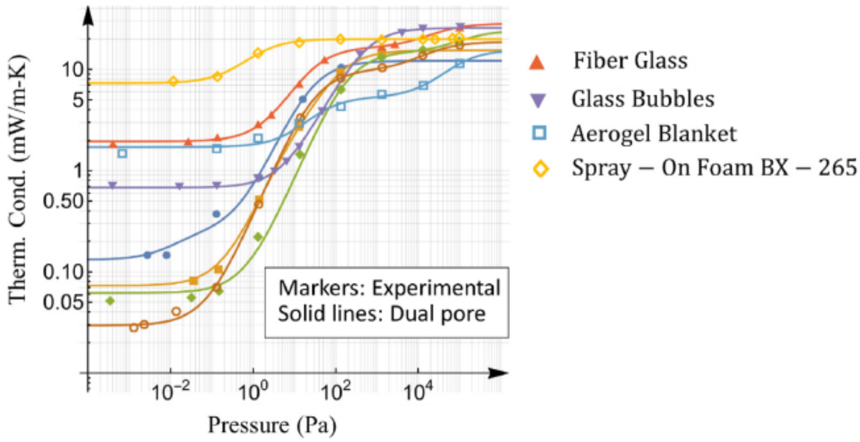

Figure 3.2: Thermal conductivity versus pressure data for various insulation material and fitted results [65]

3.2. Methodology for investigation of single-wall tank architecture

To evaluate the potential of this tank's application in hydrogen-powered aviation, a MATLAB code was developed. The first step of the methodology consists in defining the initial parameters for the single wall tank model and design points that will be investigated. Various versions of each design point are analyzed by varying the insulation thickness value through a range of values from a minimum of 0.005 mm up to 20% of the tank's external diameter. For each thickness, several key factors are calculated, including the thermal resistances of the pipes and supports, the thickness of the aluminum shell, cruise time, heat inflow from the external environment, and dormancy time. The subsequent analysis involves comparing these results to determine if the tank's performance criteria for cruise time and dormancy time could be met. The flow-chart in Figure 3.3 outlines this evaluation process in detail.

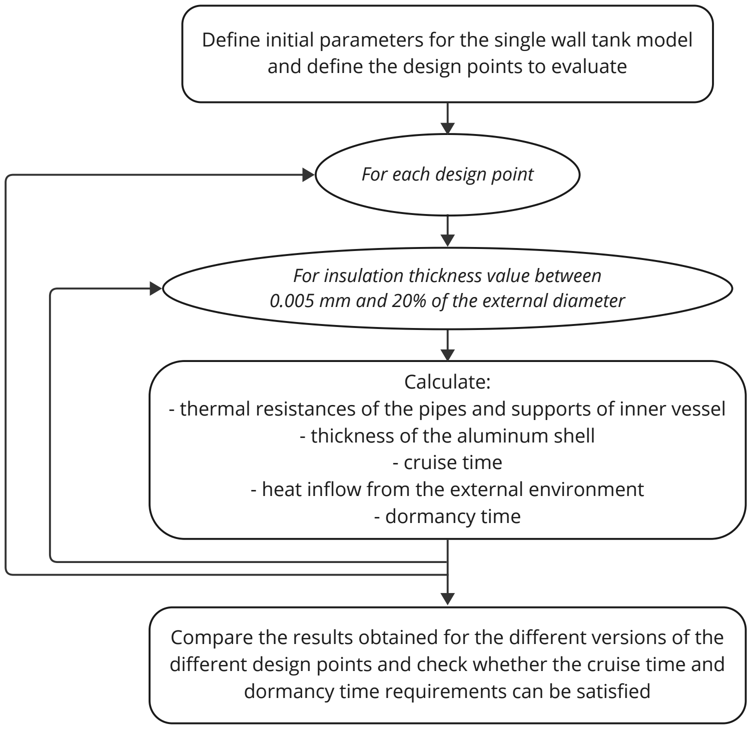

Figure 3.3: Flow chart for evaluation of single-wall tank architecture

Pressure parameters to characterise the tank model

The three pressure parameters relevant to tank modelling are the following:

- P_{vent}: the venting pressure is the pressure that, when reached inside the tank, causes the vent relief valve to open and hydrogen gas to be released. The value depends on the specific vent relief valve employed in the system and is characterised by a relative error that is generally more pronounced for low venting pressure values.
- $P_{burst-disc}$: the burst-disc pressure is the pressure that, when reached inside the tank, causes the burst disc pressure relief mechanism to activate in order to avoid over-pressurization. This value depends on the specific burst disc mechanism employed in the system and usually is expressed as a function of the venting pressure as in Equation 3.5.

$$P_{burst-disc} = SF_1 * P_{vent} \tag{3.5}$$

  where SF_1 is a safety factor that assumes the value of 1.5.
- P_{design}: the design pressure is the ultimate pressure that the tank should be able to withstand before failure. This is the pressure used in order to properly size the tank shell thickness and can be expressed using the Equation 3.6.

$$P_{design} = SF_2 * P_{burst-disc} = SF_2 * SF_1 * P_{vent} \tag{3.6}$$

  where SF_2 is a safety factor that assumes the value of 1.8. The purpose of it is to make sure that, even in the eventuality of burst disc activation, the tank is able to survive with no plastic deformation and can be made operational again simply by replacing the burst disc safety device.

In case of hydrogen fuel cell aircraft, the value of internal pressure at which hydrogen is vented must be coherent with the pressure range accepted as input by the branch leading to the fuel cells. The vent relief valve and the valve regulating the GH_2 flow to the fuel cells are both located along the outlet pipe and, for this reason, selecting a venting pressure lower than the required pressure at the inlet of the valve regulating the flow to the fuel cells would result in a system where the GH_2 flow to the fuel cells tends to zero. Therefore, it is beneficial to select P_{vent} values higher than those required in order to enter the direct branching to fuel cells so to also limit the fuel losses through venting during the flight mission. A literature research concerning the optimum operating conditions for proton-exchange membrane (PEM) fuel has uncovered numerous studies that agree that the optimum values for the operating pressure of hydrogen fuel cells can be found in the range between 1.5 and 2.5 bar [43], [16], [39], [67]. Consequently, it is considered reasonable to assume venting pressures greater than 3 bar. In this particular case study, the accepted range for venting pressures is between 3 and 5 bar. The ranges for $P_{burst-disc}$ and P_{design} are defined according to the equations 3.5 and 3.6 respectively.

Design points

The evaluated design points are retrieved by Yi-Hsiu's thesis work [82]. Additionally, it is also desired to evaluate tanks larger than those indicated for a retrofit in order to get an idea of the potential of this type of tank concept also in the case of new aircraft architectures that could accommodate an integral tank. All the considered design points and the relative characteristics are presented in Table 3.1. One important parameter to consider is the surface area-to-volume ratio, which provides insight into the extent of heat leaks.

Table 3.1: Design points considered in the analysis

External diameter [mm]	External length [mm]	Number of tanks	Surface/Volume
498	2339	15	8.65
498	2570	14	8.59
750	2600	7	5.90
2500	2500	1	2.40
1500	5000	1	2.96
2000	5500	1	2.28
2500	6500	1	1.84
3000	7500	1	1.54

Cruise time

The cruise time represents the maximum time that can be spent in the cruise phase. The value of this parameter depends on the inner dimensions of the vessel, the fill ratio, and the mission profile including the hydrogen mass flow rates and time durations for the different phases of the mission. A standard mission profile is considered and it consists of the following phases: take-off, climb, cruise, descent, and landing. The hydrogen mass flow rates values for a regional aircraft have been retrieved from the work of Onorato, Proesmans and Hoogreef [32], and are presented in Table 3.2.

Since the duration of the other phases can be considered fixed, the maximum cruise duration can be calculated based on the amount of fuel remaining by subtracting the fuel consumed in the other phases from the initial amount of hydrogen in the tank.

In making these calculations, it is necessary to introduce the assumption that there is a heater capable of providing the necessary heat so that the correct amount of liquid hydrogen is able to boil adapting to the hydrogen mass flow rate required for each specific phase of flight.

Table 3.2: Mission profile: mass rates and durations

Phase	Hydrogen mass flow [kg/s]	Phase duration [min]
Take-off	0.113	5
Climb	0.096	15
Cruise	0.051	-
Descent	0.004	15
Landing	0.081	5

Heat Input

The main component of heat input is the heat through the walls of the tank (aluminum layer + insulation layer). Multi-dimensional steady-state conduction for the aluminum layer and insulation layer of the tank has been evaluated and calculated according to equations 3.7 and 3.8.

$$\dot{Q}_{tank-wall} = \frac{T_{ext} - T_{int}}{R_{tank-wall}} \tag{3.7}$$

$$R_{tank-wall} = \frac{1}{k_{ins}S_{ins}} + \frac{1}{k_{al}S_{al}} \tag{3.8}$$

where T_{ext} is the temperature of the environment surrounding the tank, T_{int} is the temperature of the inside of the tank, $R_{tank-wall}$ is the thermal resistance of the walls of the tank, k_{ins} is the thermal conductivity of the insulation material, S_{ins} is the thermal shape factor of the insulation material, k_{al} is the thermal conductivity of aluminum alloy AL5083-O, and S_{al} is the thermal shape factor of the aluminum layer. The thermal shape factor is parameter that represents the effect of the geometry of a conducting body on the rate of heat conduction and is used to simplify complex heat conduction problems.

To achieve a more accurate assessment of the heat input, it is essential to account for the tank supports and piping. The model involves three metal pipes (inlet, outlet, and safety pipe) and two cylindrical composite supports positioned at opposite ends of the tank. A discretized 1D model has been created to evaluate thermal conduction through the piping and supports. The thermal resistance of one pipe and the thermal resistance of one support are calculated based on the geometry and material properties of the structural elements following the equations 3.9 and 3.10 respectively. The heat flow through the pipes and the supports is calculated based on equations 3.11 and 3.12 respectively.

$$R_{pipe} = \frac{L_{bridge,m}}{k_{al}A_{pipe}} \tag{3.9}$$

$$R_{support} = \frac{L_{bridge,c}}{k_{G10-CR}A_{support}} \tag{3.10}$$

$$\dot{Q}_{pipes} = N_{pipes}\frac{T_{ext} - T_{int}}{R_{pipe}} \tag{3.11}$$

$$\dot{Q}_{supports} = N_{supports}\frac{T_{ext} - T_{int}}{R_{support}} \tag{3.12}$$

where $L_{bridge,m}$ is the length of the pipe through the insulation layer, k_{al} is the thermal conductivity of aluminum alloy AL5083-O, A_{pipe} is the cross-sectional area of a pipe, $L_{bridge,c}$ is the length of the support through the insulation layer, k_{G10-CR} is the thermal conductivity of G10-CR glass fiber composite, $A_{support}$ is the cross-sectional area of a support, T_{ext} is the temperature of the environment surrounding the tank, T_{int} is the temperature of the inside of the tank, N_{pipes} is the total number of pipes in one tank, and $N_{supports}$ is the total number of supports in one tank.

Due to the temperature dependence of the thermal conductivity and the large temperature difference between the inside and the outside of the vessel, all the values of thermal conductivity are the average value between thermal conductivity at ambient temperature and thermal conductivity at cryogenic temperature.

The total heat flow into the storage vessel is expressed in Equation 3.13.

$$\dot{Q}_{total} = \dot{Q}_{tank-wall} + \dot{Q}_{pipes} + \dot{Q}_{supports} \tag{3.13}$$

Dormancy time

The dormancy time consists of the elapsed time after which the gas pressure inside the tank of a parked non-operating vehicle reaches the set point of the relief valve and some H_2 must be vented at a controlled rate. It is calculated as the time it takes to reach an internal tank pressure equal to the venting pressure and, hence, it is a function of the maximum allowable pressure and the pressure of stored H_2. The implemented model is based on the thermodynamic model for dynamic behavior of H_2 in insulated pressure vessels during dormancy presented in reference [5].

The main assumptions introduced by the thermodynamic model are the following:

- The kinetic and potential energy of H_2 entering and exiting the tank are disregarded.
- Uniform temperature and pressure conditions are assumed within the tank.
- The H_2 in the tank may be in the form of liquid, gas, or a combination of both. If H_2 is present as a mixture, then it is assumed that the gas and liquid phases are in equilibrium.
- There is a heater capable of providing the necessary heat so that the correct amount of liquid hydrogen is able to boil adapting to the hydrogen mass flow rate required for each specific phase of flight.

- H_2 is preferentially extracted from the top of the tank as a gas.
- The equilibrium between the para and ortho phases of hydrogen is ignored due to the slow conversion kinetics.

The equations used to determine the thermodynamic state of H_2 stored in the tank during the dormancy time period are retrieved from reference [5] and expressed in the matrix form as presented in Equations from 3.14 to 3.17.

$$\begin{bmatrix} 1 & -\frac{dP_s}{dT} & 0 & 0 \\ A_{21} & A_{22} & \frac{1}{\rho_g} - \frac{1}{\rho_l} & 0 \\ 0 & 0 & 1 & 1 \\ 0 & A_{42} & -(h_l - h_g) & 0 \end{bmatrix} \begin{bmatrix} \frac{dP}{dt} \\ \frac{dT}{dt} \\ \frac{dm_g}{dt} \\ \frac{dm_l}{dt} \end{bmatrix} = \begin{bmatrix} 0 \\ 0 \\ 0 \\ \dot{Q}_{\text{total}} \end{bmatrix} \tag{3.14}$$

where:

$$A_{21} = -\left[\frac{m_g}{\rho_g^2}\left(\frac{\partial \rho_g}{\partial P}\right)_T + \frac{m_l}{\rho_l^2}\left(\frac{\partial \rho_l}{\partial P}\right)_T\right] \tag{3.15}$$

$$A_{22} = -\left[\frac{m_g}{\rho_g^2}\left(\frac{\partial \rho_g}{\partial T}\right)_P + \frac{m_l}{\rho_l^2}\left(\frac{\partial \rho_l}{\partial T}\right)_P\right] \tag{3.16}$$

$$A_{42} = m_s C_s + m_l\left(\frac{\partial h_l}{\partial T}\right)_P + m_g\left(\frac{\partial h_g}{\partial T}\right)_P + \left[m_l\left(\frac{\partial h_l}{\partial P}\right)_T + m_g\left(\frac{\partial h_g}{\partial P}\right)_T\right]\frac{dP_s}{dT} \tag{3.17}$$

In the Equations from 3.14 to 3.17, T is the temperature, P is the pressure, P_s is the saturation pressure, ρ_l is the density of the liquid hydrogen, ρ_g is the density of the gaseous hydrogen, m_l is the mass of the liquid hydrogen, m_g is the mass of the gaseous hydrogen, h_l is the enthalpy of the liquid hydrogen, h_g is the enthalpy of the gaseous hydrogen, m_s is the mass of the tank structure, C_s is the specific heat of the tank structure, $\dot{Q_{total}}$ is the total heat transfer rate leaking from the outside to the inside of the tank, and V is the internal volume of the tank.

Starting from the thermodynamic conditions defined for the initial time instant and having as input the heat flow from the external environment, the thermodynamic variables describing the state of the hydrogen inside the tank are calculated for each subsequent time instant. The iterative cycle stops when the venting pressure is reached. The elapsed time to reach an internal pressure equal to the venting pressure is the dormancy time.

In general, the complexity lies in determining the optimal insulation thickness for each design point and assessing whether it allows the tank to meet the requirements of the specific case study. It is a trade off between cruise time and dormancy time. Increasing the thickness of the insulation layer while keeping the outer dimensions of the tank fixed, leads to a decrease in the internal volume of the tank and thus a decrease in the amount of hydrogen that can be transported. Consequently, less fuel will be available for the cruise phase. At the same time, an increase in the thickness of the insulation layer implies a decrease in heat input and thus an increase in dormancy time.

3.3. Results and discussion

Consistently with what is described in the flow chart in Figure 3.3, every design point from Table 3.1 has been evaluated from the point of view of cruise time and dormancy time. The feasibility region is defined by a cruise time of more than 20 minutes (1200 seconds) and a dormancy time of more than 1 day (86400 seconds).

For every design point different versions have been created by varying the insulation thickness value in a range bounded by a minimum value of 0.005 mm and a maximum value equal to 20$\%$ of the respective outer diameter of the tank. This range has been defined so as to prevent excessively fine insulation layers that are impossible to manufacture in reality, as well as excessively thick insulation layers that end up occupying most of the tank's internal volume, thus substantially reducing the volume dedicated to liquid hydrogen storage.

The results presented in Figure 3.4 refer to the feasibility study conducted for a tank model which is characterised by $k_{insulation-material}$ = $k_{nominal}$ = 0.015 W/mK, P_{vent} = 4 bar, $P_{burst-disc}$ = 1.5 * P_{vent} = 6 bar, and P_{design} = 1.8 * $P_{burst-disc}$ = 10.8 bar. In order to show more clearly what the dependence of cruise time and dormancy time actually is on insulation thickness, these have been depicted individually in figures 3.5 and 3.6 respectively. Particularly relevant is also the relation between the heat inflow through the tank wall and the insulation thickness which is presented in Figure 3.7.

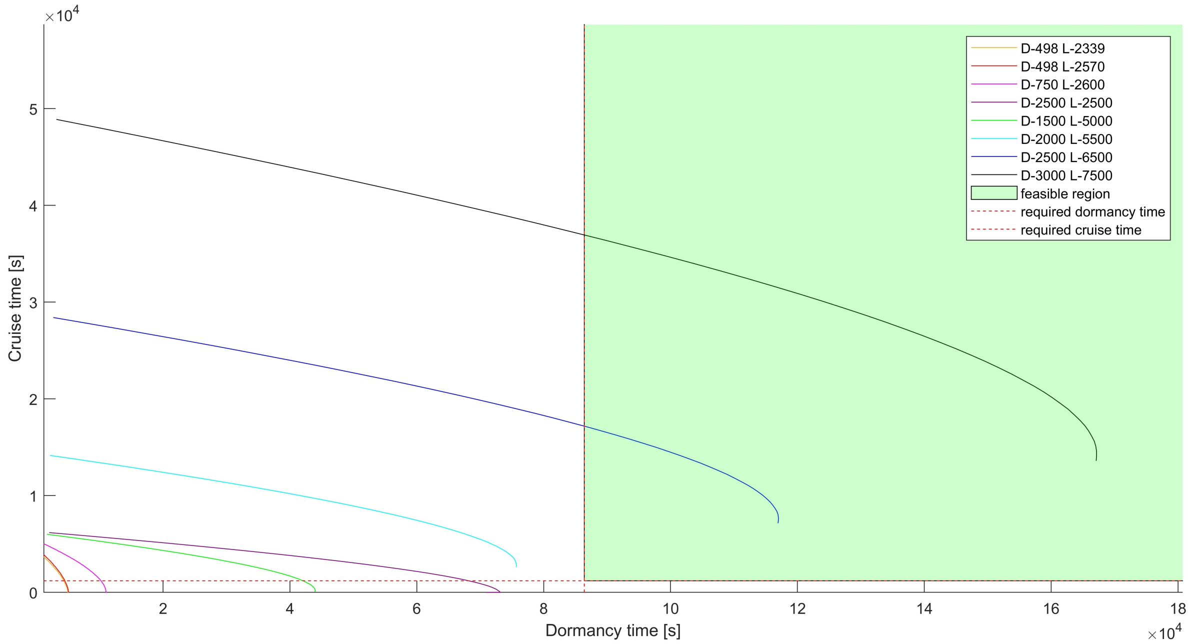

Figure 3.4: Evaluation of various insulation thickness values for different design points

From Figure 3.4 it is possible to ascertain that the minimum cruise time requirement can be met for all design points, at least for some values of insulation thickness. However, the minimum dormancy time requirement is only met for two design points (D-2500 L-6500 and D-3000 L-7500), both of which have large dimensions beyond the size requirements for the aircraft retrofit case study.

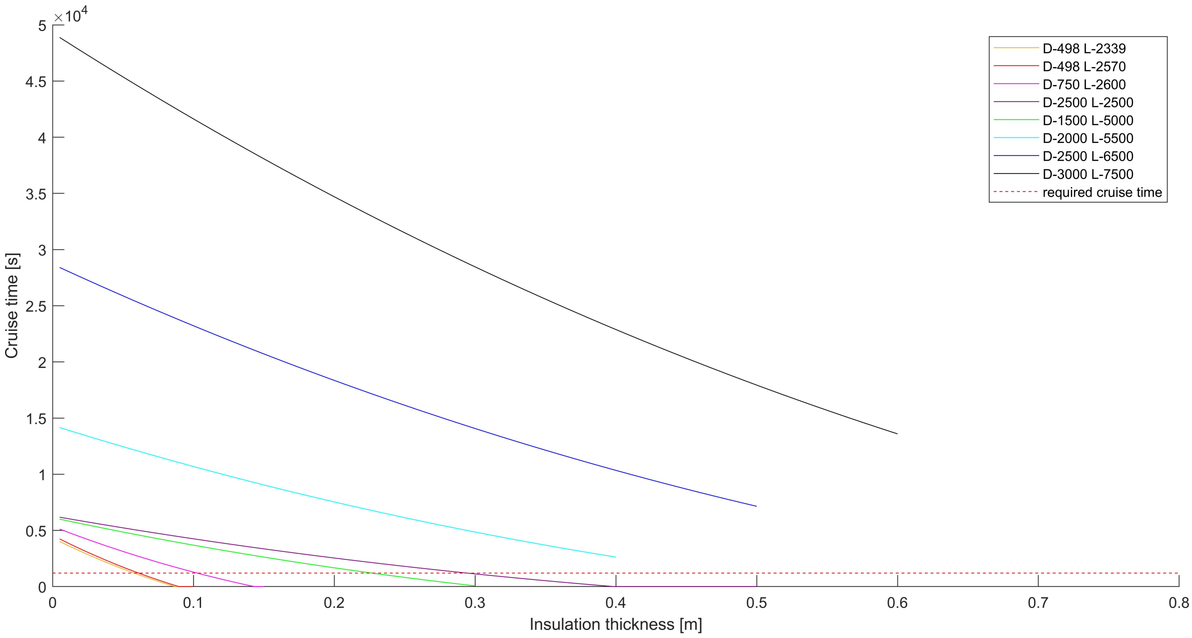

Figure 3.5: Evaluation of cruise time for various insulation thickness values and different design points

Figure 3.5 makes it clear that cruise time decreases as insulation thickness increases in an almost linear way. This is because a thicker layer of insulation material reduces the internal tank volume, which limits the amount of hydrogen that can be stored inside. As a result, less hydrogen is available during the cruise phase.

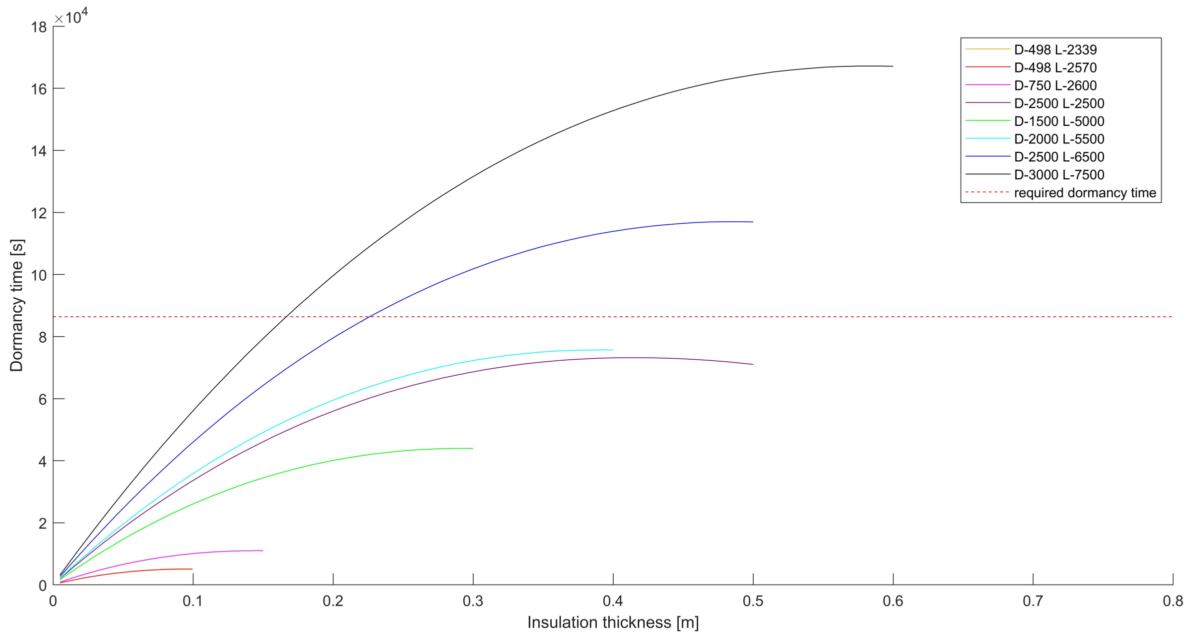

Figure 3.6: Evaluation of dormancy time for various insulation thickness values and different design points

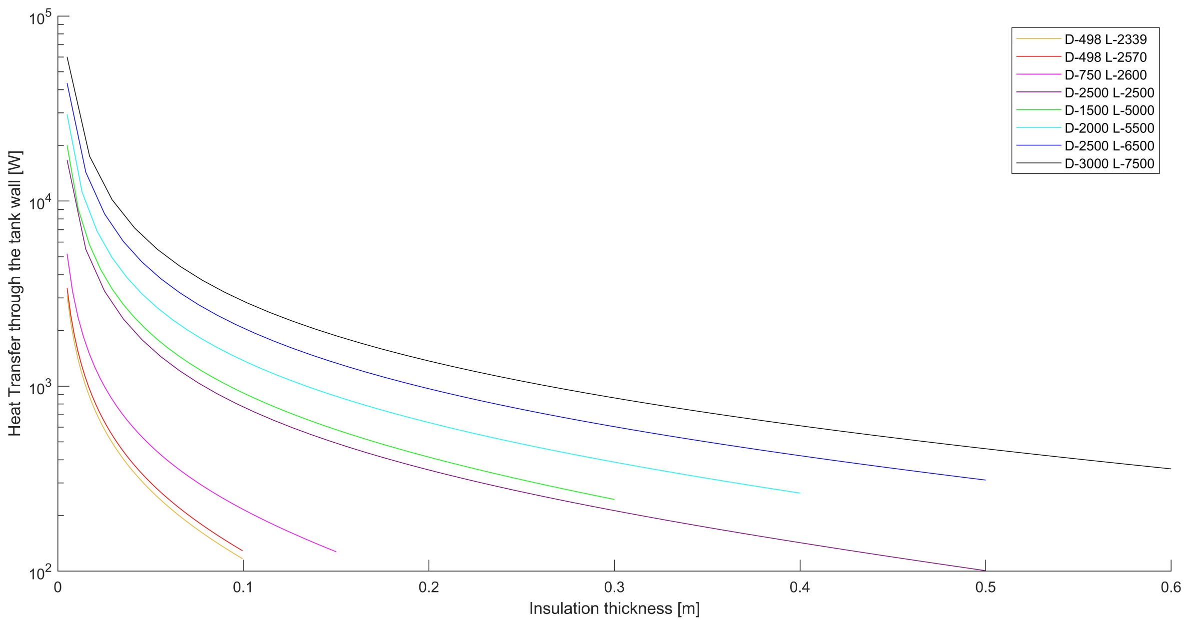

Figure 3.7: Evaluation of heat transfer through the tank walls for various insulation thickness values and different design points

On the other hand, dormancy time generally increases with increasing insulation thickness (Figure 3.6). This is because the heat flow input from the external environment decreases as insulation thickness increases (Figure 3.7). However, beyond a certain insulation thickness, the effect on the heat inflow and thus dormancy time is attenuated. This is evident from the nearly asymptotic trend in Figures 3.6 and 3.7. The explanation for this behaviour is that, initially, increasing the thickness of the insulation layer improves dormancy time by enhancing thermal resistance and reducing heat inflow. However, this positive effect is considerably mitigated once an optimal insulation thickness is surpassed. In fact, while thicker insulation improves thermal performance, it also reduces the tank's internal volume. A smaller internal volume means less hydrogen can be stored, which negatively affects dormancy time because it means that the same amount of heat from outside will act on a smaller amount of hydrogen. This suggests that beyond a certain insulation thickness, pushing further becomes non-beneficial as dormancy time won't be significantly increased, but cruise time will be affected in an almost linear manner.

3.3.1. Sensitivity analysis

The values of certain parameters characterising the single wall tank model are defined with a certain degree of arbitrariness and may therefore assume any value within a well-defined range depending on the choices made by the designer. It is therefore worth performing a sensitivity analysis in order to evaluate what impact varying these parameters has on the tank's overall performance.

Thermal conductivity of the insulation material

In the section 3.1, three different possible values for the thermal conductivity of the insulation material has been defined: $k_{best} = 0.010$ W/mK (best value of the range), $k_{nominal} = 0.015$ W/mK (average value of the range), and $k_{worst} = 0.020$ W/mK (worst value of the range). Since the results that have been previously presented refers to $k_{nominal}$, it is important to assess the impact of assuming a different thermal conductivity value for the insulation material on the thermal performance of the tank model.

The feasibility study has been performed again considering three different versions of each design point depending on the value assumed by the thermal conductivity parameter of the insulation material. The results are presented in Figure 3.8.

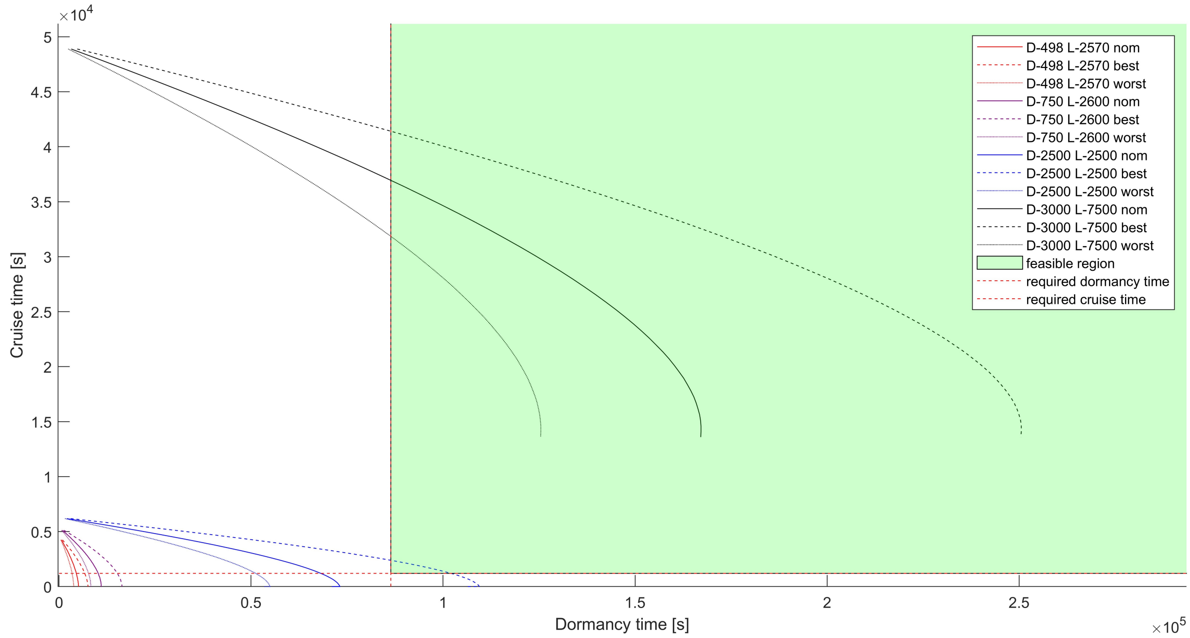

Figure 3.8: Evaluation of various insulation thickness values for different design points varying the thermal conductivity value

It can be deduced from Figure 3.8 that using an insulation material characterised by lower thermal conductivity leads to a direct increase in dormancy times. This is true if all other factors, such as insulation thickness, remain equal. Additionally, by using an insulation material with lower thermal conductivity, it is possible achieve a longer cruise time at the same dormancy time. This is because the heat flow through the insulation material is directly proportional to the thermal conductivity of the material used.

While it is always preferable to use a more performant insulation material, there are other important factors to consider. These include cost, Technology Readiness Level (TRL), and other structural characteristics of the material. These factors play a crucial role in determining the feasibility and effectiveness of the insulation system and, therefore, it is important to carefully weigh thermal performance considerations alongside these additional factors when making design decisions.

Nevertheless, even if the thermal conductivity value of the insulating material is varied, the dormancy time requirement is only achieved by tanks that are considerably larger than those specified for the retrofit case study.

Venting pressure

Previously in this section, the three pressure parameters that characterised the tank model has been defined as P_{vent}, $P_{burst-disc}$, and P_{design}. Furthermore, $P_{burst-disc}$ and P_{design} can be expressed as function of P_{vent} using the equations 3.5 and 3.6 respectively. In conclusion, varying P_{vent} will have a direct impact on the two other pressure values, which will consequently have an impact on the sizing of the pipes and tank walls.

Three different possible values of P_{vent} has been defined: $P_{vent,high}$ = 5 bar (implying $P_{burst-disc,high}$ = 7.5 bar and $P_{design,high}$ = 13.5 bar), $P_{vent,nom}$ = 4 bar (implying $P_{burst-disc,nom}$ = 6 bar and $P_{design,nom}$ = 10.8 bar), $P_{vent,low}$ = 3 bar (implying $P_{burst-disc,low}$ = 4.5 bar and $P_{design,low}$ = 8.1 bar). The results are presented in Figure 3.9.

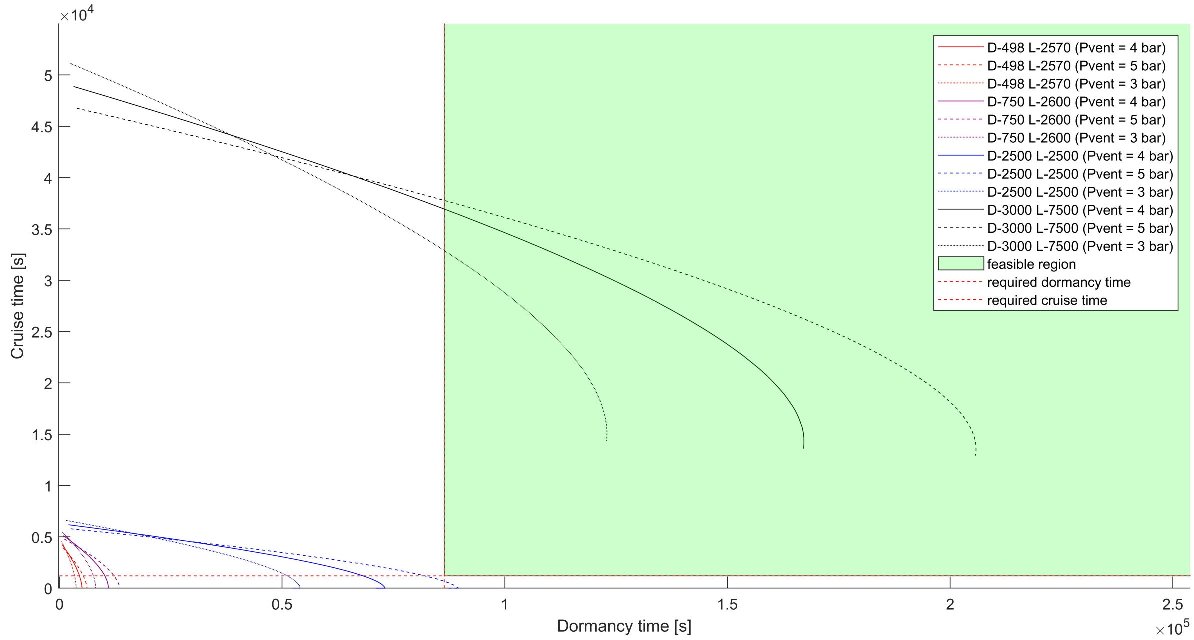

Figure 3.9: Evaluation of various insulation thickness values for different design points varying the P_{vent} value

The variation of P_{vent}, and thus $P_{burst-disc}$ and P_{design}, can significantly impact the overall performance of a tank. An increase in venting pressure means that a greater pressure difference needs to be overcome to reach the point when the vent relief valve opens to release hydrogen gas. This results in a longer time needed to reach the venting pressure, also known as dormancy time.

However, a higher venting pressure also leads to an increase in burst disc pressure and design pressure, which affects the sizing of pipes and the shell. Thicker pipes lead to a higher heat inflow through them, and thicker shells result in a reduction of the tank's internal volume affecting the cruise time. Moreover, both factors contribute to an increase in the total weight of the tank, which is generally not desirable.

This complex combination of effects is clearly visible in Figure 3.9 for the D-3000 L-7500 design point. For low insulation thicknesses (on the left-hand side of the curves), the insulation is not effective enough to prolong dormancy times, regardless of the venting pressure applied. The design pressure affects the shell thickness and internal volume of the tank, leading to a clear impact on the cruise time. A higher venting pressure (and design pressure) results, in fact, in a shorter cruise time. However, if the insulation thickness is increased enough to achieve a considerable thermal effectiveness of the insulation system, the impact of increasing the venting pressure becomes more evident. For the same dormancy time, the tank with higher venting pressure will have a higher cruise time.

Therefore, evaluating the optimal design choice for a tank becomes complex and depends on the specific application and desired outcome, particularly in the case study. Nevertheless, even if the venting pressure value is varied, the dormancy time requirement is only achieved by tanks that are considerably larger than those specified for the retrofit case study.

3.3.2. Final considerations

The analysis of the single-wall tank architecture reveals significant challenges that render this design unfeasible for the case study. In fact, even when varying the parameters characterising the architecture within the respective permissible ranges, the result is that the dormancy time requirement is not met for the three design points of the retrofit case study. The primary limitations arise from the inability to adequately manage thermal loads and maintain the necessary insulation to ensure compliance with the dormancy time requirement. The high heat leakage through the tank walls significantly reduce the dormancy time, preventing the tank from meeting operational requirements.

As a result, alternative approaches for viable design solutions are needed.

4 Double wall tank

As stated in the literature review (chapter 2), double-wall architecture with vacuum-based insulation could offer a better thermal performance than single-wall architecture with material-based insulation. These tanks, known as Dewar type tanks, consist of two structural walls with minimal physical contact and feature a vacuum layer in between. The vacuum jacket is evacuated to reduce convective heat transfer and residual gas conduction between the liquid hydrogen and the external environment. Additionally, reflective membranes like multi-layer insulation (MLI) are incorporated to further reduce the radiation heat flux and consequently boil-off rates. However, the double-wall architecture requires a support system for the inner vessel in order to maintain its proper positioning, adding complexity to the design of the structure. In general, therefore, the disadvantages are related to the higher cost and complexity associated with this type of architecture.

As has been done in the chapter 3 for the single wall tank, it is important to check whether a double-wall architecture would be able to meet the requirements regarding both time of flight (cruise time of at least 20 minutes) and dormancy time (dormancy time of at least 24 hours). If this type of architecture proves to be suitable to meet the requirements, then the structural evaluation of the tank will be performed with particular attention to the design of the inner tank supports.

4.1. Double wall tank model

The subject of this section is a cylindrical double-wall LH_2 vessel with hemispherical ends. The proposed design entails outer and inner aluminum vessels, an insulation system consisting of HV-MLI (high vacuum multi-layered insulation), two composite structural supports, and three aluminum pipes. As far as pipes and vessel structural supports are concerned, the choices and considerations valid for this model are the same as for the single-wall model presented in section 3.1. The double-wall tank model is presented schematically in Figure 4.1.

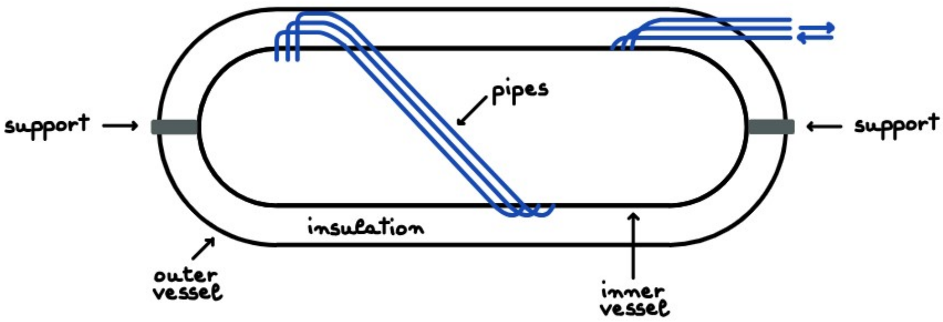

Figure 4.1: Double wall tank model

Shells

The design choices concerning shape and material of inner and outer vessels are the same as those made for the single wall tank model presented in section 3.1. The selected shape is in fact a cylinder with hemispherical ends and the material is the aluminum alloy AL5083-O.

For the double-wall architecture, the sizing process is different for inner and outer vessels: the inner vessel is subject to internal pressure while the outer vessel is subject to external pressure. For both cases, the guidelines followed are derived from the ASME standards [13]. For the inner vessel, the reference is the general requirement UG-27 (”thickness of shells under internal pressure”) while, for the outer vessel, the reference is the general requirement UG-28 (”thickness of shells and tubes under external pressure”).

Insulation

The insulation system selected for the double-wall tank model is high-vacuum insulation coupled with multi-layer insulation (HV-ML), given its wide use for storage of cryogenic liquids. As previously presented in subsection 2.4.1, the vacuum jacket is installed between the outer vessel (warm boundary) and the inner vessel (cold boundary), and the high vacuum (HV) function reduces the residual gas conduction and convective heat transfer between the external environment and cryogenic liquids. Multi-layer insulation (MLI) is also introduced in order to further improve the thermal performance of the insulation system, reducing heat transfer by radiation, while keeping heat conduction through the spacer material and the residual gas low. The performance of HV-MLI systems is influenced by several critical parameters, each contributing to the overall effectiveness of the insulation (reference to subsection 2.4.1):

- *Vacuum pressure*: in order to maintain the apparent thermal conductivity of the insulation system below 10^{-4} W/mK, the vacuum pressure should remains below 10^{-1} Pa. As the vacuum pressure exceeds 10^{-1} Pa, there is a considerable rise in the apparent thermal conductivity that would compromise the performance of the insulation system.
- *Layer density*: while increasing the number of shields can reduce radiative heat transfer, a higher packing density can enhance solid conduction through improved contact between radiation shields and spacers. This presents a trade-off, emphasizing the need to find an optimal layer density for each specific application.
- *Emissivity of the radiation shields*: for the double wall tank model, double aluminized Mylar with an emissivity value of 0.04 is assumed.
- *Thermal conductivity of the spacer material*: for the double wall tank model, the material is assumed to be Dacron net which is a polyester fiber made by DuPont. The thermal conductivity of this material is expressed as a function of temperature (later presented in Equation 4.11).
- *Type of residual gas*: the preferable residual gas choice consists of a residual gas characterised by low EAC and low apparent thermal conductivity across varied vacuum conditions. This would allow the insulation system to maintain low apparent thermal conductivity throughout the transition from molecular to continuum regimes.

4.2. Methodology for investigation of double-wall tank architecture

To evaluate the potential of this tank's application in hydrogen-powered aviation, a MATLAB code was developed. Similarly to the algorithm developed for single-wall tank architecture (section 3.2), after initialising the parameters that characterize the double-wall tank model, the code considers the various design points selected in order to evaluate both cruise time and dormancy time. For every version of each design point, it is then necessary to calculate the the thickness of the inner and outer aluminium shells, thermal resistances of the pipes and supports of the inner vessel, the cruise time, the heat inflow through the tank walls (aluminium shells + vacuum layer) and the dormancy time. Once these are calculated, it is possible to assess whether and which design points are able to meet the requirements.

In the calculations to be performed for the double wall tank model, there are several similarities with what has been done for the single wall tank model. The pressure parameters characterising the tank model are defined in exactly the same way and the calculation of cruise time and dormancy time follow the same steps and equations. The design points evaluated are exclusively those from Yi-Hsiu's thesis work [82] as this type of model is expected to meet the requirements for the considered case study. These are shown in the table 4.1.

Table 4.1: Design points considered in the analysis

External diameter [mm]	External length [mm]	Number of tanks	Surface/Volume
498	2339	15	8.65
498	2570	14	8.59
750	2600	7	5.90

For each of the design points, the following versions are evaluated:

- varying vacuum pressure P_{vacuum} between 10^{-5} and 1 Pa
- varying the number of MLI layers N_{MLI} between 10 and 50
- varying the thickness of HV-MLI insulation layer t_{vacuum} between a minimum value depending on the diameter of the pipes and a maximum value equal to 20% of the external diameter of the tank
- varying the type of residual gas (gases presented in Figure 2.5)

Heat Input

The total heat flow into the storage vessel is expressed in Equation 4.1.

$$\dot{Q}_{total} = \dot{Q}_{tank-wall} + \dot{Q}_{pipes} + \dot{Q}_{supports} \tag{4.1}$$

where $\dot{Q}_{tank-wall}$ is the heat flow through the tank wall (inner and outer shells + HV-MLI layer), $\dot{Q}_{pipes}$ is the heat flow through the three pipes, and $\dot{Q}_{supports}$ is the heat through the inner vessel supports. Regarding the calculation of $\dot{Q}_{pipes}$ and $\dot{Q}_{supports}$, the methodology is the same as what has been described in section 3.2. The heat flow through the tank wall $\dot{Q}_{tank-wall}$ is calculated according to equations 4.2 and 4.3.

$$\dot{Q}_{tank-wall} = \frac{T_{ext} - T_{int}}{R_{tank-wall}} \tag{4.2}$$

$$R_{tank-wall} = \frac{1}{k_{al,inner} S_{al,inner}} + R_{HV-MLI} + \frac{1}{k_{al,outer} S_{al,outer}} \tag{4.3}$$

where T_{ext} is the temperature of the environment surrounding the tank, T_{int} is the temperature of the inside of the tank, $R_{tank-wall}$ is the thermal resistance of the walls of the tank, $k_{al,inner}$ and $k_{al,outer}$ are the thermal conductivity values of aluminum alloy AL5083-O for the inner shell and outer shell respectively, $S_{al,inner}$ and $S_{al,outer}$ are the thermal shape factors of the inner shell and outer shell respectively, and R_{HV-MLI} is thermal resistance of the HV-MLI insulation layer.

In order to quantify the heat flow through the insulation layer, a heat transfer model has been implemented based on the one presented in reference [85]. The following assumptions are introduced to simplify the problem as a one-dimensional conduction:

- The spacer placed between two consecutive layers of low-emissivity metal foil does not have an impact on the radiation heat leakage.
- The spacer placed between two consecutive layers of low-emissivity metal foil is a finite space.
- The longitudinal conduction through MLI is not taken into account, and conduction is assumed to be solely radial.

In order to obtain the thermal resistance of the entire HV-MLI insulation system, the contribution of each individual layer bounded by two adjacent surfaces must be calculated. The HV-MLI insulation system model considered is presented in Figure 4.2.

The boundary surfaces of a certain layer can be either one of the low-emissivity metal foils or the inner surface of the outer vessel (first layer) or the outer surface of the inner vessel (last layer). The main contributions to the thermal resistance of each individual layer of the insulation system come from radiation between the reflection shields, residual gas conduction, and solid conduction through the spacers. So, to summarise the calculation steps, the equivalent thermal resistance of each individual layer is calculated by considering the three thermal resistances of the three heat transfer modes as resistances in parallel, and then the total thermal resistance is subsequently calculated by considering all the equivalent thermal resistances of the various layers of the insulation system in series.

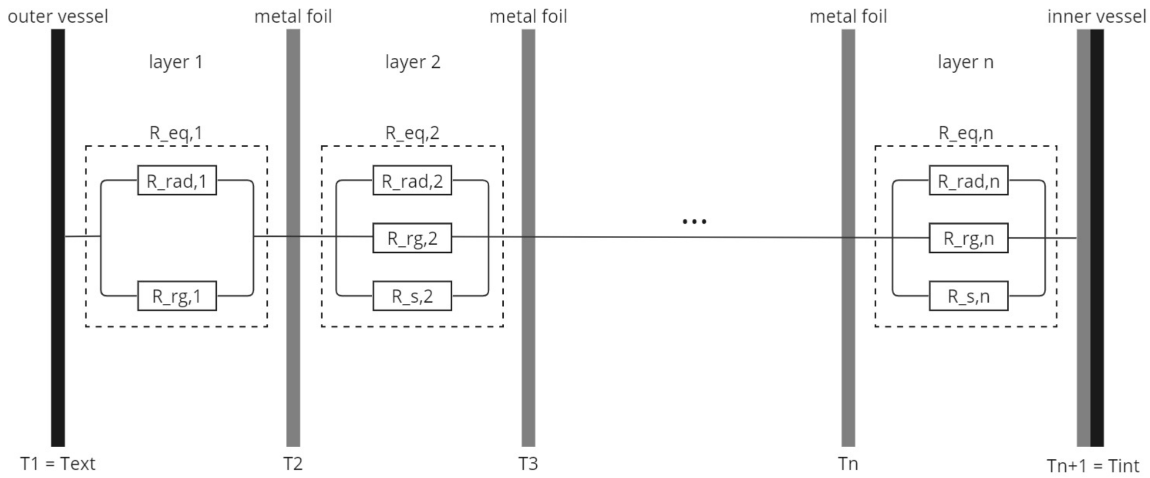

Figure 4.2: Schematic of MLI interlayer thermal resistance

The thermal resistance of the i-th layer can be expressed by Equations 4.4, 4.5, 4.6, and 4.7.

$$R_{eq,i} = (\frac{1}{R_{rad,i}} + \frac{1}{R_{rg,i}} + \frac{1}{R_{s,i}})^{-1} \tag{4.4}$$

$$R_{rad,i} = \frac{1}{AK_{rad,i}} \tag{4.5}$$

$$R_{rg,i} = \frac{1}{AK_{rg,i}} \tag{4.6}$$

$$R_{s,i} = \frac{1}{AK_{s,i}} \tag{4.7}$$

where $R_{rad,i}$ is the thermal resistance of radiation heat transfer between two adjacent reflection shields, $R_{rg,i}$ is the thermal resistance of residual gas, $R_{s,i}$ is the thermal resistance of solid conduction through the spacer, A is the area of boundary surface, $K_{rad,i}$ is the radiation heat transfer coefficient, $K_{rg,i}$ is the residual gas heat transfer coefficient, and $K_{s,i}$ is the solid heat transfer coefficient.

The radiation heat transfer between two adjacent reflection shields can be modeled using the formulas for radiation heat transfer in two-surface enclosures. This represents the case where the net rate of radiation heat transfer from surface 1 to surface 2 equals the net rate of radiation heat transfer from surface 1 and the net rate of radiation heat transfer to surface 2 [24]. The radiation heat transfer coefficient $K_{rad,i}$ can then be expressed by Equation 4.8.

$$K_{rad,i} = \frac{\sigma(T_{i+1}^2 + T_i^2)(T_{i+1} + T_i)}{\frac{1}{\varepsilon_i} + \frac{A_{i+1}}{A_i}(\frac{1}{\varepsilon_{i+1}} - 1)} \tag{4.8}$$

where σ is the Stefan-Boltzmann coefficient $\sigma = 5.67 * 10^{-8} W/m^2K^4$, T_{i+1} and T_i are the temperatures of the outer boundary and the inner boundary of the i-th layer respectively, ε_{i+1} and ε_i are the emissivity of the outer boundary surface and the inner boundary surface of the i-th layer respectively ($\varepsilon = 0.04$ for double aluminized Mylar [40]), A_{i+1} and A_i are the area of the outer boundary surface and the inner boundary surface of the i-th layer respectively.

The conduction in residual gas is modeled using Kennard's law. This law describes the heat transfer between two surfaces in a gas with Knudsen characteristics, where the gas molecules' mean free path is larger than the gap between the two surfaces. This implies that the gas molecules mostly interact with the surfaces rather than with each other. Kennard's law is derived by analyzing how the speed distribution, density, and temperature of the gas molecules affect this process of heat transfer [80]. The residual gas heat transfer coefficient $K_{rg,i}$ can be expressed by Equation 4.9.

$$K_{rg,i} = P_{vacuum}\alpha\sqrt{\frac{R}{8\pi MT_{g,i}}\frac{\gamma+1}{\gamma-1}} \tag{4.9}$$

where P_{vacuum} is the residual gas pressure, α is the accommodation coefficient ($\alpha = 0.3678$ for Argon [72]), R is the universal gas constant $R = 8.314 J/molK$, M is the molecular weight of the residual gas ($M = 39.948 g/mol$ for Argon), $T_{g,i}$ is the temperature of the gas in the i-th layer $T_{g,i} = (T_{i+1} - T_i)/2$, $\gamma = c_p/c_v$ where c_p and c_v are the isobaric specific heat and isochoric specific heat, respectively ($\gamma = 1.667$ for Argon).

The solid heat transfer coefficient $K_{s,i}$ can be expressed by equations 4.10 and 4.11 [55].

$$K_{s,i} = \frac{2\pi C_2 f \lambda}{\Delta x} \tag{4.10}$$

$$\lambda = 0.017 + 7 \cdot 10^{-6}(800 - T_{avg,i}) + 0.0228 log(T_{avg,i}) \tag{4.11}$$

where C_2 is an empirical constant ($C_2 = 0.008$ for Dacron net [86]), f is the relative density of the spacer to the solid material ($f = 0.03$ for Dacron net [86]), Δx is the actual thickness of the spacer between adjacent radiation shields, and λ is the thermal conductivity of the spacer material which, for Dacron net material, is expressed as a function of the average temperature of the layer $T_{avg,i} = (T_{i+1} - T_i)/2$. The thermal resistance of the entire HV-MLI insulation system can be calculated using Equation 4.12.

$$R_{HV-MLI} = \sum_{i=1}^{n} R_{eq,i} \tag{4.12}$$

4.3. Results and discussion

Consistently with what is described in the methodology (section 4.2), every design point from table 4.1 has been evaluated from the point of view of time cruise and dormancy time. The feasibility region is defined by a cruise time of more than 20 minutes (1200 seconds) and a dormancy time of more than 1 day (86400 seconds). For every design point different versions have been created by varying thickness of HV-MLI insulation layer t_{vacuum}, vacuum pressure P_{vacuum}, number of MLI layers N_{MLI}, and type of residual gas.

In this phase of analysis, the support structure of the inner vessel is simplified to two cylindrical composite supports extending longitudinally through the insulation layer. This is justified by the fact that the main objective is to provide a realistic approximation of the heat leakage through the support structure. However, it is important to define the actual budget for the heat leakage through the support structure, i.e. the maximum allowable heat inflow through the supports that still allows to meet the dormancy time requirement.

4.3.1. Varying the thickness of HV-MLI insulation layer t_{vacuum}

The thickness of HV-MLI insulation layer t_{vacuum} is defined in a range between minimum value depending on the diameter of the pipes and a maximum value equal to 20% of the external diameter of the tank. This range has been defined so as to prevent excessively thin insulation layers that do not allow enough distance between the walls of the shells and the pipes (the aim is to avoid contact between the walls of inner and outer vessels and the pipes, which are located in the insulation layer), as well as excessively thick insulation layers that end up occupying most of the tank's internal volume, thus substantially reducing the volume dedicated to liquid hydrogen storage.

For tank sizes considered as design points, the pipe sizing process leads to diameter values of approximately 0.020 m. Based on this, the minimum insulation layer value is set at 0.025 m.

Varying the thickness of HV-MLI insulation layer has an impact on both cruise time (variation of the internal tank volume) and dormancy time (variation of layer density, implying variation of heat transfer through the insulation layer). The general results are presented in the Figure 4.3 and, in order to show more clearly what the dependence of cruise time and dormancy time actually is on insulation thickness, these have been depicted individually in Figures 4.5 and 4.4 respectively. The following parameters take on their respective values at this stage: P_{vent} = 4 bar, P_{vacuum} = 10^{-3} Pa, N_{MLI} = 30, Argon as residual gas.

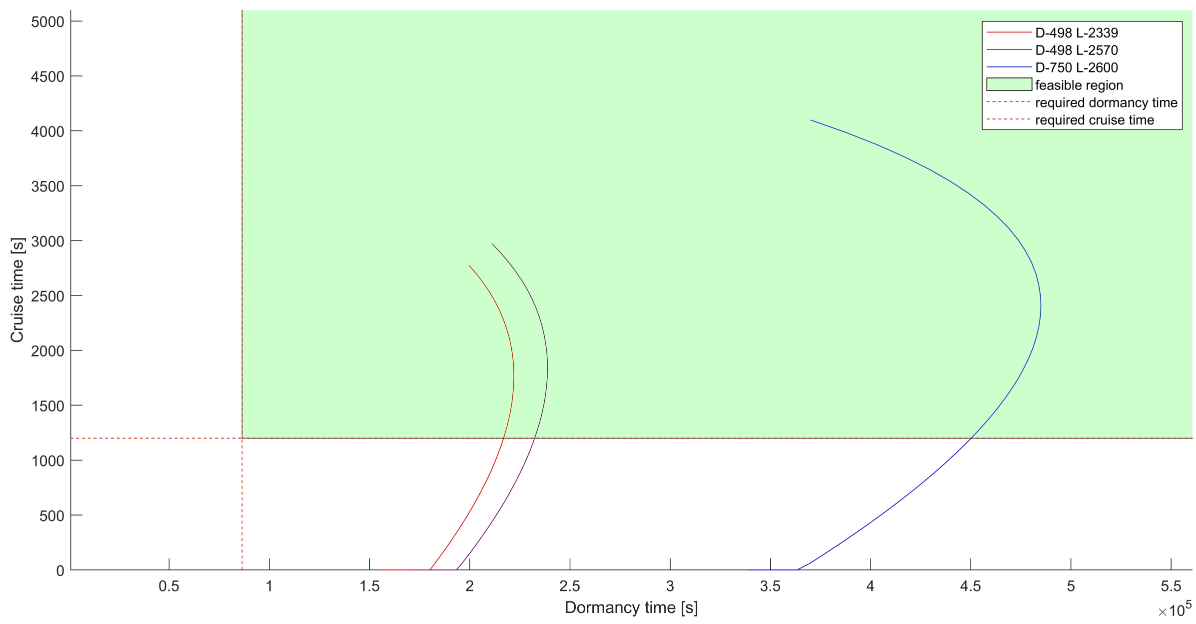

Figure 4.3: Evaluation of various HV-MLI insulation thickness values for different design points

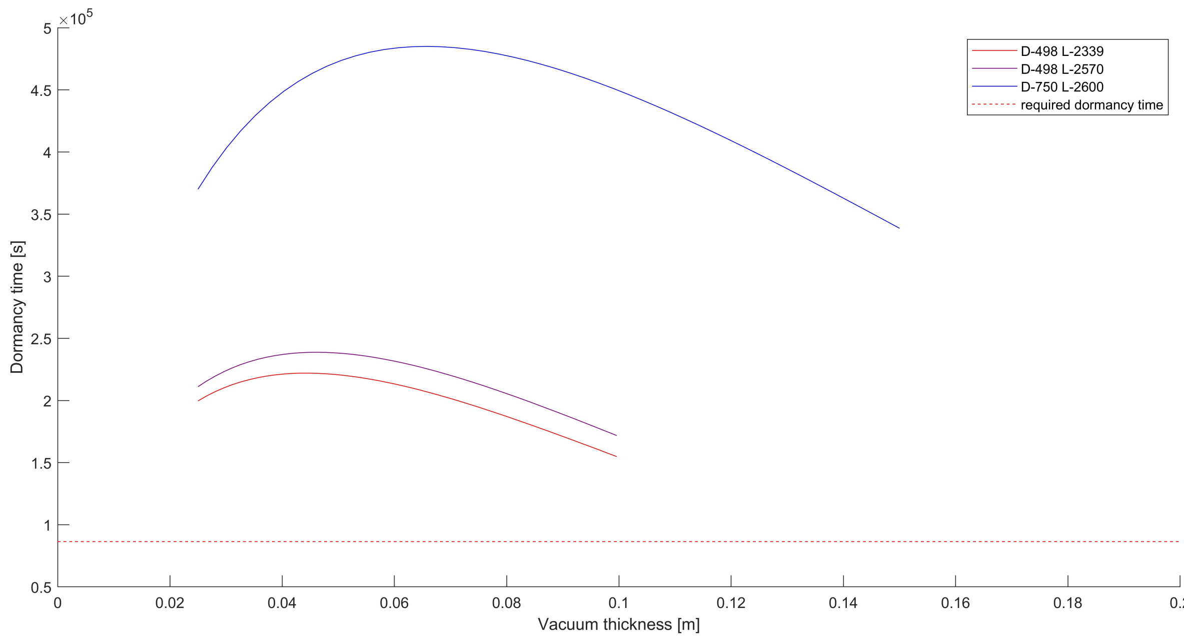

Figure 4.4: Evaluation of dormancy time for various HV-MLI insulation thickness values and different design points

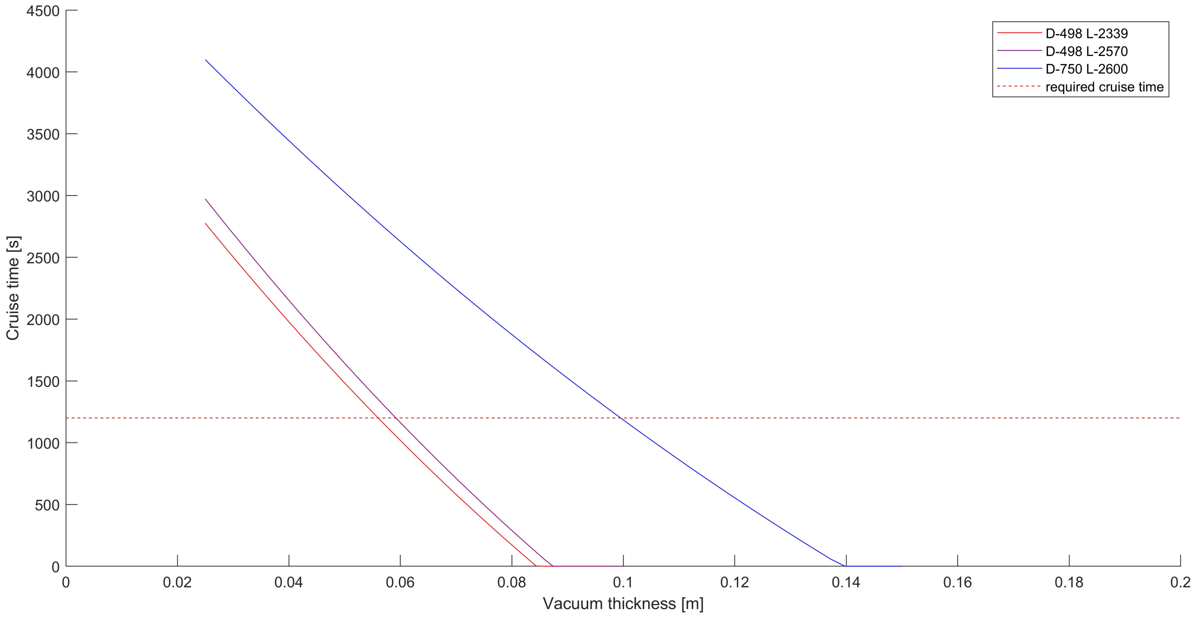

Figure 4.5: Evaluation of cruise time for various HV-MLI insulation thickness values and different design points

The dependence of cruise time on vacuum thickness is immediately apparent from Figure 4.5: for every increase in vacuum thickness, the internal volume of the tank decreases, implying that less hydrogen can be carried and made available during the cruise phase. For some values of vacuum thickness the minimum value required for cruise time cannot even be met.

The dependence of dormancy time on vacuum thickness, on the other hand, is a little more complex (Figure 4.4): initially, an increase in vacuum thickness seems to be beneficial as it leads to an increase in dormancy time. However, this trend is reversed once an optimum value is reached. Beyond this point, a further increase in vacuum thickness leads to a decrease in dormancy time.

This behaviour can be explained by two coexisting trends. First, increasing the insulation thickness leads to an increase in the thermal resistance of the insulation layer and thus a decrease in heat inflow. This definitely has a positive effect as it allows an increase in dormancy time. At the same time, however, increasing the insulation thickness also leads to a decrease in the internal volume of the tank and thus a decrease in the mass of hydrogen that can be stored in it. This negatively affects dormancy time because it means that the same amount of heat from the outside will act on a smaller mass of hydrogen. This graph shows us that, above a certain limit, having an inner volume that is too small can compromise the performance of the tank in terms of dormancy time, even if the thermal performance of the insulation increases.

4.3.2. Varying vacuum pressure P_{vacuum}

The vacuum pressure P_{vacuum} is defined in a range between 10^{-5} Pa and 1 Pa. The upper bound has been defined based on the consideration presented in section 4.1: the vacuum pressure should definitely remain below 1 Pa so as to avoid apparent thermal conductivity values that are in the order of magnitude of the thermal conductivity of material insulation systems, thus losing the benefits of the vacuum layer. As for the lower limit, there are technical limitations related to the difficulty of obtaining vacuum pressure values that are lower than $10^{-4} - 10^{-5}$ Pa.

Varying the vacuum pressure at the same insulation thickness has no impact on the internal tank volume and consequently there is no change in cruise time. Consequently, only the effects on dormancy time will be evaluated. The results are presented in the Figure 4.6. The following parameters take on their respective values at this stage: P_{vent} = 4 bar, N_{MLI} = 30, t_{vacuum} = 0.04 m, Argon is selected as residual gas.

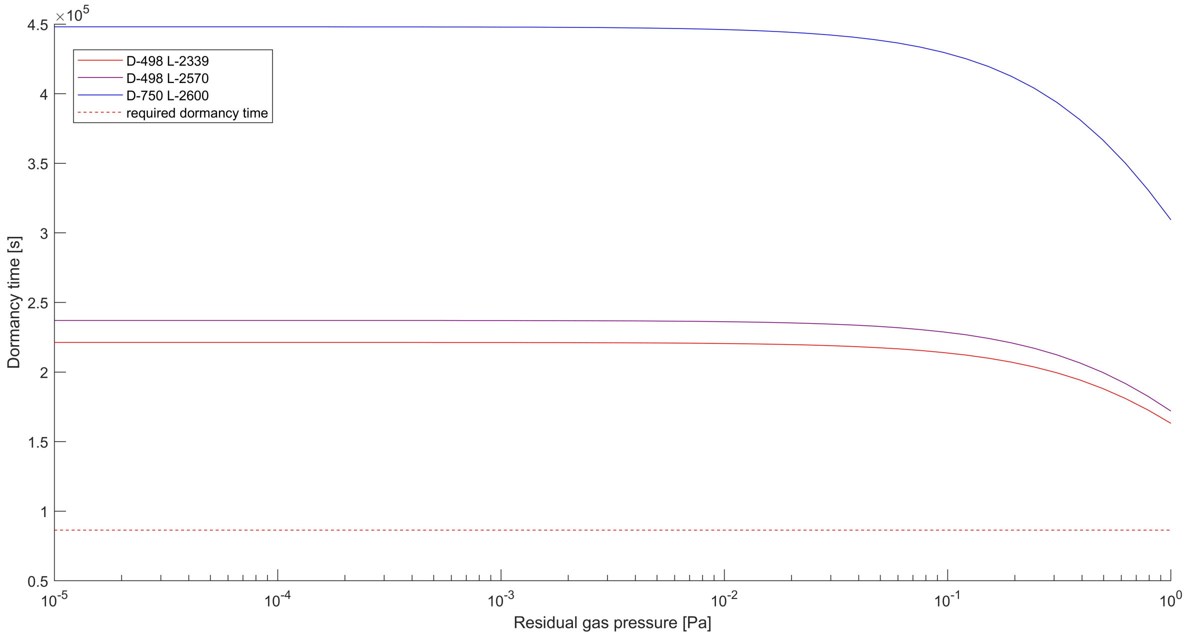

Figure 4.6: Evaluation of dormancy time for various vacuum pressure values and different design points

As expected from the considerations presented in reference [78] and Figure 2.4, when the vacuum pressure remains below 10^{-1} Pa, the heat inflow stays almost constant implying that also the dormancy time stays almost constant. Consequently, in order to be certain to keep the thermal performance of the insulation system constant during the operational life of the tank, it is necessary to remain below 10^{-1} Pa by a certain margin: values of vacuum pressure P_{vacuum} of 10^{-2} Pa or lower (on the basis of the tools available for vacuum creation) are then recommended.

4.3.3. Varying number of MLI layers N_{MLI}

The number of MLI layers N_{MLI} is defined in a range between 10 and 50. As has been presented in section 4.1 when discussing the influence of MLI layer density, the heat transfer by radiation can be reduced by increasing the number of shields, but heat transfer by solid conduction increases with increasing packing density since the thermal contact between the radiation shields and spacers gets better. Furthermore, if the distance between two successive radiation shields decreases (increasing the layer density), then the thickness of the spacers will decrease as well, implying shorter heat paths and greater heat transfer by solid conduction. In general, therefore, for the same insulation thickness, the goal is to obtain a number of MLI layers that allows for a sufficient reduction of the heat transfer by radiation and at the same time does not lead to an excessive packing density, which would results in a substantial increase of the heat transfer by solid conduction through the spacers.

Varying the number of MLI layers at the same insulation thickness has no impact on the internal tank volume and consequently there is no change in cruise time. Consequently, only the effects on dormancy time will be evaluated. The results are presented in the Figure 4.7. The following parameters take on their respective values at this stage: P_{vent} = 4 bar, P_{vacuum} = 10^{-3} Pa, t_{vacuum} = 0.04 m, Argon is selected as residual gas.

As can be deduced from the graph in the Figure 4.7, increasing the number of MLI layers in the range considered (between 10 and 50) results in an increasing dormancy time. This shows how the heat transfer by radiation can be reduced by increasing the number of shields. It can then be concluded that, in the range considered, the packing density does not reach values that would considerably increase the heat transfer by solid conduction through the spacers and impact the general performance of the insulation system.

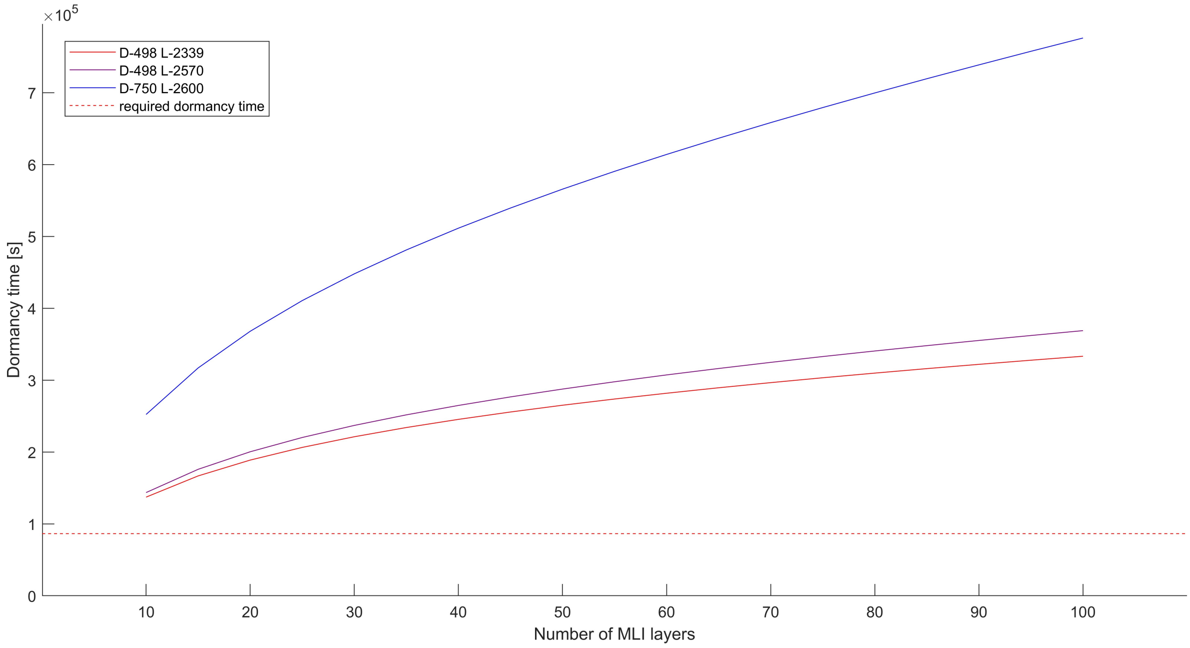

Figure 4.7: Evaluation of dormancy time for various number of MLI layers and different design points

4.3.4. Varying the type of residual gas

In the section 4.1, it has been discussed how the type of residual gas could have an impact on the general performance of the HV-MLI insulation system. In general, the procedure leading to the creation of vacuum in the space between the inner and outer shells involves the removal of gas molecules from the defined volume through the use of vacuum pumps, which may be based on different principles (mechanical pumps operating according to the compression-expansion principle, molecular-driven pumps such as turbopumps, and physical draw pumps such as cryopumps) [38]. Generally, the gas initially present in the space between inner and outer vessel is air. Since the complete removal of all molecules is technically impossible, the result will be the presence of residual gas, which may be air or another gas that has been actively introduced to take the place of air.

Based on the characterisation of various residual gas examples presented in the reference [72], the effect of the presence of different types of residual gas on the thermal performance of the tank was evaluated. In particular, the focus was brought to the design point D-518 L-2500, as it is the most critical based on shortest dormancy time.

Varying the type of residual gas at the same insulation thickness has no impact on the internal tank volume and consequently there is no change in cruise time. Consequently, only the effects on dormancy time will be evaluated. The results are presented in the Figure 4.8. The following parameters take on their respective values at this stage: P_{vent} = 4 bar, P_{vacuum} = 10^{-3} Pa, t_{vacuum} = 0.04 m, N_{MLI} = 30.

From Figure 4.8 it can be concluded that, in the case where the vacuum pressure is less than 10^{-2} Pa, the difference in terms of dormancy time for the different versions with different types of residual gas is practically negligible. In the range between 10^{-2} and 1 Pa, however, the differences become more pronounced. For some gases (Air, D_2, H_2, and N_2) even the minimum requirement for dormancy time can no longer be met for pressures approaching 1 Pa.

From this it can be deduced that under optimum operating conditions for vacuum pressures below 10^{-2} Pa, the difference between the various types of gas is practically imperceptible. However, considering sub-optimal operating conditions where, for example, a malfunction occurs in the vacuum pressure maintenance system, some gases prove to be better then others at coping with these possible increases in vacuum pressure. In general, it may be favourable to choose these gases characterised by a more stable thermal conductivity in the transition from molecular to continuum regimes in order to be able to accommodate minor malfunctions of the vacuum pressure maintenance system without excessive damage.

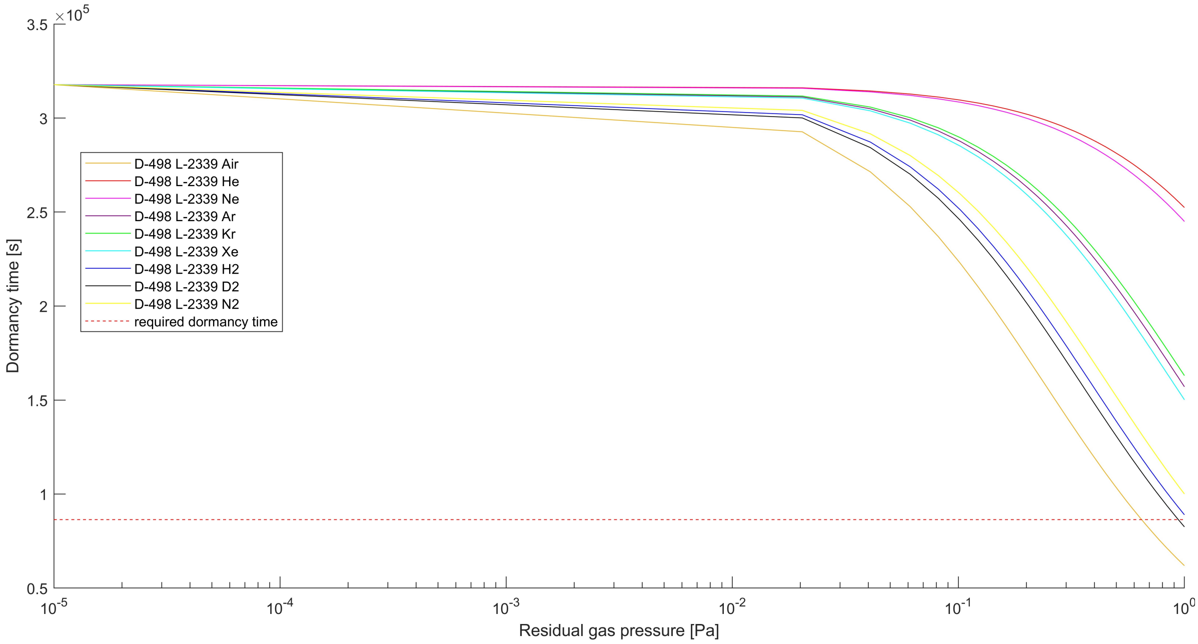

Figure 4.8: Evaluation of dormancy time for various residual gases

4.3.5. Budget for the heat leakage through the support structure $\dot{Q}_{supports,max}$

The budget for the heat leakage through the support structure, denoted as $\dot{Q}_{supports,max}$, represents the maximum allowable heat inflow through the supports that still allows to meet the dormancy time requirement. This parameter must be calculated for each tank design in order to obtain specific thermal performance requirements for the inner vessel support structure.

The direct approach would be to calculate the total heat inflow from the external environment that corresponds to the minimum acceptable dormancy time for a specific tank. Then, subtract the other two contributions to the heat inflow, i.e. heat inflow through the tank walls and through the piping.

Calculating dormancy time is, however, a complex process as it requires determining iteratively the thermodynamic state of the hydrogen stored in the tank at each time step until the internal pressure reaches the characteristic venting pressure value P_{vent} of the tank considered (see section 3.2). A more straightforward approach to estimate the budget for the heat leakage through the support structure for a given tank involves evaluating the dormancy time performance for various iterations of the original design (i.e. the one including two longitudinal composite supports). In each iteration, the heat leakage through the support structure is gradually increased from its initial value until the version that corresponds to the minimum acceptable dormancy time is identified. At that point, the value taken for the heat leakage through the support structure will correspond to the maximum allowed, i.e $\dot{Q}_{supports,max}$.

For every design point from table 4.1, different versions have then been created by varying the parameter $\dot{Q}_{supports}$. In particular, for every design point, the original heat leakage through the support structure is multiplied by a factor f_q defined in a range from 1 to 200.

It is clear that varying the heat leakage through the support structure for the same insulation thickness has no impact on the internal volume of the tank and consequently no change in cruise time. Consequently, only the effects on dormancy time will be evaluated. The result are presented in Figure 4.9. The following parameters take on their respective values at this stage: P_{vent} = 4 bar, N_{MLI} = 30, t_{vacuum} = 0.04 m, Argon as residual gas, P_{vacuum} = 10^{-3} Pa.

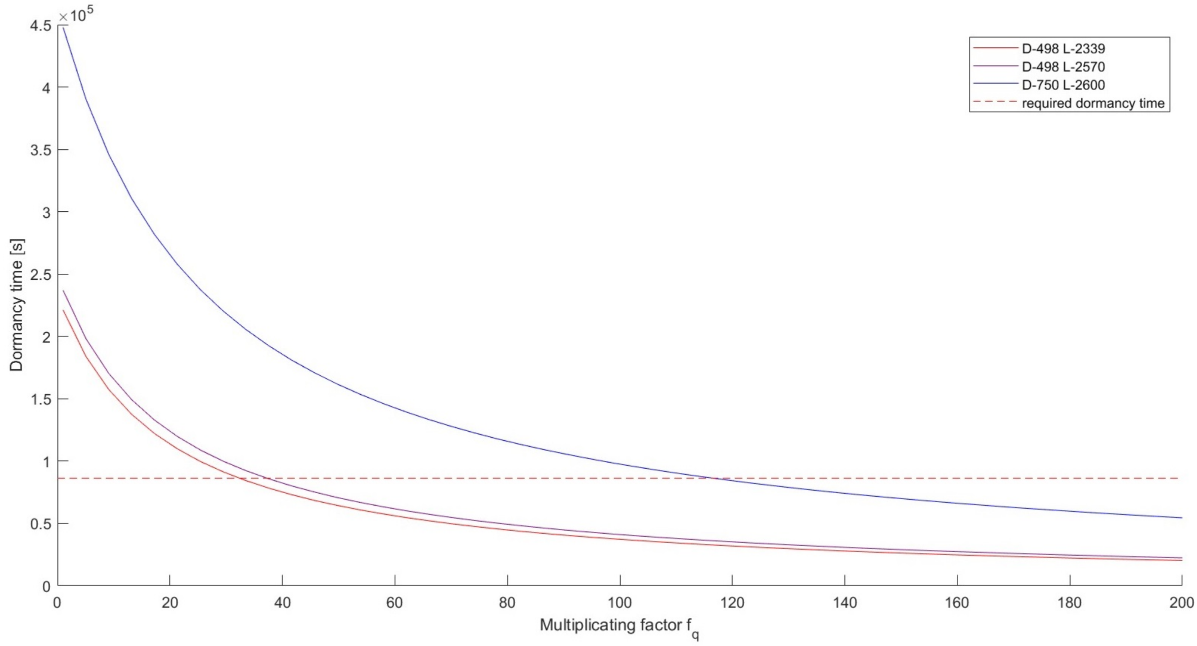

Figure 4.9: Effect of increased heat leak through the support system on dormancy time

From this graph, it is possible to extrapolate the maximum multiplication factor $f_{q,max}$ that still allows to meet the dormancy time requirement for the specific tank design. Multiplying the original value of $\dot{Q}_{supports}$ by the factor $f_{q,max}$ gives the $\dot{Q}_{supports,max}$. The original value of heat leakage through the support structure $\dot{Q}_{supports}$ which was considered in the previous analysis, is calculated on the basis of the values presented in table 4.2 and the Equation 4.13 (reference to section 3.2).

Table 4.2: Values characterising the simplified support structure

$N_{supports}$	T_{ext}	T_{int}	$L_{bridge,c}$	k_{G10-CR}	$A_{support}$
2	305 K	20.26 K	t_{vacuum}	0.25 W/mK	$7.23 * 10^{-05} m^2$

$$\dot{Q}_{supports} = N_{supports}\frac{T_{ext} - T_{int}}{R_{support}} = N_{supports}\frac{T_{ext} - T_{int}}{L_{bridge,c}} k_{G10-CR} A_{support} \tag{4.13}$$

where $L_{bridge,c}$ is the length of the support through the insulation layer (equal to the thickness of the insulation layer t_{vacuum}), k_{G10-CR} is the thermal conductivity of G10-CR glass fiber composite, $A_{support}$ is the cross-sectional area of a support, T_{ext} is the temperature of the environment surrounding the tank, T_{int} is the temperature of the inside of the tank, and $N_{supports}$ is the total number of supports.

Knowing that the insulation thickness value assumed for this analysis is t_{vacuum} = 0.04 m, it is possible to calculate the original values of $\dot{Q}_{supports}$ for every design point and, after extracting the respective maximum multiplication factors $f_{q,max}$, finally obtain the budgets for the heat leakage through the support structure $\dot{Q}_{supports,max}$. The results are presented in table 4.3.

Table 4.3: Values characterising the simplified support structure

	D-498 L-2339	**D-498 L-2570**	**D-750 L-2600**
$\dot{Q}_{supports}$ **[W]**	0.2572	0.2572	0.2572
$f_{q,max}$	32	37	116
$\dot{Q}_{supports,max}$ **[W]**	8.2297	9.5156	29.8328

The results presented in Table 4.3 demonstrate that the heat leakage budget through the support structure $\dot{Q}_{supports,max}$ for all the evaluated designs exceeds the original heat leakage values $\dot{Q}_{supports}$.

This difference indicates that there is additional thermal margin available, providing flexibility to introduce different support structure configurations without compromising the overall thermal performance of the tank. This thermal margin enables the exploration of different materials and/or geometries for the supports, offering the possibility to further optimize the tank's design for operational and safety requirements.

Furthermore, it can be noticed that the larger tank (D-750 L-2600), with all the other parameters being equal, has a significantly higher budget for the heat leakage through the support structure than the other two tanks (D-498 L-2339 and D-498 L-2570), which have very similar dimensions. This reconfirms the concept that a larger tank characterised therefore by a lower surface area-to-volume ratio will have a lower heat inflow from the external environment, resulting in a higher thermal performance. This leaves room for a larger heat inflow budget through the support structure.

Obviously, the same procedure must be repeated if one of the parameters characterising the geometry or performance of the tank is changed.

4.3.6. Final considerations

The evaluation of the double-wall tank architecture indicates significant potential for successful application in the case study. This design provides enhanced thermal performance through vacuum-based insulation, which significantly minimizes heat transfer. As a result, the tank is able to meet the stringent dormancy time requirements across all three design points considered for the retrofit. The overall benefits in terms of performance make the double-wall architecture a viable and attractive option for hydrogen storage in aviation applications.

Moreover, the analysis of the heat leakage budget through the support structure $\dot{Q}_{supports,max}$ reveals that the maximum allowable heat leakage is higher than the originally calculated values. This offers additional thermal margin, providing flexibility to introduce alternative support structures or optimize the existing ones without compromising the overall thermal performance. This available heat leakage budget also imposes a thermal requirement for the support structure, as any introduced design must stay within the allowable heat inflow limit while meeting structural and operational demands.

However, to fully demonstrate the feasibility of this architecture, the next step involves designing an inner vessel support structure capable of withstanding even the most extreme operational conditions. This introduces additional complexity to the design, as the support structure must satisfy both structural and thermal requirements. The development and analysis of the inner vessel support structure will be addressed in the following chapter 5.

5
Inner vessel and support structure

In the case of double-wall tank design, the presence of both an outer and inner vessel necessitates a comprehensive approach to maintain proper positioning and overall structural integrity. A key element of this approach is the support system for the inner vessel, which is crucial to prevent contact between the inner vessel and the walls of the outer shell, while also accommodating thermal contraction and expected G-forces in all directions.

Finding the optimal design for the inner vessel supports is challenging since it involves balancing structural integrity, thermal insulation, and weight optimization. These supports need to withstand dynamic forces, accommodate thermal expansion/contraction of the inner vessel, and minimize heat transfer while meeting space and weight constraints.

This chapter aims to give an overview of the requirements that a possible design for inner vessel supports must fulfill, to assess the inner vessel displacements caused by temperature and pressure variation (ΔT and Δp), to develop a methodology for analysing the thermal and structural performance of possible support structures' designs, to propose design concepts that might be appropriate, and to evaluate the results.

5.1. Requirements

In the design process of the inner vessel support system, it is important to take into account all the criticalities that the tank may encounter during its operational life in order to achieve a safe and robust design.

First filling of the tank

The step into the operational life of a tank involves the first filling after the tank has been manufactured. During this process, the inner vessel of a double-wall LH_2 tank experiences a significant temperature difference. The manufacturing process of the tank takes place under standard environmental conditions, with an ambient pressure of approximately 101000 Pa and a temperature of around 300 K. However, when the tank is filled with liquid hydrogen for the first time, the inner vessel experiences an extreme change in temperature, dropping to cryogenic levels of about 20 K. This results in a significant temperature differential of approximately 280 K between the manufacturing and operational states. Additionally, once the tank becomes operational (right after being filled), the internal pressure rises to a level just below the venting pressure. This operational pressure typically falls within the range of 300000 to 500000 Pa, as discussed in section 3.2, leading to a pressure differential in the order of 200000 to 400000 Pa.

Therefore, the inner tank must endure varying temperature and pressure conditions going from the manufacturing phase to the operational phase. Understanding how much a vessel expands or contracts when pressure and temperature undergo a change is essential, especially when designing the inner vessel supports. It is crucial to ensure that these dimensional changes do not lead to significant thermomechanical stresses in the support structure and its connection.

Another effect that must be considered is that the introduced temperature change directly affects the supports of the inner vessel. Initially, both the outer and inner boundaries of the support system (which correspond to the outer and inner vessel, respectively) were at ambient temperature. However, after filling, the inner boundary's temperature is determined by the presence of liquid hydrogen, reaching 20 K. As a result, the outer and inner boundaries are now at different temperatures, leading to the development of a temperature distribution through the connection structure between the inner and outer vessel. This temperature distribution could be responsible for a distribution of thermal stresses: different portions of the support structure are subjected to different temperature variations between before and after first filling (depending on the temperature distribution in the support structure after filling) and would like to expand/contract accordingly, but at the same time are constrained by the surrounding portions and the external boundaries.

Operational and crash loads

Over its operational life, a particular airplane will experience discrete maneuvers that could generate high maneuver loads, which are expressed in terms of accelerations. These loads arise from such activities as a very sharp turn or rapid upward or downward movement or other dynamic flight activities that repeatedly apply extensive forces to the structure of an airplane. The crash loads originate from an impact event and, by nature, are more severe and much more critical than maneuver loads for the structural integrity of the airplane. Due to these reasons, maneuver loads appear much less relevant, and in this study, the understanding and mitigation of crash loads is a major concern for safety and structural soundness.

The general emergency landing provisions (regulated in chapters 25.561 25.563 of CS-25 and chapter 25.561 25.563 of FAR-25) define the ultimate inertia forces acting separately relative to the surrounding structure as presented in Table 5.1.

Table 5.1: Ultimate inertia forces acting separately relative to the surrounding structure

Upward	Forward	Sideward	Downward	Rearward
3.0 g	9.0 g	4.0 g	6.0 g	1.5 g

The equipment, and any large items of mass in general, must be securely restrained to withstand all loads up to those specified above. Furthermore, in order to comply with AMC 25.963, the fuel tanks must be designed to endure the prescribed inertial load factors for emergency landing conditions within the fuselage contour. It is important to note that if the tanks are required to be frequently removed, an additional multiplying factor of 1.33 must be applied to these load factors to account for the increased demands on the structural design.

The emergency landing dynamic conditions (according to CS 25.562 and FAR 25.562) involve stringent requirements to protect occupants by maintaining specific deceleration limits and ensuring that the injury criteria are not exceeded. During an emergency landing scenario, in fact, the aircraft experience a change in downward vertical velocity and forward longitudinal velocity. The analysis of how these conditions determine the acceleration spectrum applied to tanks (which also depends on the type of support structure and the specific location of the tank) was part of the thesis project carried out by TU Delft master student Yi-Hsiu Wu [82]. The dynamic loading condition considered consists of a drop test conducted on the section of the fuselage containing the hydrogen tanks with a vertical impact speed of 9.14 m/s. This test provided valuable data on the acceleration spectra measured at the tank heads, which serve as the foundation for understanding how the impulse generated by the drop test on the fuselage is transmitted to the internal components of the tank: the internal vessel and its support system [82].

Tank performance

Once the minimum requirements in terms of loads (thermal and mechanical) that the support structure must be able to support have been defined, it is necessary to evaluate which strategies to adopt in order to minimize the heat leak between external and internal environment. In fact, an excessive heat leak through the support structure could seriously compromise the general thermal performance of the tank and, consequently, the ability to meet the dormancy time requirement.

Evaluating the heat leakage budget for the support structure is essential for each tank design. Denoted as $\dot{Q}_{supports,max}$, this budget represents the maximum allowable heat inflow through the supports while still meeting the dormancy time requirement. This parameter must be calculated in order to establish specific thermal performance requirements for the inner vessel's support structure. Although minimizing heat leakage is ideal, this threshold is crucial as it defines the upper limit of allowable heat inflow, ensuring the tank's thermal performance stays within acceptable limits.

The heat transfer rate from outer to inner vessel through the inner vessel support system is influenced by the dimensions and shape of the supports, the thermal conductivity of the material they are made from, and the contact thermal conductivity between them and the walls. The inner tank-supporting structure materials should then be characterised by a combination of high strength and low thermal conductivity. Some possible configurations have been presented in section 2.4.1, based on the literature study conducted previously.

To summarize, a suitable design for the inner vessel support system must meet the following requirements to be considered for use in a double wall tank for an aircraft retrofit:

- Accommodate the inner vessel's displacements while minimizing the risk of inducing excessive stresses that could lead to plastic deformation or even structural failure
- Withstand the crash loads without failing or causing damage to other components: both quasi static accelerations and dynamic crash conditions
- Minimize the heat leak from the outside to the inside of the tank in order to meet the dormancy requirement and enhance the thermal performance of the tank

5.2. Model of the outer vessel

The outer vessel is a shell that consists of three main regions: spherical dome 1, cylinder, and spherical dome 2. In the analysis performed, the outer vessel is consistently modeled as a rigid body for the following reasons:

- Firstly, the outer vessel is not exposed to significant differences in temperature or pressure, meaning that no substantial expansion or contraction is expected to occur. The temperature differential between the environment and the outer vessel remains relatively stable, minimizing any deformation resulting from thermal effects.
- Secondly, the external support structure of the tank is designed to ensure that no deformations are introduced to the vessel itself. The structural framework is specifically constructed to prevent any external forces or loads from distorting the tank, ensuring that the outer vessel maintains its integrity under operational conditions and emergency landing conditions. This design consideration is further supported by the analysis performed in Yi-Hsiu's thesis, which demonstrated that no plastic deformation or damage was found on the tanks [82].

5.3. Model of the support structure

The supports are modeled as beams characterised by axial stiffness and flexural stiffnesses.
In Figure 5.1, a schematic of the interaction between a single support and the two vessels is presented.

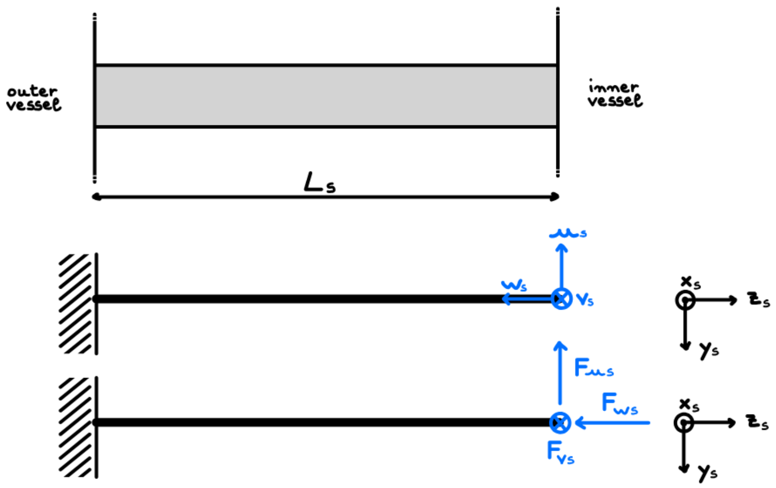

Figure 5.1: Model of the interaction between a single support and the two vessels

For ease of modelling, it is assumed that all supports in the support system have the same geometrical and material characteristics. Furthermore, the geometry assumed for the cross-section of the supports is axisymmetric.

The coordinate system of the support is composed by the following:

- x_s coordinate: one of the two orthogonal axes within the plane of the beam's cross-section.
- y_s coordinate: the other orthogonal axis within the plane of the beam's cross-section.
- z_s coordinate: aligned with the axial direction of the beam.

Each support connects the outer vessel to the inner vessel, with one end in contact with each of the vessels. The connection with the outer vessel is fixed, so the beam can be modeled as a cantilever beam. The connection with the inner vessel is pinned, so that axial and lateral movements are confined without impeding rotational motion. The axial and lateral loads exerted by each support on the inner vessel result from the support's reaction to the vessel's displacements at the contact point (u_s, v_s, and w_s), which depend on the stiffness properties of the support, and have same direction but opposite orientation of the displacement vectors at the contact point.

The forces that are applied by the inner vessel on the support are simply the reaction forces that develop at the contact point. They are therefore exactly equal and opposite to the forces exerted by the support on the inner vessel. These loads ($F_{u,s}$, $F_{v,s}$, and $F_{w,s}$) can be considered as applied at the free end of the beam, which is the one in contact with the inner vessel.

The values of axial stiffness ($k_{z_s z_s}$) and flexural stiffnesses ($k_{x_s z_s}$ and $k_{y_s z_s}$) can then be respectively expressed as presented in the Equation 5.1.

$$k_{z_s z_s} = k_{ax} = \frac{A_s E_s}{L_s} = \frac{F_{u,s}}{u_s} \qquad k_{x_s z_s} = k_{y_s z_s} = k_{flex} = \frac{3 E_s I_s}{L_s^3} = \frac{F_{v,s}}{v_s} = \frac{F_{w,s}}{w_s} \tag{5.1}$$

where E_s is the Young's modulus of the material selected for the support, A_s is the cross-sectional area of the support, L_s is the length of the support (equal to the thickness of the vacuum layer t_{vacuum}), and I_s is the moment of inertia about the neutral axis of the beam.

5.3.1. Assumptions for the support structure

As previously presented in section 4.3.5, for each specific tank design, it is possible to obtain the maximum allowable heat inflow through the supports that still allows to meet the dormancy time requirement (budget for the heat leakage through the support structure $\dot{Q}_{supports,max}$). This parameter is of fundamental importance in the design of the support structure as it limits the design possibilities to only combinations of support structure variables capable of guaranteeing compliance with the dormancy time requirement.

The variables influencing the heat inflow through the support structure are: the length of the support through the insulation layer (equal to the thickness of the insulation layer t_{vacuum} in case of straight supports), the thermal conductivity $k_{support}$ of the material selected, the cross-sectional area of the supports $A_{support}$, and the total number of supports $N_{supports}$. The thermal performance requirement must then be translated into requirements for the design variables considering that the expression for calculating the heat inflow through the support structure is the one presented in Equation 5.2.

$$\dot{Q}_{supports} = N_{supports} \frac{T_{ext} - T_{int}}{t_{vacuum}} k_{support} A_{support} \tag{5.2}$$

Once the tank design has been selected, the value of the thickness of the insulation layer t_{vacuum} will then already be fixed. For the remaining parameters, the following considerations can be made:

- *Total number of supports $N_{supports}$:* wanting an axisymmetrical configuration of the support structure, the minimum number of supports must be 2.
- *Thermal conductivity $k_{support}$ of the material selected:* this parameter refers to a material's intrinsic ability to transfer or conduct heat. For this specific application, the goal is generally to limit heat transfer through the support structure and therefore the choice would be materials with low thermal conductivity. Considering most known materials, possible thermal conductivity values are defined in a wide range from 0.01 W/mK to 1000 W/mK.

- *Cross-sectional area of the supports $A_{support}$:* when defining the size and characteristics of the cross-section, it is important to keep into account the phenomenon of local buckling. Considering a cross-section under compression/shear as a combination of individual plate elements connected together, one must assess the risk that these plate elements, laterally supported along edges and subjected to membrane compression or shear, may buckle prematurely (before the overall column buckling or overall beam failure by lateral buckling or yielding) [74]. Thus, local buckling imposes a limit to the extent to which sections can be made thin-walled. Assuming a circular ring cross-section, the local buckling phenomenon is called wrinkling and observed as symmetric corrugations on a tube wall under axial compressive loading [45]. Theoretical equations have been derived to predict the critical axial compressive stress that causes a tubular member to become unstable, leading to the formation of wrinkles. Assuming ideal conditions (homogeneous and isotropic tubular material, concentric and uniform loading, and flat, burr-free tube edges) the expression and the corresponding t/R ratio requirement are presented in Equation 5.3.

$$\sigma_{cr} = \frac{1}{\sqrt{3(1-\nu_s^2)}}\frac{E_s t_s}{R_s} \qquad\qquad \frac{t_s}{R_s} = \frac{\sigma_{cr}\sqrt{3(1-\nu_s^2)}}{E_s} \tag{5.3}$$

where σ_{cr} is critical axial compressive stress, ν_s and E_s are respectively the Poisson's ratio and the Young's modulus of the material selected for the supports, R_s and t_s are respectively the outer radius and the thickness of the circular ring section. To avoid the phenomenon of local buckling in the elastic regime of the component, σ_{cr} must be bigger than or equal to the yield stress of the material selected for the supports $\sigma_{y,s}$. The condition on the t/R ratio can be finally expressed as Equation 5.4.

$$\frac{t_s}{R_s} \geq \frac{\sigma_{y,s}\sqrt{3(1-\nu_s^2)}}{E_s} \tag{5.4}$$

For a specific tank design, it is crucial to understand which combinations of these parameters are actually acceptable from the point of view of the budget for the heat leakage through the support structure $\dot{Q}_{supports,max}$. This feasibility study for the various options can be carried out by analysing what is the maximum number of supports $N_{s,max}$ allowed for a certain combination of cross-sectional area of the supports $A_{support}$ and thermal conductivity of the material considered $k_{support}$. If the maximum number of supports allowed to respect the heat leakage budget is equal to or more than 2, then the combination can be considered as potentially feasible.

Using the characteristics of the specific tank as input, the respective value of $\dot{Q}_{supports,max}$ can be obtained by following the method presented in section 4.3.5. For each combination of $A_{support}$ and $k_{support}$, the maximum permissible number of supports can be calculated according to the Equation 5.5.

$$N_{s,max,c} = \frac{\dot{Q}_{supports,max} t_{vacuum}}{A_{support,c} k_{support,c}(T_{ext} - T_{int})} \tag{5.5}$$

where $N_{s,max,c}$ is the maximum number of supports allowed for the combination c, $\dot{Q}_{supports,max}$ and t_{vacuum} are respectively the budget for the heat leakage through the support structure and the thickness of the insulation layer for the tank design considered, $A_{support,c}$ and $k_{support,c}$ are respectively the cross-sectional area of the supports and the thermal conductivity for the combination c, T_{ext} is the temperature of the environment surrounding the tank and T_{int} is the temperature of the inside of the tank.

After analysing all possible combinations, it will be possible to differentiate between combinations that are potentially feasible or not and, for potentially feasible combinations, know what the maximum allowed number of supports is.

It is important to specify 'potentially feasible' because there are several other requirements to consider before attesting to actual feasibility. In fact, the mechanical characteristics of the material and the geometric characteristics of the supports must be such that the support structure can also withstand the stresses induced by the shrinkage of the inner vessel without plastic deformation and the crash loads without failure. In fact, the study of potentially feasible configurations is a tool for learning which configurations meet the thermal requirements and provides a basis of possible configurations for evaluating the structural performance of the support structure.

5.3.2. Analysis of stresses in the support structure

In order to evaluate the stresses in the supports, Navier's formula for beam normal stress can be applied (Equation 5.6) [41].

$$\sigma_{z,s} = \frac{N}{A_s} - \frac{M_{yz}}{I_y} x_s + \frac{M_{xz}}{I_x} y_s \tag{5.6}$$

where $\sigma_{z,s}$ is the normal stress, x_s, y_s, and z_s are the principal axes of inertia of the support, N is the axial force, A_s is the cross-sectional area of the beam, M_{yz} and M_{xz} are the bending moments, I_y and I_x are the moments of inertia of the beam's cross-section.

By understanding the boundary conditions and the external forces applied to the beam, it is possible to derive the expressions for the axial load and bending moments along the beam. This involves analyzing the structural system, which includes evaluating the constraint reactions and constructing the internal force diagrams.

Figure 5.2 shows the steps of the analysis performed for the generic support previously described in section 5.3. As presented in Figure 5.2, the expressions for the bending moments M_{xz} and M_{yz} along the beam expressions can be found by exploiting the relations between bending moments and shear loads (T_x and T_y), and the understanding of the constraint reactions.

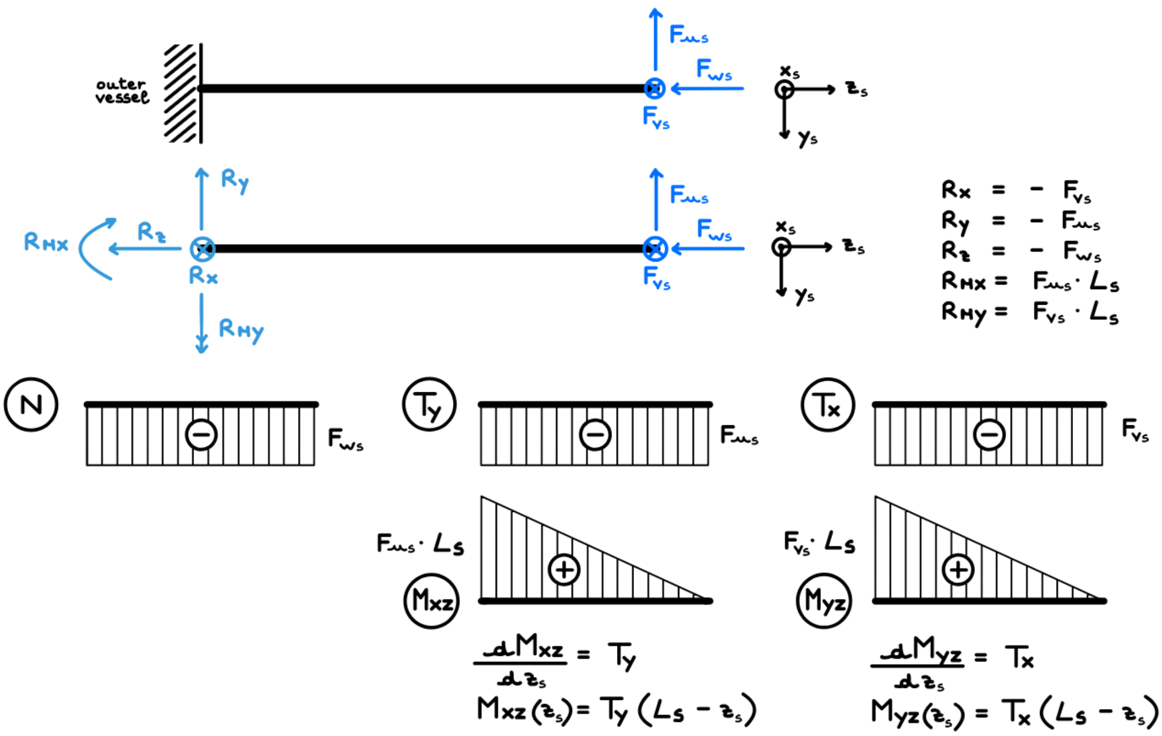

Figure 5.2: Determination of the generic support's structural system

To conclude, the expressions obtained should be substitued in Navier's formula (Equation 5.6), obtaining the final expression for the normal stress in the generic support (Equation 5.7).

$$\begin{aligned}\sigma_{z,s} &= \frac{-F_{w,s}}{A_s} - \frac{F_{v,s}(L_s - z_s)}{I_y} x_s + \frac{F_{u,s}(L_s - z_s)}{I_x} y_s \\ &= -\frac{k_{ax} w_s}{A_s} - \frac{(k_{flex} v_s)(L_s - z_s)}{I_y} x_s + \frac{(k_{flex} u_s)(L_s - z_s)}{I_x} y_s \end{aligned} \tag{5.7}$$

where $\sigma_{z,s}$ is the normal stress, x_s, y_s, and z_s are the principal axes of inertia of the support, $F_{u,s}$, $F_{v,s}$, and $F_{w,s}$ are the forces applied by the inner vessel on the support (reaction forces developed at the contact point), $-F_{w,s}$ is the axial force, A_s is the cross-sectional area of the beam, $F_{v,s}(L_s - z_s)$ and $F_{u,s}(L_s - z_s)$ are expressions for the bending moments $M_y z$ and $M_x z$, I_y and I_x are the moments of inertia of the beam's cross-section, u_s, v_s, and w_s are the vessel's displacements at the contact point, k_{ax} is the axial stiffness of the support, and k_{flex} is the flexural stiffness of the support.

Equation 5.7 will be employed to calculate the stress values at key locations within the cross-section of the beam, known as *stress recovery points*. These points are carefully selected to ensure the critical stresses, which significantly impact the beam's design and safety, are accurately captured during structural analysis. Here are some common stress recovery points on a typical beam cross-section:

- *Extreme fibers:* These are the outermost points on the top and bottom surfaces of the cross-section, where normal stresses due to bending are usually at their maximum or minimum.
- *Centroid:* The geometric center of the cross-section. For symmetrical sections, the centroid lies on the neutral axis. Stresses are sometimes recovered at the centroid to evaluate the average stress distribution.
- *Corners:* In non-circular cross-sections, such as rectangular or I-beams, corners often experience complex stress states.
- *Points along the height:* Depending on the analysis, stresses might be evaluated at multiple points along the height of the cross-section, such as at intermediate points between the neutral axis and the extreme fibers.

Based on the cross section specification then the coordinates (x_s, y_s) of the stress recovery points must be defined. Furthermore, in order to assess the maximum values of the stresses along the beam, the section at the clamped location must be evaluated (z_s = 0).

5.4. Model of inner vessel

This chapter details the methodology for modelling and analysing the inner vessel. A theoretical approach is developed to investigate how the inner vessel performs when subjected to the pressure difference Δp and temperature difference ΔT in the transition to operational life.

The inner vessel is modeled as a shell which consists of three regions: spherical dome 1, cylinder, and spherical dome 2. A scheme is presented in Figure 5.3.

The coordinate system is composed by the following:

- x coordinate: tangential to the shell surface. For the spheres, the x coordinate direction is defined by the angle θ. For the cylinder, the x coordinate represents the longitudinal direction.
- y coordinate: tangential to the shell surface. For both the cylinder and the spheres, the y coordinate is defined by the angle ϕ.
- z coordinate: perpendicular to the shell surface.

The dimensions of the inner vessel (diameter, length, and thickness) follows the sizing process presented in section 4.1 and, based on the solutions proposed by Yi-Hsiu Wu in his master thesis [82], there are three possible sets of external dimensions of the tank depending on the packing strategy chosen for the retrofit design. These are presented in table 5.2.

Table 5.2: Possible external dimensions of the tank

Retrofit design	Option n.	External diameter [m]	External length [m]
LSP	1	0.498	2.339
LHP	2	0.498	2.570
LCP	3	0.750	2.600

According to the information in section 4.1, the material selected for the inner vessel is the aluminum alloy AL5083-O and the relevant material properties are summarised in table 5.3 [29] [61].

Table 5.3: Relevant material properties of AL5083-O

Young's modulus E [Pa]	$8.093 * 10^{10}$
Poisson's ratio ν	0.33
Ultimate strength S_u [Pa]	$4.21 * 10^{8}$
Coefficient of Thermal Expansion α [m/m*K]	$25 * 10^{-6}$
Thermal conductivity k [W/m*K]	80

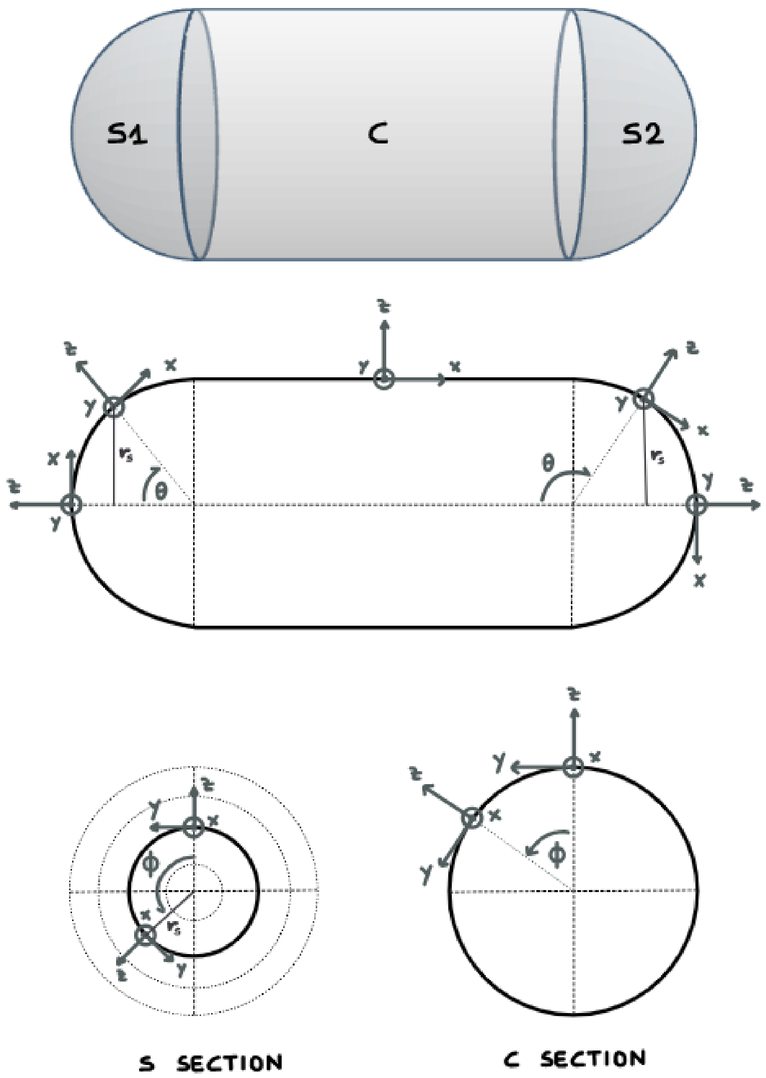

Figure 5.3: Model of the inner vessel

5.4.1. Deformation of the inner vessel due to ΔT and Δp

As presented in section 5.1, the inner vessel experiences a significant variation of temperature and pressure conditions going from the manufacturing phase to the operational phase. This can be expected to result in an expansion/contraction of the inner vessel and quantifying this phenomenon is important also for the design of inner vessel supports. In order to evaluate how the inner vessel would deform in this condition, a MATLAB code that applies the principle of minimum total potential energy was implemented.

The minimum total potential energy principle is one of the basic principles in structural mechanics, which states that the state of stable equilibrium of a conservative system occurs at the minimum value of total potential energy. This means that, among all the admissible displacements, the one that would make the total potential energy a minimum will be the most accurate solution [51]. The admissible displacement in this respect should be compatible with compatibility equations and the essential or kinematic boundary condition [68]. This principle is a fundamental basis for the analysis of deformations and stresses in structural systems. In fact, for constrained structural systems, the applied forces introduce deformation which is the incremental change to the new deformed state from the original undeformed state. Deformation is actually the main unknown in any structural analysis, which leads to the strains and finally the stresses within the system.

The total potential energy for a conservative mechanical system is defined as the internal elastic deformation energy (strain energy) minus the work performed by external forces in the process of deformation (or the potential energy lost) [68], as expressed by Equation 5.8 [51].

$$\delta\Pi_t = \delta(U - W_f) = 0 \tag{5.8}$$

where Π_t is the total potential energy, U is the strain energy, and W_f is the work performed by the external forces.

Strain energy

The strain energy is calculated using the volume integral over the strain energy density throughout the volume of the structure. The strain energy density is defined as the total energy stored per unit volume of material under consideration and, for linearly elastic materials, it can be expressed by Equation 5.9

$$U_d = \sum_{i,j} \frac{\sigma_{ij}\epsilon_{ij}}{2} \tag{5.9}$$

where σ_{ij} and ϵ_{ij} are respectively the stress and strain in the ij direction ($i, j = x, y, z$).

The linear theory of thin elastic shells with arbitrary shape of the middle surface is derived on the basis of Kirchhoff's assumptions [76], which state that:

- Normals to the undeformed middle surface remain straight and normal to the deformed middle surface and do not experience any extension. This assumption means that all strain components (both normal and shear) in the direction normal to the middle surface are zero: $\epsilon_{zz} = \epsilon_{xz} = \epsilon_{yz} = 0$
- The transverse normal stress is negligible compared to the other normal stress components and can be disregarded. It can then be assumed that: $\sigma_{zz} = 0$

The strain energy for the current case study is then expressed by Equation 5.10.

$$U = \int_V U_d \mathrm{d}V = \int_V \sum_{i,j} \frac{\sigma_{ij}\epsilon_{ij}}{2} \mathrm{d}V = \int_V \frac{1}{2} \left(\sigma_{xx}\epsilon_{xx} + \sigma_{yy}\epsilon_{yy} + 2\sigma_{xy}\epsilon_{xy}\right) \mathrm{d}V \tag{5.10}$$

Another formulation of the strain energy for the current case study is presented in Equation 5.11 [76].

$$\begin{aligned} U = \int_S \frac{1}{2} \big(& A_{11}\epsilon_{xx0}^2 + 2A_{12}\epsilon_{xx0}\epsilon_{yy0} + A_{22}\epsilon_{yy0}^2 + 4A_{66}\epsilon_{xy0}^2 + \\ & + D_{11}k_{xx}^2 + 2D_{12}k_{xx}k_{yy} + D_{22}k_{yy}^2 + 4D_{66}k_{xy}^2 \ \big) \mathrm{d}S \end{aligned} \tag{5.11}$$

where A_{11}, A_{12}, A_{22}, and A_{66} are terms of the extensional stiffness matrix A, D_{11}, D_{12}, D_{22}, and D_{66} are terms of the bending stiffness matrix D, ϵ_{xx0}, ϵ_{yy0}, and ϵ_{xy0} are the mid-surface strain terms in the respective directions, and k_{xx}, k_{yy}, and k_{xy} are the mid-surface curvature terms in the respective directions. The extensional stiffness matrix A and bending stiffness matrix D for isotropic plates are expressed by Equations 5.12 and 5.13 respectively [35].

$$A = \begin{bmatrix} \frac{Et}{1-\nu^2} & \nu\frac{Et}{1-\nu^2} & 0 \\ \nu\frac{Et}{1-\nu^2} & \frac{Et}{1-\nu^2} & 0 \\ 0 & 0 & \frac{1-\nu}{2}\frac{Et}{1-\nu^2} \end{bmatrix} \tag{5.12}$$

$$D = \begin{bmatrix} \frac{Et^3}{12(1-\nu^2)} & \nu\frac{Et^3}{12(1-\nu^2)} & 0 \\ \nu\frac{Et^3}{12(1-\nu^2)} & \frac{Et^3}{12(1-\nu^2)} & 0 \\ 0 & 0 & \frac{1-\nu}{2}\frac{Et^3}{12(1-\nu^2)} \end{bmatrix} \tag{5.13}$$

where E is the Young's modulus, t is the thickness of the plate, and ν is the Poisson's ratio.

The strain-displacement relations for a general shell are expressed by the kinematics equations [76]. They define the compatibility conditions for strains and displacements, appropriately tailored for the specific shell theory being considered. For this specific case study, the contribution of thermal strains also must be taken into account. The thermal strains are due to the temperature difference experienced during the first filling of the tank (ΔT of approximately 300 K) and can be expressed as $\alpha\Delta T$ where α is the coefficient of linear thermal expansion of the material selected for the inner shell.

For the specific case of a *cylindrical shell* strain-displacement relations are expressed by Equations 5.14, 5.15, and 5.16.

$$\epsilon_{xx_c} = \epsilon_{xx0_c} + zk_{xx_c} \qquad \epsilon_{yy_c} = \epsilon_{yy0_c} + zk_{yy_c} \qquad \epsilon_{xy_c} = \epsilon_{xy0_c} + zk_{xy_c} \tag{5.14}$$

$$\epsilon_{xx0_c} = \frac{\partial u}{\partial x} - \alpha\Delta T \qquad \epsilon_{yy0_c} = \frac{1}{R}\frac{\partial v}{\partial \phi} + \frac{w}{R} - \alpha\Delta T \qquad \epsilon_{xy0_c} = \frac{1}{2}\left(\frac{\partial v}{\partial x} + \frac{1}{R}\frac{\partial u}{\partial \phi}\right) \tag{5.15}$$

$$k_{xx_c} = -\frac{\partial^2 w}{\partial x^2} \qquad k_{yy_c} = -\frac{1}{R}\frac{\partial}{\partial \phi}\left(\frac{1}{R}\frac{\partial w}{\partial \phi}\right) \qquad k_{xy_c} = -\frac{\partial}{\partial x}\left(\frac{1}{R}\frac{\partial w}{\partial \phi}\right) \tag{5.16}$$

where u, v, and w are the displacement functions in the x, y, and z direction respectively, ϵ_{xx0_c}, ϵ_{yy0_c}, and ϵ_{xy0_c} are the mid-surface strain terms for the cylinder in the respective directions, and k_{xx_c}, k_{yy_c}, and k_{xy_c} are the mid-surface curvature terms for the cylinder in the respective directions, ΔT is the temperature difference at which the inner vessel is subjected during the first filling, α is the coefficient of linear thermal expansion of the material selected for the inner shell, and R is the radius of the cylinder.

For the specific case of a *spherical shell* strain-displacement relations are expressed by Equations 5.17, 5.18, and 5.19.

$$\epsilon_{xx_s} = \epsilon_{xx0_s} + zk_{xx_s} \qquad \epsilon_{yy_s} = \epsilon_{yy0_s} + zk_{yy_s} \qquad \epsilon_{xy_s} = \epsilon_{xy0_s} + zk_{xy_s} \tag{5.17}$$

$$\epsilon_{xx0_s} = \frac{\partial u}{\partial x} + \frac{w}{R} - \alpha\Delta T \qquad \epsilon_{yy0_s} = \frac{1}{r_s}\frac{\partial v}{\partial \phi} + \frac{w}{R} - \alpha\Delta T \qquad \epsilon_{xy0_s} = \frac{1}{2}\left(\frac{\partial v}{\partial x} + \frac{1}{r_s}\frac{\partial u}{\partial \phi}\right) \tag{5.18}$$

$$k_{xx_s} = -\frac{\partial^2 w}{\partial x^2} \qquad k_{yy_s} = -\frac{1}{r_s}\frac{\partial}{\partial \phi}\left(\frac{1}{r_s}\frac{\partial w}{\partial \phi}\right) \qquad k_{xy_s} = -\frac{\partial}{\partial x}\left(\frac{1}{r_s}\frac{\partial w}{\partial \phi}\right) \tag{5.19}$$

where u, v, and w are the displacement functions in the x, y, and z direction respectively, ϵ_{xx0_s}, ϵ_{yy0_s}, and ϵ_{xy0_s} are the mid-surface strain terms for the sphere in the respective directions, and k_{xx_s}, k_{yy_s}, and k_{xy_s} are the mid-surface curvature terms for the sphere in the respective directions, ΔT is the temperature difference at which the inner vessel is subjected during the first filling, α is the coefficient of linear thermal expansion of the material selected for the inner shell, R is the radius of the sphere, and r_s is the local radius for a specific section of the sphere (reference to Figure 5.3).

By comparing Equations 5.14, 5.15, 5.16 and Equations 5.17, 5.18, 5.19, it is evident that the definition of the strain components for cylindrical shell and for spherical shell is different. Comparing the definition of the strain ϵ_{xx0} for the spherical shell and for the cylindrical shell, it can be seen that ϵ_{xx0_s} contains an additional term (w/R). Furthermore, in the definitions of ϵ_{yy} and ϵ_{xy}, for the cylinder the only value of radius is the geometry's own radius R, while for the sphere the term local radius r_s appears, which is not constant but varies according to the section of the sphere considered.

The compatibility between the three domains (sphere 1, cylinder, sphere 2) is ensured by using the same displacement functions across the entire inner vessel, even though the kinematic equations differ between the spherical and cylindrical sections.

The stress-strain relations for a general shell are expressed by the constitutive equations (Equation 5.20) assuming a plane stress state whereby the stresses normal to the shell are assumed to be zero [76].

$$\sigma_{xx} = \frac{E}{1-\nu^2}\left(\epsilon_{xx} + \nu\epsilon_{yy}\right) \qquad \sigma_{yy} = \frac{E}{1-\nu^2}\left(\epsilon_{yy} + \nu\epsilon_{xx}\right) \qquad \sigma_{xy} = \frac{E}{1+\nu}\epsilon_{xy} \tag{5.20}$$

where E is the Young's modulus, ν is the Poisson's ratio, ϵ_{xx}, ϵ_{yy}, and ϵ_{xy} are the strain terms for the shell in the respective directions.

Work potential

Work potential is the negative of the work done by applied forces, which is given by the product of the applied forces and the corresponding displacements. In this case study, the two contributions to the work potential are:

- W_p: the work done by the internal pressure difference acting on the inner walls of the vessel. This can be calculated by integrating the product of the pressure difference Δp and the displacement function w over the vessel's surface S (Equation 5.21).

$$W_p = \int_S \Delta p w \mathrm{d}S \tag{5.21}$$

- W_s: the work done by the supports positioned between the inner and outer vessels (with the outer vessel considered as a rigid body). The total contribution is determined by summing the contributions from each support, which depends on its inherent stiffness in a particular direction and the value of the displacement function in the same direction at the point in the vessel where the support is positioned. As described in section 5.3, the supports are characterized by axial stiffness k_{ax} and flexural stiffness k_{flex}. The displacement experienced by a support in the axial direction is given by the value of the w displacement function at that point ($w_{s,i}$), displacements in the two tangential directions are given by the u and v displacement functions at the same point ($u_{s,i}$ and $v_{s,i}$, respectively). These relations are expressed in Equation 5.22.

$$W_{s,i} = \frac{1}{2}k_{ax}w_{s,i}^2 + \frac{1}{2}k_{flex}u_{s,i}^2 + \frac{1}{2}k_{flex}v_{s,i}^2 \tag{5.22}$$

  Assuming that N is the total number of supports, the total work done by the inner vessel's support system can be expressed by Equation 5.23.

$$W_s = \sum_{i,1}^{N} W_{s,i} \tag{5.23}$$

To conclude, the formula for the total work potential is expressed in Equation 5.24.

$$W_f = W_p + W_s = \int_S \Delta p w \mathrm{d}S + \sum_{i,1}^{N}\left(\frac{1}{2}k_{ax}w_{s,i}^2 + \frac{1}{2}k_{flex}u_{s,i}^2 + \frac{1}{2}k_{flex}v_{s,i}^2\right) \tag{5.24}$$

Application of the minimum total potential energy principle

The minimum total potential energy principle may be applied by using either generalized displacements or an assumed form of displacements [64]. The method of generalized displacements will provide the most complete solution, but will generally become too complex for even relatively intricate structures. Thus, in this research, the decision was to opt for assuming a form for the displacements functions, so to make the problem more manageable and concrete by accepting a loss of generality. In general, this is considered acceptable if a specific solution is sought for a specific problem. The method employed is based on the Ritz method, which allows for the assumption of displacement functions that need only satisfy the geometric boundary conditions.

The assumed form for the displacement functions u, v and w are presented respectively in Equations 5.25, 5.26, and 5.27. The structure is the same for all three displacement functions. First, the polynomials in x variable describes the contribution of the solution that would be obtained assuming the problem as axisymmetric. Then, a term expressed as a function of the variable ϕ multiplied by the variable x. This dependency on ϕ is intended to allow the representation of cross-sectional deformations including ovalisation.

$$\begin{gathered} u = \left(a_5^u x^5 + a_4^u x^4 + a_3^u x^3 + a_2^u x^2 + a_1^u x + a_0^u\right) + \\ x\left(a_{cos}^u \cos(\phi) + a_{sin}^u \sin(\phi) + a_{2cos}^u \cos(2\phi) + a_{2sin}^u \sin(2\phi)\right) \end{gathered} \tag{5.25}$$

$$\begin{gathered} v = \left(a_5^v x^5 + a_4^v x^4 + a_3^v x^3 + a_2^v x^2 + a_1^v x + a_0^v\right) + \\ x\left(a_{cos}^v \cos(\phi) + a_{sin}^v \sin(\phi) + a_{2cos}^v \cos(2\phi) + a_{2sin}^v \sin(2\phi)\right) \end{gathered} \tag{5.26}$$

$$\begin{aligned} w = \left(a_5^w x^5 + a_4^w x^4 + a_3^w x^3 + a_2^w x^2 + a_1^w x + a_0^w\right) + \\ x\left(a_{cos}^w \cos(\phi) + a_{sin}^w \sin(\phi) + a_{2cos}^w \cos(2\phi) + a_{2sin}^w \sin(2\phi)\right) \end{aligned} \tag{5.27}$$

The undetermined coefficients of the supposed displacement expressions will then become the unknown variables to be determined (Equation 5.28).

$$\begin{aligned} \boldsymbol{c} = [&a_5^u, a_4^u, a_3^u, a_2^u, a_1^u, a_0^u, a_{cos}^u, a_{sin}^u, a_{2cos}^u, a_{2sin}^u, \\ &a_5^v, a_4^v, a_3^v, a_2^v, a_1^v, a_0^v, a_{cos}^v, a_{sin}^v, a_{2cos}^v, a_{2sin}^v, \\ &a_5^w, a_4^w, a_3^w, a_2^w, a_1^w, a_0^w, a_{cos}^w, a_{sin}^w, a_{2cos}^w, a_{2sin}^w] \end{aligned} \tag{5.28}$$

The next step involves replacing these displacement functions in the calculations and obtain the expressions for strain energy and work potential. From these, the total potential energy, Π_t, is derived. To find the minimum value of Π_t, the Ritz method is applied, where the variation of the total potential energy Π_t is expressed with respect to variations of the independent degrees of freedom (DOFs), specifically the Ritz coefficients. Starting from the general expression of Π_t (as shown in Equation 5.8), the stationary condition is satisfied when the partial derivatives of Π_t with respect to each undetermined Ritz coefficient are zero. This process yields a set of linear algebraic equations. The general form of one of these algebraic equations is presented in Equation 5.29 and each equation corresponds to the condition that the potential energy is at a minimum with respect to a particular Ritz coefficient.

$$eq_j : \frac{\partial \Pi_t}{\partial \boldsymbol{c}_j} = 0 \tag{5.29}$$

where Π_t is the total potential energy defined in Equation 5.8 and $\boldsymbol{c}_j$ is the j^{th} Ritz coefficient of the supposed displacement expressions. This linear system can be solved to obtain the values of the Ritz coefficients $\boldsymbol{c}$, which can be readily substituted back into the displacement functions in order to obtain the solution to the deformation problem.

In order to evaluate the stresses in the inner vessel, it is necessary to substitute the solutions obtained for the displacement functions into the expressions for the strains (Equations from 5.14 to 5.19) and then use these to evaluate the stresses according to Equation 5.20

5.5. Analysis of fatigue life

The temperature and pressure changes experienced by the tank during the filling process can occur multiple times throughout the aircraft's operational life. It is reasonably expected that the tanks may be completely emptied and subsequently filled approximately once every six months. However, this is only an estimate, as there is no specific official requirement or certification specification that mandates a precise frequency for such operations. It is anyway important to assess how the stresses experienced by the inner vessel and supports during the specific condition translate into the overall life expectancy of the component in order to ensure the reliability and safety of the tank over time.

The load cycle in this case is characterised by a minimum stress $S_{min} = 0$ and a maximum stress S_{max} which depends on the specific conditions of the case study. This means that the stress range $\Delta S = S_{max} - S_{min} = S_{max}$, the stress amplitude $S_a = \Delta S/2 = S_{max}/2$ and the mean stress $S_m = (S_{max} - S_{min})/2 = S_{max}/2$. The stress ratio R, which is defined as the ratio between S_{min} and S_{max}, assumes then a value equal to 0.

Fatigue behavior in metals and composites differs significantly due to their distinct material structures and failure mechanisms. The two different approaches to fatigue analysis are presented below.

5.5.1. Fatigue analysis for metals

Fatigue in metals generally starts with crack initiation, often at surface flaws or stress concentrations. These cracks propagate over time until the material ultimately fails. In fact, metal fatigue refers to the unexpected failure of metal parts by progressive fracturing while in service and is directly related to the number of stress cycles undergone by a part and the level of stress imposed on the part. The presence of an endurance limit in some metals means they can theoretically endure an infinite number of cycles if the stress is below a certain threshold.

The S-N curve (or Wöhler curve) is commonly used in metal fatigue analysis to predict how long a material can withstand repeated stress before failing. It consists in a graphical representation of the relationship between the cyclic stress amplitude S_a and the number of cycles to failure N [11]. This is due to the fact that, in metals, the stress amplitude is more decisive for the failure life then for example the mean stress. The S-N curve is usually obtained as a result of a number of fatigue tests at different stress levels. In an approximate approach, the fatigue S-N curve for a specific component can be reconstructed based on the ultimate strength of the material and the fatigue limit.

As presented previously, the mean stress S_m of the load cycle is not zero, meaning that the mean stress effect has to be accounted for [11]. In fact, for the same stress amplitude S_a, a positive mean stress S_m > 0 implies that the maximum stress applied S_{max} is greater than when the mean stress $S_m = 0$. In other words, an increase in mean stress S_m at constant stress amplitude S_a results in a higher maximum stress S_{max}, which leads to a shorter fatigue life and a lower fatigue limit. In order to account for the mean stress effect, it is possible to apply the Goodman relation presented in Equation 5.30 [11].

$$S_N = (S_N)_{S_m=0}\left(1 - \frac{S_m}{S_u}\right) \tag{5.30}$$

where S_N is the fatigue strength at N cycles for the loading case considered, $(S_N)_{S_m=0}$ is the fatigue strength at N cycles for the case of completely reversed loading, S_m is the mean stress, and S_u is the ultimate strength of the material. For the specific case of a loading cycle characterised by a stress ratio $R = 0$, stress amplitude S_a and mean stress S_m always coincide. This allows to rewrite the Goodman relationship as presented in Equation 5.31.

$$S_N = \frac{(S_N)_{S_m=0} S_u}{S_u + (S_N)_{S_m=0}} \tag{5.31}$$

In order to obtain an approximate S-N curve for the metal component under considerations, the following parameters need to be defined:

- *Upper asymptote:* it relates to the ultimate strength of the material S_u. The value of the upper asymptote taking into account the mean stress effect is calculated substituting S_u for $(S_N)_{S_m=0}$ in the Goodman relation 5.31. The resulting value for the upper asymptote is equal to $S_u/2$.
- *Lower asymptote:* it represents the fatigue limit S_f. If no experimental data are available, the fatigue limit can be approximated using the linear relation with the ultimate strength: $S_f = \alpha_m S_u$, where α_m is a coefficient that depends on the material. The value of the lower asymptote taking into account the mean stress effect is calculated substituting $S_f = \alpha_m S_u$ for $(S_N)_{S_m=0}$ in the Goodman relation 5.31. The resulting value for the lower asymptote is equal to $(\alpha_m S_u)/(\alpha_m + 1)$.

Based on what has been discussed so far and standard practices for this type of graph [11], the approximated fatigue S-N curve of the metal component under investigation will look something like Figure 5.4. Having then defined the approximate graph, it is sufficient to check which number of cycles N corresponds to the stress amplitude S_a to which the component is subjected in order to have an indication of the fatigue life of the component.

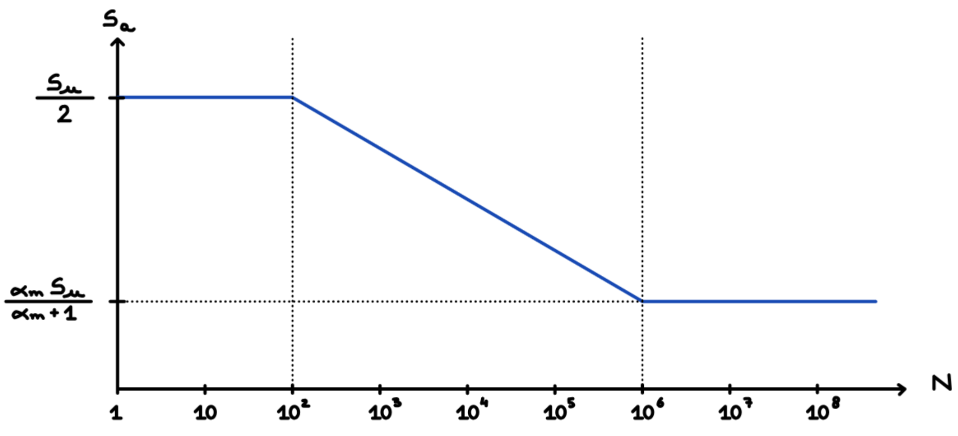

Figure 5.4: Approximated fatigue S-N curve

5.5.2. Fatigue analysis for composites

Composites are inhomogeneous and anisotropic materials, and their fatigue behaviour is influenced by multiple factors, including the interaction between the fibers and the matrix, fiber orientation, and matrix properties. Fatigue failure in composites is more complex and can involve several modes such as matrix cracking, fiber-matrix debonding, fiber breakage, and delamination (separation of layers). Damage typically accumulates in various forms throughout the material rather than a single dominant crack. Fatigue in composites is defined as the phenomena/mechanisms by which fluctuating loads induce permanent structural changes through the initiation and propagation of damages, including a loss of material stiffness and/or load carrying capability which may lead to structural failure below the monotonic failure stress [11].

Fatigue prediction in composites is more complex and less standardized due to the multi-mode damage mechanisms. Methodologies diverge into a range of different approaches, many of which are empirical, and can be categorised in the following groups [11]:

- *Stress life methods (S-N curves) and constant life diagrams*: the *S-N curve* for composites is used to predict how long a material can withstand repeated stress before failing and consists in a graphical representation of the relationship between the cyclic maximum stress S_{max} and the number of cycles to failure N [11]. It is a highly empirical approach, depending on the specific characteristics of the material considered. The *constant life diagram* is the same representation as Goodman and Gerber diagrams are for metals. The amplitude or stress range is plotted against the mean or maximum stress, where the individual curve represent the same failure life.
- *Damage mechanics methods*: these methods describe the consequence of damage that developed on the mechanical response of material and structure. The focus is not on the understanding the individual damage phenomena, but on providing predictive capabilities.
- *Fracture mechanics methods*: the aim of this kind of approach is to describe the growth of physical damage modes.
- *Residual strength methods*: this methods introduce the fatigue modulus parameter, which is defined by the slope of a line between the origin of the strain-stress graph and the applied stress and resultant strain at a specific load cycle. This parameter is convenient for the purpose of predicting the residual strength of a composite structure containing fatigue damage.

5.6. Emergency landing scenario

As presented in section 5.1, one of the requirements for the hydrogen tank is to be able to remain functional in the event of a controlled crash scenario. It is then important to validate that the support system is adequately designed to withstand emergency conditions without compromising the structural integrity of the hydrogen tank. This encompasses both static and dynamic emergency landing conditions: the static conditions involve ultimate inertia forces acting on the inner vessel independently of the surrounding structure, while the dynamic conditions involve an acceleration spectrum applied to the outer vessel.

5.6.1. Ultimate inertia forces

This analysis is focused on determining displacements and stresses experienced by the support system under emergency landing static conditions. The final objective is to ensure that displacements and stresses within the support system remain within safety limits ensuring that both the contact between inner and outer vessels and the failure of the supports are avoided.

In this study, the inner and outer tanks are considered as rigid bodies. The outer tank is considered fixed and immovable, while the inner tank is supported by the support system and subjected to the ultimate inertia forces. This simplification ignores the flexible-body modes of the tanks and does not account for the potential deformations and vibrations that could occur in a more realistic scenario. This is important because, depending on the distribution of supports and the properties of the inner vessel, these flexible-body modes could have natural frequencies that resonate with the frequency of the dynamic loads. Such resonance could become critical, leading to potentially dangerous oscillations or structural failures. Therefore, while the rigid-body assumption simplifies the analysis, it does so by neglecting the possibility of resonance effects, which could be significant depending on the system's characteristics. Additionally, this assumption is also applied in the dynamic model used to evaluate the acceleration spectrum load case. This approach is valid for an initial assessment, but further analysis would be required to fully understand the impact of the ultimate inertia forces and dynamic loads on a system that includes flexible-body effects.

Based on the general emergency landing provisions (regulated in chapters 25.561 25.563 of CS-25 and chapter 25.561 25.563 of FAR-25), the support system shall be able to properly restrain the inner vessel under all loads up to the ultimate forces (which are acting separately) presented in Equations from 5.32 to 5.36.

$$F_{upward} = 3.0 \cdot g \cdot m_{inner} \tag{5.32}$$

$$F_{forward} = 9.0 \cdot g \cdot m_{inner} \tag{5.33}$$

$$F_{sideward} = 4.0 \cdot g \cdot m_{inner} \tag{5.34}$$

$$F_{downward} = 6.0 \cdot g \cdot m_{inner} \tag{5.35}$$

$$F_{rearward} = 1.5 \cdot g \cdot m_{inner} \tag{5.36}$$

where g is the gravity acceleration $g = 9.81\ m/s^2$ and m_{inner} is the mass of the inner vessel, obtained by summing up the mass of the aluminum vessel, the mass of the piping, and the hydrogen mass contained inside the tank (fill rate $FR = 0.95$ is assumed).

As an initial step, the support system configuration to be analysed must be defined. It can consist of individually defined supports placed in specific locations and orientations or groups of supports arranged in ring or half-ring configurations around the inner vessel.

Subsequently, the equivalent stiffness of the whole support system in each of the three direction (global coordinates system: x_g, y_g, and z_g) must be calculated. This involves summing up the equivalent stiffness values of the individual supports based on their orientation and characteristics.

With the positioning options of the supports established, the ultimate inertia forces that could be acting on the free end of the generic i support can be classified into two categories: forces lying in the plane defined by the y_i and z_i axes and forces perpendicular to this plane, which means forces in the x_i direction. The process of calculating equivalent stiffness of a specific support therefore varies from case to case based on the direction considered.

Equivalent stiffness in direction j lying in the plane defined by directions y_i and z_i

Consider Figure 5.5: a generic support i characterised by the coordinate system $x_{s,i}$, $y_{s,i}$, $z_{s,i}$ and a force F_j applied to the free end of the support in direction j which lies in the $y_{s,i} - z_{s,i}$ plane.

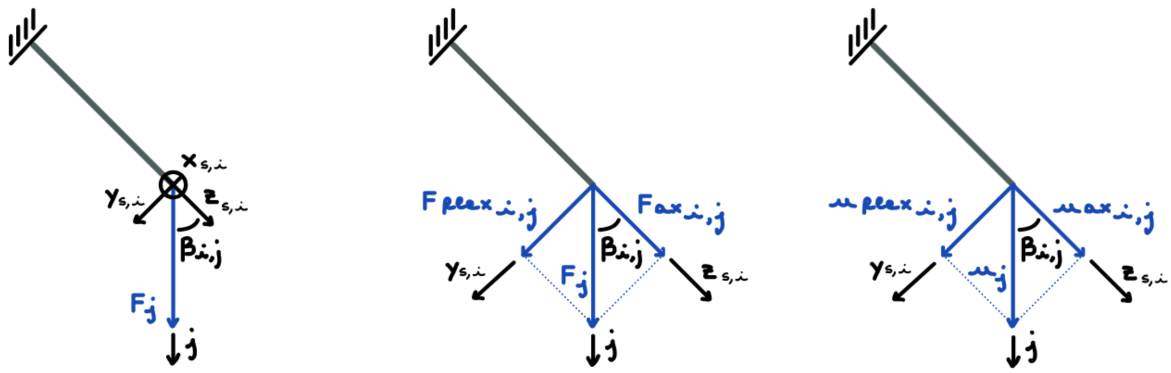

Figure 5.5: Decomposition of applied force and consequent displacement for a generic support

The induced displacement u_j and the applied force F_j (both in direction j) are related by the equation $F_j = k_{eq,i,j} u_j$ where $k_{eq,i,j}$ is the equivalent stiffness of the support i in direction j.

The force F_j can be decomposed into the axial component $F_{ax_{i,j}}$ and the flexural component $F_{flex_{i,j}}$ using basic trigonometric relations. Furthermore, $F_{ax_{i,j}}$ and $F_{flex_{i,j}}$ can be expressed as the product of the respective stiffness and displacement in the axial z_i and flexural y_i directions. To determine the displacements in the axial $z_{s,i}$ and flexural $y_{s,i}$ directions (denoted as $u_{ax_{i,j}}$ and $u_{flex_{i,j}}$ respectively), basic trigonometric relations should be again applied. These relationships are expressed in the

Equations 5.37 and 5.38.

$$F_{ax_{i,j}} = F_j cos(\beta_{i,j}) \qquad F_{ax_{i,j}} = k_{ax} u_{ax_{i,j}} = k_{ax} u_j cos(\beta_{i,j}) \tag{5.37}$$

$$F_{flex_{i,j}} = F_j sin(\beta_{i,j}) \qquad F_{flex_{i,j}} = k_{flex} u_{flex_{i,j}} = k_{flex} u_j sin(\beta_{i,j}) \tag{5.38}$$

where $\beta_{i,j}$ is the angle defined between the axial direction of the i^{th} support $z_{s,i}$ and the direction j.

Putting together the information gathered, it is possible to express the equivalent stiffness of the generic support i in direction j lying in the plane defined by directions $y_{s,i}$ and $z_{s,i}$ according to the Equation 5.39.

$$\begin{aligned} k_{eq,i,j} &= \frac{F_j}{u_j} = \frac{\sqrt{F^2_{ax_{i,j}} + F^2_{flex_{i,j}}}}{u_j} = \frac{\sqrt{(k_{ax} u_j cos(\beta_{i,j}))^2 + (k_{flex} u_j sin(\beta_{i,j}))^2}}{u_j} = \\ &= \sqrt{(k_{ax} cos(\beta_{i,j}))^2 + (k_{flex} sin(\beta_{i,j}))^2} \end{aligned} \tag{5.39}$$

Equivalent stiffness in direction j coincident with the $x_{s,i}$ direction of the support

In the case where direction j coincides with the $x_{s,i}$ direction of support i, the stiffness characteristics that come into play are exclusively the flexural ones. Consequently, the equivalent stiffness in direction j coincident with the $x_{s,i}$ direction of the support i $k_{eq,i,j}$ is equal to k_{flex} (Equation 5.40).

$$k_{eq,i,j} = k_{flex} \tag{5.40}$$

Total resulting displacement

The overall displacement that the inner vessel will experience when ultimate inertia forces are individually applied depends then on the modulus of the applied force and the equivalent stiffness of the system in that direction, as expressed by Equation 5.41.

$$d_{tot,j} = \frac{F_{applied,j}}{k_{eq,j}} = \frac{F_{applied,j}}{\sum_{i,1}^{N} k_{eq,i,j}} \tag{5.41}$$

where $d_{tot,j}$ is total displacement experienced by the inner vessel in direction j, F_j is the applied force in direction j, and $k_{eq,j}$ is the equivalent stiffness of the whole support system in direction j obtained by summing up the equivalent stiffness values of the N individual supports $k_{eq,i,j}$.

Analysis of stresses in the supports

In order to evaluate the stresses in the supports due to the total displacement experienced by the inner vessel in direction j, it is necessary to decompose the total displacement $d_{tot,j}$ into the displacement components along the directions x_s, y_s and z_s of each support. After determining the displacements u_s, v_s and w_s for each support at the contact point, it is possible to apply Navier's formula for beam normal stress as previously presented in subsection 5.4.1, Equation 5.7.

Since one of the requirements of the design is to avoid failure of the supports during an emergency landing scenario, it is necessary to check that the stress values in all supports for all ultimate inertial loading conditions remain below the ultimate strength of the material selected for the supports.

5.6.2. Acceleration spectra

To verify the dynamic load condition, a drop test can be conducted on the section of the fuselage containing the hydrogen tanks, in accordance with the packing strategies outlined in section 2.8. This type of test was thoroughly explored in Yi-Hsiu Wu's master's thesis project [82]. Among the various results produced, the test provided valuable data on the acceleration spectra measured at the tank heads, both at and near the center point of the domes of the external vessel. This location is crucial because it is where the tanks connect to the fuel systems. The results from Yi-Hsiu Wu's study serve as the foundation for understanding how the impulse generated by the drop test on the fuselage is transmitted to the internal components of the external vessel: the internal vessel and its support system.

The acceleration inputs that the different tanks experience during an emergency landing scenario in which the aircraft experiences a change in downward vertical velocity depend on which packing and support strategy for positioning the tanks in the fuselage is adopted. For the following analysis, it was decided to consider only the worst-case condition for each packing solution, i.e. the acceleration spectrum characterised by higher acceleration peaks. This is due to the assumption that the acceleration spectrum with the highest peak is the worst for the tank. These are presented in Figure 5.6 for the lateral square packing (LSP) retrofit design, the lateral hexagonal packing (LHP) retrofit design, and the longitudinal circle packing (LCP) retrofit design respectively.

By analyzing these acceleration spectra, it is possible to gain insights into the dynamic response of the tanks and evaluate the effectiveness of the support system in mitigating the impact loads. This analysis is essential for ensuring the structural integrity and safety of the hydrogen storage system under dynamic loading conditions.

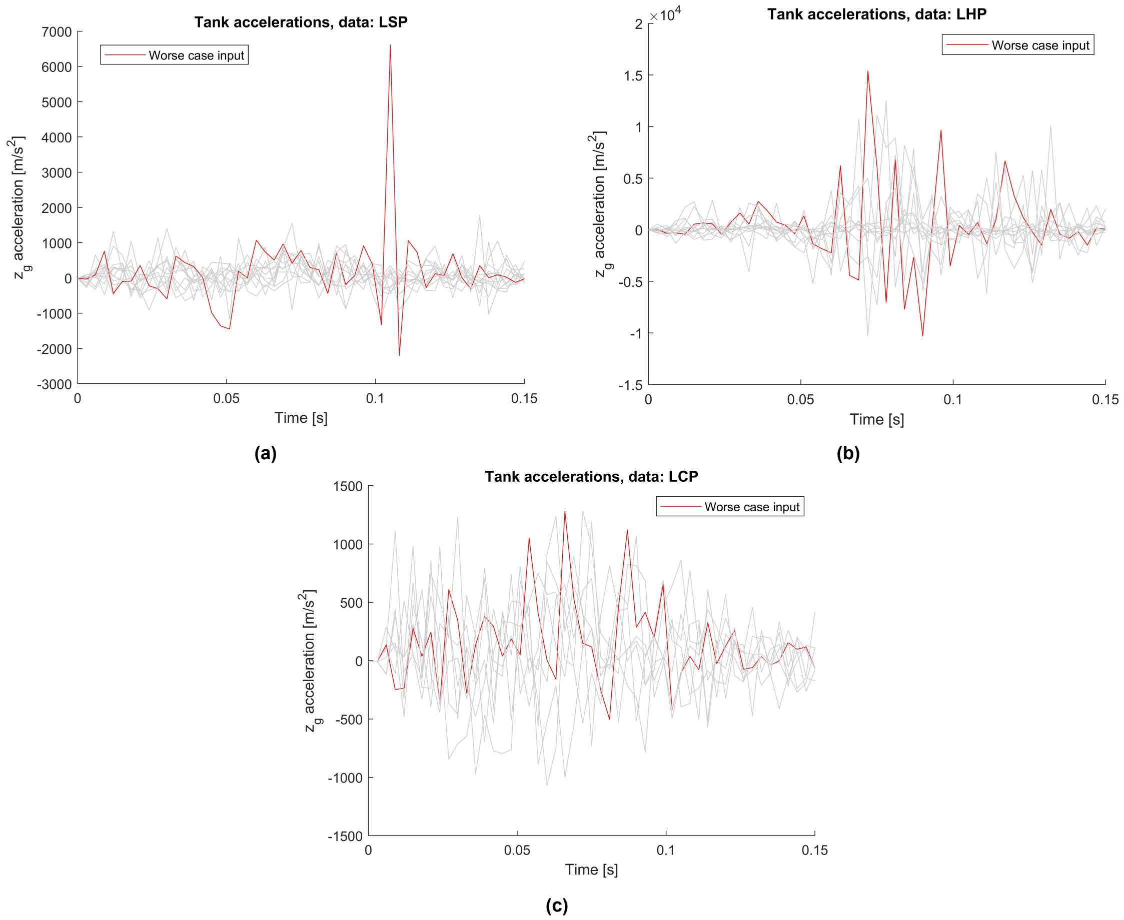

Figure 5.6: Acceleration spectra for different retrofit design

The system consisting of external vessel, inner vessel and respective support system can be modelled as presented in the Figure 5.7.

In the presented scheme, m_i is the mass value of the mass point representing the inner vessel, k is the stiffness value of the spring that represents the support system (equivalent stiffness value in the vertical direction), c is the damping coefficient of the support system, the base represents the outer vessel, $z_1(t)$ represents the displacement of the outer vessel (considered as rigid body) over time due to impact, $z_2(t)$ represents the displacement of the inner vessel (considered as rigid body) over time due to impact. The difference between $z_1(t)$ and $z_2(t)$ is $\delta(t)$: the displacement imposed on the support system over time.

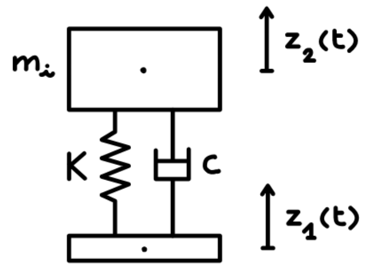

Figure 5.7: Model of the tank for evaluation of acceleration spectrum

The solution to this system is part of the material in the 'Stability and Analysis of Structures II' course taught at the Department of Aerospace Structures and Materials, Delft University of Technology [22]. The expression for the relative displacement between inner and outer vessel over time $\delta(t)$ in this specific system is then expressed in Equations from 5.42 to 5.45.

$$\delta(t) = \begin{cases} 0 & \text{if } t < t_n \\ p_0 h(t-t_n) & \text{if } t \geq t_n \end{cases} \tag{5.42}$$

$$h(t-t_n) = \frac{1}{\omega_d} e^{-\zeta\omega_n(t-t_n)} \sin\omega_d(t-t_n) H(t-t_n) \tag{5.43}$$

$$\omega_n = \sqrt{\frac{k}{m_i}} \tag{5.44}$$

$$\omega_d = \omega_n\sqrt{1-\zeta^2} = \omega_n\sqrt{1-\left(\frac{c}{c_c}\right)^2} = \omega_n\sqrt{1-\left(\frac{c}{2m_i\omega_n}\right)^2} \tag{5.45}$$

where p_0 is the assumed acceleration impulse that happen at the respective time t, t_n is the threshold time after which the system starts responding, and $h(t-t_n)$ is the impulse response function of the system (Equation 5.43), ω_n is the natural frequency of the system (Equation 5.44), k is the stiffness value of the spring that represents the support system, m_i is the mass value of the mass point representing the inner vessel, ω_d is the damped natural frequency of the system (Equation 5.45), ζ is the damping factor, c is the damping coefficient, c_c is the critical damping coefficient, and $H(t-t_n)$ is the Heaviside step function which ensures that the impulse response starts at $t = t_n$.

Analysis of stresses in the supports

In order to evaluate the stresses in the supports over time due to the displacement imposed on the support system over time $\delta(t)$, it is necessary to assess the situation instant by instant.

For every time instant t_i, it is necessary to decompose the total displacement $\delta(t_i)$ into the displacement components along the directions x_s, y_s and z_s of each support. After determining the displacements u_s, v_s and w_s for each support at the contact point and at time instant t_i, it is possible to apply Navier's formula for beam normal stress as previously presented in section 5.4.1, Equation 5.7.

For a complete analysis of the entire impulse interval, all the time instants must be analysed. Since one of the requirements of the design is to avoid failure of the supports during an emergency landing scenario, it is necessary to check that the stress values in all supports throughout the impact timeframe remain below the ultimate strength of the material selected for the supports.

5.7. Design methodology for inner vessel support structure

The design methodology for the inner vessel support structure is outlined in the flowchart in Figure 5.8. The presented approach is systematic and iterative, bringing together the elements previously introduced individually in subsection 5.4.1, section 5.5, and section 5.6. Earlier, the focus was on analyzing various critical scenarios that the tank must endure throughout its operational life. Now, this design methodology demonstrates how those insights are integrated into a cohesive preliminary design process, addressing the most critical aspects of the tank's lifecycle. This ensures that all key factors are considered within a unified framework for a reliable and robust tank design.

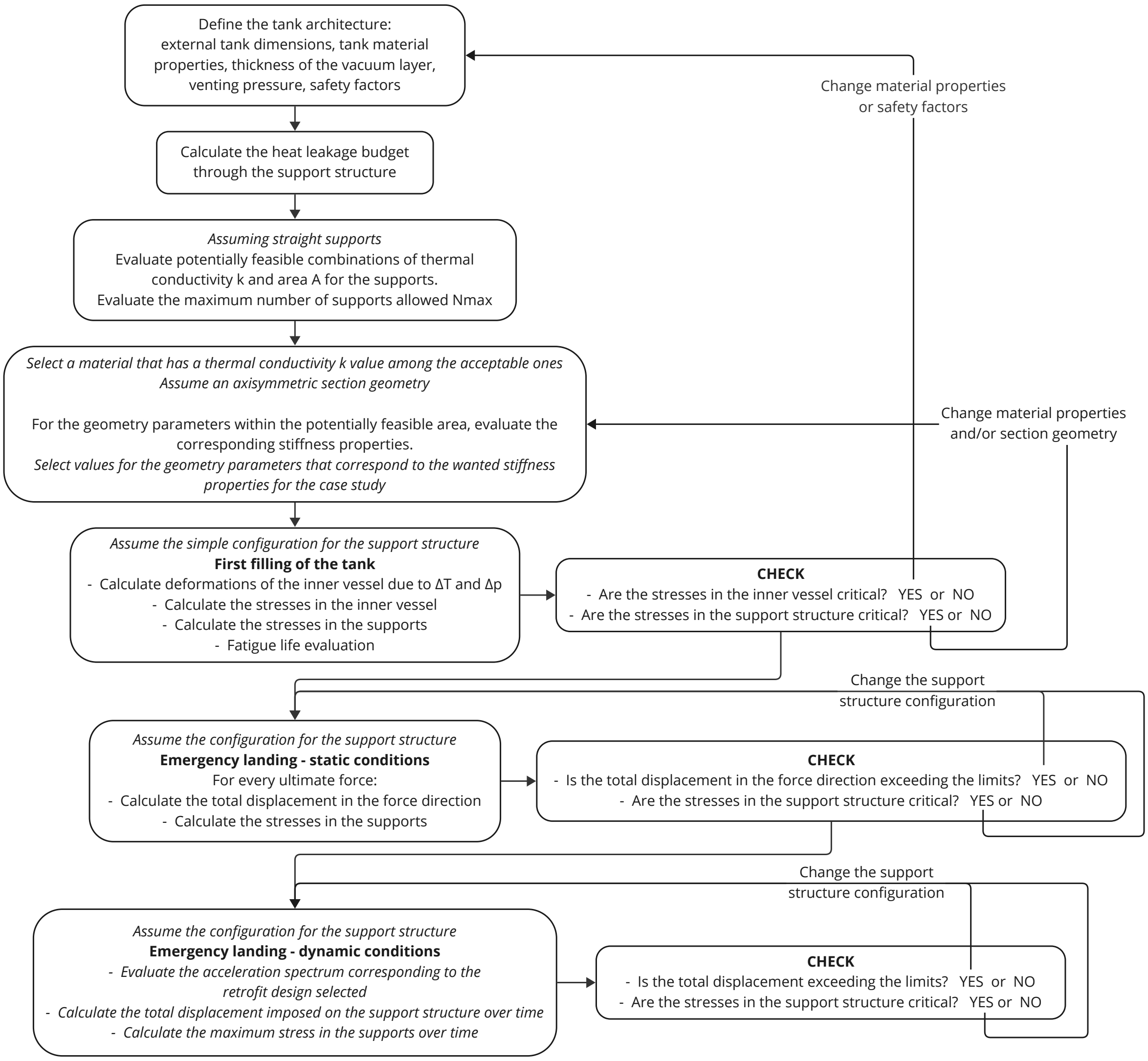

Figure 5.8: Flow chart - Design methodology for inner vessel support structure

The process begins by defining key architectural elements, including external tank dimensions, tank material properties, vacuum layer thickness, venting pressure, and safety factors. These initial parameters guide the subsequent analyses. Next, the heat leakage budget through the support structure is calculated to ensure the dormancy time requirement is met.

Once thermal considerations are addressed, the analysis proceeds by assuming a straight support configuration so that the length of the individual support equals the thickness of the insulation layer. This assumption is introduced to reduce the number of variables and simplify the problem. Various feasible combinations of thermal conductivity and cross-sectional area for the support design are evaluated, determining the maximum number of supports permissible for every combination. With thermal and geometric constraints identified, a material with acceptable thermal conductivity has to be selected. The stiffness properties of the supports are then analyzed, with particular focus on stiffness values that align with the requirements of the case study. Adjustments to material properties or geometry may be made to meet the desired criteria.

The design procedure is then tested against multiple loading scenarios, starting with the simplest configuration for the support structure (Figure 5.9) which allows for the establishment of baseline stiffness properties. In this phase, the first filling of the tank is analyzed by evaluating the deformations of the inner vessel due to thermal and pressure differences. Stresses in both the inner vessel and the supports are calculated, followed by a fatigue life evaluation. If critical stress levels are detected, iterations are performed by changing the material properties, safety factors, or section geometry. Afterward, the structure is tested under emergency landing conditions, both for static and dynamic scenarios. In static conditions, the total displacement and stresses are evaluated to ensure compliance with design limits. Similarly, for dynamic conditions, the acceleration spectrum is considered, and the maximum stress and displacement over time are calculated. The design proceeds through iterative checks and balances, ensuring that each configuration is evaluated, and modifications are made when necessary to optimize performance. This iterative methodology ensures that the final design is robust, compliant with critical safety standards, and optimized for both operational and emergency conditions.

5.8. Results and discussion

Consistently with what is described in the methodology (section 5.4), the inner vessel and the support system have been analysed in order to verify their behaviour in the most critical conditions that may occur during operational life.

In the analyses performed, the value of certain parameters can be decided quite arbitrarily. The first thing to do is therefore to define acceptable ranges of values and, in order to reduce the amount of possible combinations, one can decide to assume a specific value which is then maintained in the analyses. The parameters in question are as follows:

- *External dimensions of the tank:* the possible external dimensions of the tank (diameter and length) are the 3 solutions proposed by Yi-Hsiu Wu in his master thesis [82] and depend on the packing strategy selected. These are presented in table 5.2.
- *Thickness of the vacuum layer t_{vacuum}:* As discussed in section 4.3.1, the thickness of the vacuum insulation layer significantly affects the performance of the tank. Determining the optimal thickness is complex and depending on the specific design requirements. However, an optimal range can be established that ensures both satisfactory cruise time and dormancy time and, at the same time, respects the constraints imposed. Within this range, selecting the exact thickness can be somewhat flexible. For each possible external tank size, the evaluated ranges are obtained from the the results presented in section 4.3.1 and are presented in table 5.4.

Table 5.4: Evaluated thickness ranges for vacuum insulation layer by external tank size

Option number	Min t_{vacuum} [m]	Max t_{vacuum} [m]
1	0.03	0.05
2	0.03	0.05
3	0.04	0.10

- *Venting pressure P_{vent}:* As discussed in section 3.2, the venting pressure is a crucial parameter in tank design as it has a significant impact on the maximum achievable dormancy time and on the sizing process of the inner vessel, and must be compatible with the characteristics of the rest of the fuel system. The range that has been considered acceptable for venting pressure is between 3 and 5 bar.
- *Thickness of the inner vessel t_{inner}:* As discussed in section 3.1, the minimum required thickness of shell under internal pressure is determined following the ASME standards guidelines [13]. The actual thickness selected for the inner vessel can be calculated by multiplying the minimum required value by a safety factor SF_t whose value can be defined depending on the design strategy adopted.
- *Properties of the single support:* The support structural properties of interest in the analysis are mainly axial and flexural stiffness (k_{ax} and k_{flex} respectively). These values depend on the geometrical and material characteristics of the support as described in the formula 5.1 in section 5.3. The relevant parameters that should be set are the Young's modulus E_s, the length of the support L_s, and the geometrical properties of the cross-sectional area which define both the area A_s and the second moment of inertia about the neutral axis of the beam I_s. To reduce the number of options during the first analyses, a circular ring cross-sectional area is going to be considered. The important parameters that define the geometry are the radius R_s and the thickness t_s. The values of the area A_s and the second moment of inertia about the neutral axis of the beam I_s are calculated using Equation 5.46 and 5.47 respectively.

$$A_s = \pi t_s \left(2R_s - t_s\right) \tag{5.46}$$

$$I_s = \frac{\pi t_s}{4}\left(4R_s^3 - 6R_s^2 t_s + 4R_s t^2 - t_s^3\right) \tag{5.47}$$

The minimum allowed thickness value t_s is set to 0.001 m, in order to avoid compromising the manufacturability of the component. A minimum allowable radius value R_s of 0.002 m can therefore realistically be assumed. Considering the dimensions of the space between the inner and outer vessel and the fact that the support is modelled as a beam, it is realistic to assume that the maximum radius considered will be 1/4 the length of the support (t_{vacuum}). This results in a minimum area value of approximately $10^{-5}\ m^2$ and a maximum area value depending on t_{vacuum}. Furthermore, based on the considerations presented in section 5.3.1 regarding the phenomenon of local buckling, the ratio between thickness t_s and radius R_s is subject to a lower limit which depends on the characteristics of the material. For each radius R_s, the minimum allowed thickness value is presented in Equation 5.48.

$$t_{s,min} = R_s \frac{\sigma_{y,s}\sqrt{3(1-\nu_s^2)}}{E_s} \tag{5.48}$$

where $\sigma_{y,s}$ is the yield stress of the material selected for the supports, ν_s and E_s are respectively the Poisson's ratio and the Young's modulus of the material selected for the supports. Furthermore, with regard to thermal performance of the support structure, the material parameter of interest is the thermal conductivity $k_{support}$.

- *Location of the supports:* The positioning of supports must also be defined before carrying out an analysis. The choice is rather arbitrary, but the basic rule is to obtain an axisymmetric composition. To reduce the number of options during the first analyses, it is possible to consider a simple configuration comprising 2 horizontal (in blue), 6 vertical (in green) and 6 lateral supports (in light blue) as presented in the Figure 5.9.

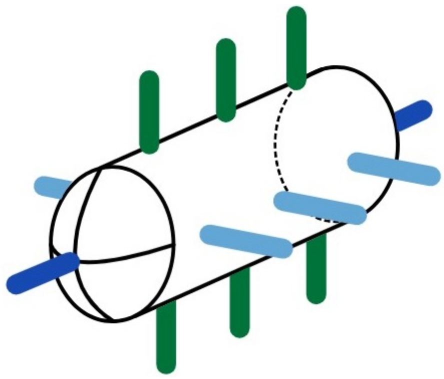

Figure 5.9: Simple configuration of the support system

Three set of analysis parameters can be then defined based on the three retrofit design presented in section 2.8. The external tank dimensions considered are directly associated with the packing strategy considered: option 1 for LSP (lateral square packing), option 2 for LHP (lateral hexagonal packing), and option 3 for LCP (longitudinal circle packing) (reference to table 5.2). For each retrofit design, the other parameters are chosen according to the guidelines presented. The values assumed are summarised in the table 5.5.

Table 5.5: Assumed parameters for the analysis

Retrofit design	External dimentions	t_{vacuum}	P_{vent}	SF_t	Support section
LSP	option 1	0.04 m	4 bar	1.5	Circular
LHP	option 2	0.04 m	4 bar	1.5	Circular
LCP	option 3	0.06 m	4 bar	1.5	Circular

The variables of the analysis are thus the size of the circular ring cross-sectional area of the individual support, the material selected for the supports, and their location around the inner vessel.

Referring to the conclusions presented in the thesis project carried out by TU Delft master's student Yi-Hsiu Wu [82], the LCP design has the greatest potential for retrofitting the baseline aircraft, primarily due to its superior crashworthiness and extended range, both critical factors for the operation of the aircraft after the retrofit. In the following discussion, therefore, the retrofit design under investigation will be the longitudinal circle packing. In addition to the parameters defined in the table 5.5, the other parameters defined for the case study are as follows: N_{MLI} = 30, Argon as residual gas, P_{vacuum} = 10^{-3} Pa, T_{ext} = 305 K, and T_{int} = 20.26 K.

5.8.1. Evaluation of the characteristics of the support structure

Referring to the methodology presented in section 5.3.1, the fist step in the analysis is to limit the design possibilities to only combinations of support structure variables capable of guaranteeing compliance with the dormancy time requirement. In this perspective, it is crucial to first define the maximum allowable heat inflow through the supports that still allows to meet the dormancy time requirement (budget for the heat leakage through the support structure $\dot{Q}_{supports,max}$). To achieve this, the dormancy time is evaluated across various iterations of the original design obtained by gradually increase the initial value of the heat leakage through the support structure until the version that corresponds to the minimum acceptable dormancy time is identified (reference to the method presented in section 4.3.5).

The results of this analysis are presented in Figure 5.10. It is then possible to extrapolate the maximum multiplication factor $f_{q,max}$ that still allows to meet the dormancy time requirement for the specific tank design. Multiplying the original value of $\dot{Q}_{supports}$ by the factor $f_{q,max}$ gives the $\dot{Q}_{supports,max}$. The results are summarised in table 5.6.

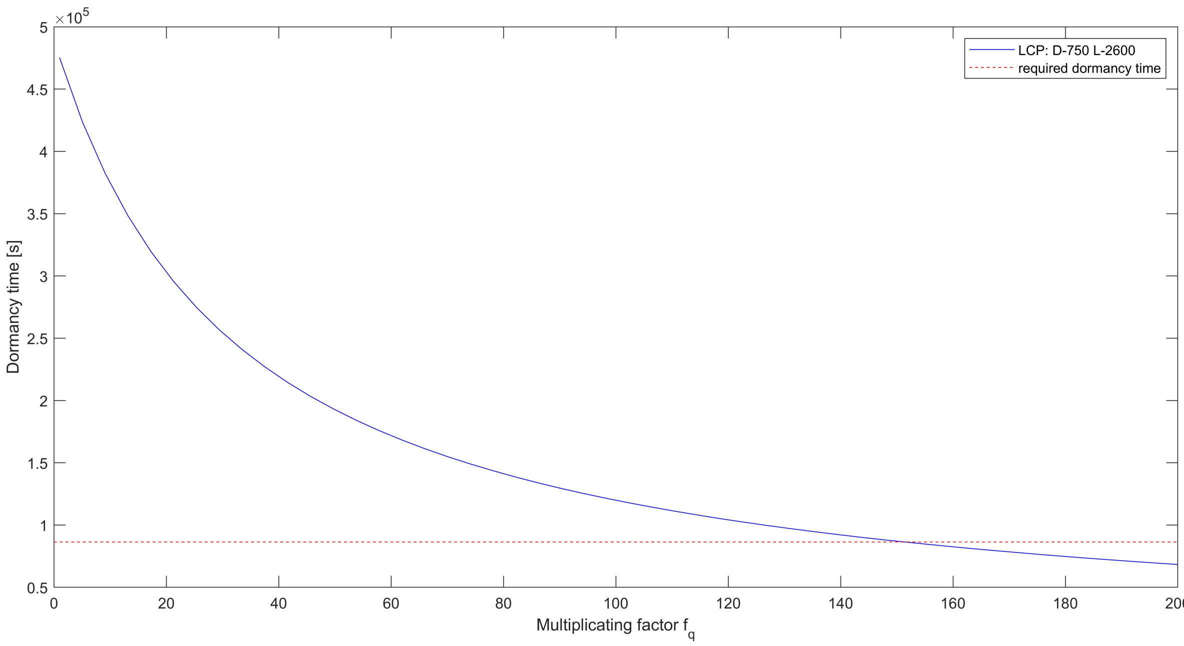

Figure 5.10: Effect of increased heat leak through the support system on dormancy time

Table 5.6: Values of $\dot{Q}_{supports}$, $f_{q,max}$ and $\dot{Q}_{supports,max}$ for the tank design evaluated

$\dot{Q}_{supports}$ **[W]**	$f_{q,max}$	$\dot{Q}_{supports,max}$ **[W]**
0.1715	151	25.8965

Based on the value of $\dot{Q}_{supports,max}$, the feasibility study can be carried out by analysing what is the maximum number of supports $N_{s,max}$ allowed for all the combinations of cross-sectional area of the supports $A_{support}$ and thermal conductivity of the material considered $k_{support}$. The range considered for the thermal conductivity is rather wide in order to give a general overview of all the materials (range between 0.01 W/mK to 1000 W/mK). The cross-sectional area values considered are between the minimum area value 10^{-5} m^2 and the maximum area value $7 \cdot 10^{-4}$ m^2 (considering an external radius equal to 1/4 of t_{vacuum} and the minimum internal radius of 0.001 m). The results of this analysis are presented in Figure 5.11 restricting the field to the area where acceptable combinations are present.

A certain combination can be considered potentially feasible if the maximum number of supports allowed to respect the heat leakage budget is greater than or equal to 2. For every thermal conductivity value considered, it is possible to know what is the maximum area of the cross-section that could lead to a feasible design from the perspective of thermal performance, i.e. that area value which corresponds to a maximum number of supports of 2. For lower area values, a higher value of $N_{s,max}$ is expected.

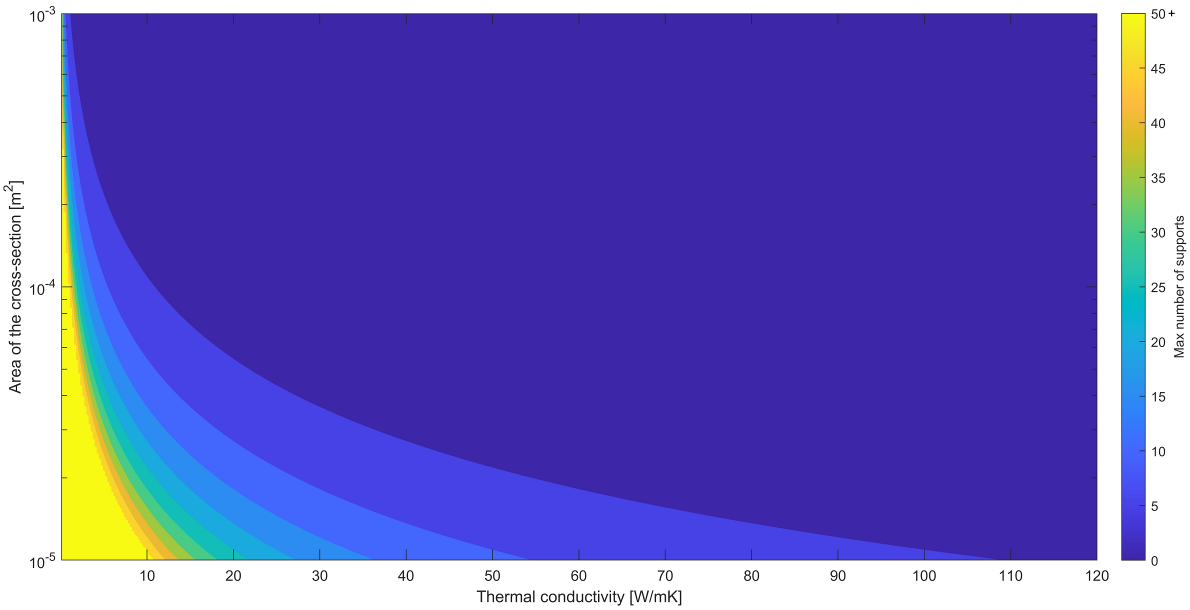

Figure 5.11: Feasibility study for combinations of $A_{support}$ and $k_{support}$

The range of thermal conductivity values within the feasibility area is between 0.01 W/mK and 109 W/mK, while the range of cross-sectional area values within the feasibility area is between 10^{-5} m^2 and 10^{-3} m^2. At this point, the potentially feasible combinations of material and section geometry are countless. The choice of starting point for the analysis is strictly dependent on the case study considered and the requirements and constraints associated with it.

For this specific case, it has been decided to start from the choice of material, evaluating options considered potentially akin to the specific application. Referring to the chapter 2.5 of the literature study, the material selected for the following discussion is the G-10 CR, a high-pressure glass-reinforced epoxy laminate. It is a version of G-10 specifically designed for enhancing the performance in low-temperature environments for cryogenic applications and characterised by extremely high strength and high dimensional stability over temperature. The material characteristics that are relevant to the following analysis are summarised in table 5.7 [62] [42].

Table 5.7: G-10 CR material properties

Young's modulus E [Pa]	$2.8 \cdot 10^{10}$
Poisson's ratio ν	0.2
Ultimate strength S_u [Pa]	$4.7 \cdot 10^{8}$
Thermal conductivity k [W/m*K]	0.25

For the specific thermal conductivity value of the material G-10 CR, the range of cross-sectional area values A_s that correspond to a maximum number of supports greater than or equal to 2 spans the entire range of considered area values. This confirms that for the selected material, every cross-sectional area value within the evaluated range is potentially feasible. Moreover, since the maximum number of supports allowed is consistently greater than 14 for the selected material, it is always possible to evaluate the simple support structure configuration (Figure 5.9).

The number of potentially feasible combinations of A_s and N_s allows for a wide selection of possible support characteristics that can be tailored to meet the other design requirements. It is generally advisable to select a cross-sectional area that corresponds to a sufficiently large maximum number of supports, in order to avoid being limited in the choice of support structure configurations afterwards.

It is now interesting to assess which combinations of radius R_s and thickness t_s fall within the permitted area range. As far as the radius is concerned, it has already been specified that the permitted range is realistically between 0.002 m and 0.015 m. Furthermore, for each radius value, the corresponding thickness must meet the requirements to avoid the phenomenon of local buckling in the elastic regime (Equation 5.48). The results of the study of combinations of R_s and t_s are presented in Figure 5.12.

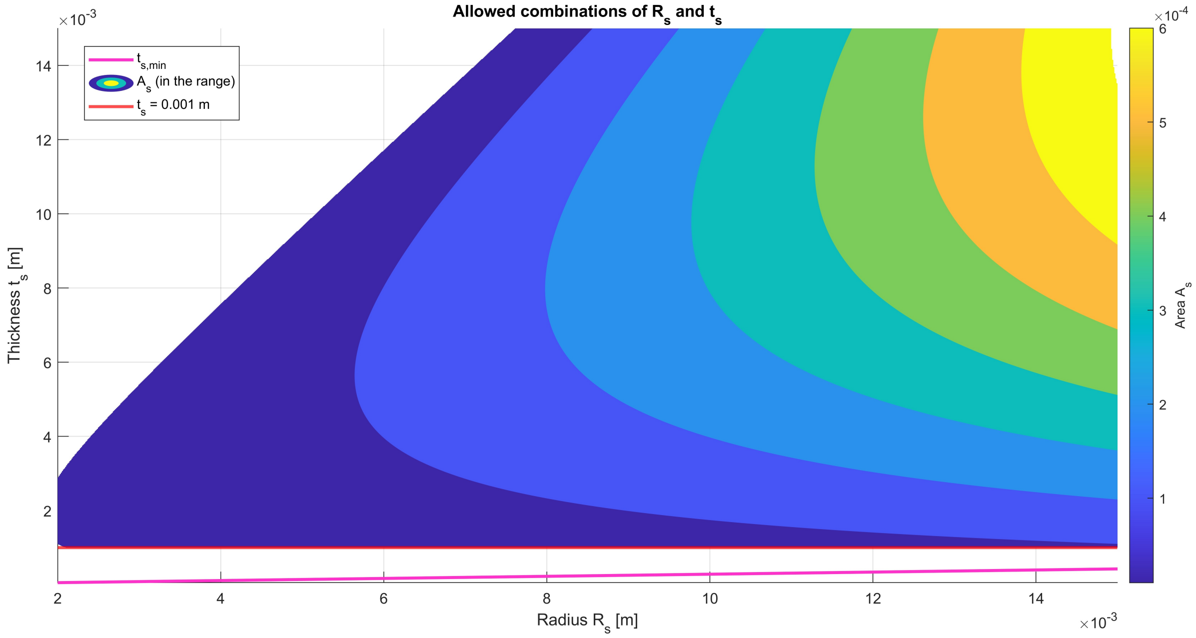

Figure 5.12: Allowed combinations of R_s and t_s

First of all, it can be seen that, for the range of radii considered, the minimum thickness requirement to avoid local buckling in the elastic regime is less stringent than the requirement to have a thickness greater than 0.001 m (for practical reasons related to manufacturability).

Furthermore, not all combinations of radius and thickness considered give an area within the permitted range. There remains, however, a wide choice of permissible combinations. At this point, the focus should be on identifying the combination of thickness and radius that defines satisfactory characteristics of the individual support. This combination should ensure that the support can accommodate the displacement of the tank subjected to changes in temperature and pressure (ΔT and Δp). Simultaneously, it should result in an area that corresponds to a maximum number of supports that allows for structural configurations capable of withstanding emergency loads.

The first step is then to assess how the geometric dimensions of the section affect the stiffness characteristics of the support. For each allowed combination of radius and thickness, the values of axial stiffness k_{ax} and flexural stiffness k_{flex} were calculated (formulas presented in section 5.3).

The results are presented in Figure 5.13. For the material selected and the size range considered, it is possible to obtain axial stiffness values between $4.667 \cdot 10^6\ N/m$ and $3.266 \cdot 10^8\ N/m$, and flexural stiffness values between $4.685 \cdot 10^3\ N/m$ and $1.546 \cdot 10^7\ N/m$.

Considering the methodology presented for the analysis of normal stresses in section 5.3.2 supports, it can be concluded that the forces acting at the free end of the beam representing the support are directly proportional to the displacements imposed by the inner tank at that point and to the stiffness characteristics of the support. For the same displacements, therefore, a support characterised by lower stiffness values will develop lower stresses than a support characterised by higher stiffness values. In general, the choice is then directed towards values of radius and thickness associated with relatively low stiffness values.

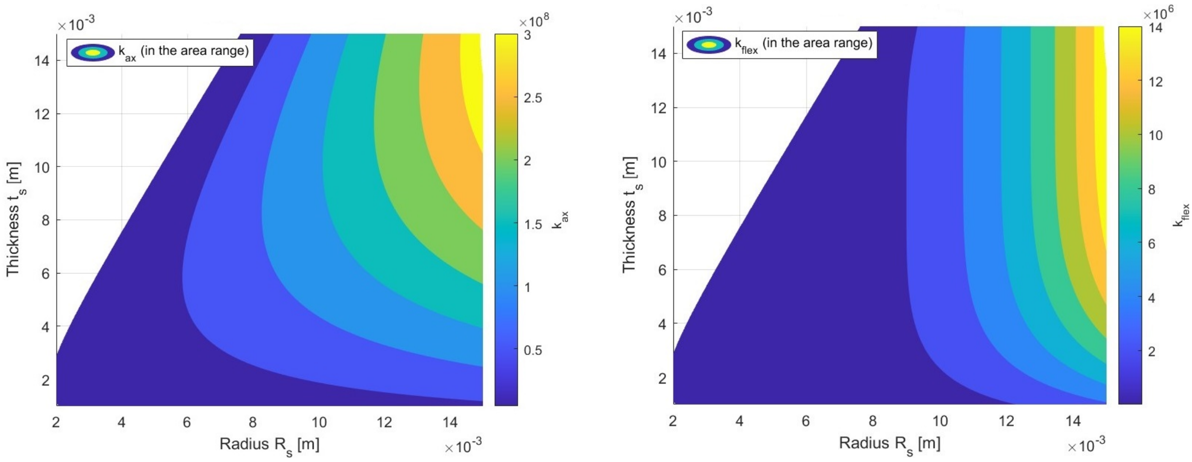

(a) Axial stiffness k_{ax} **(b)** Flexural stiffness k_{flex}

Figure 5.13: Evaluation of stiffness properties of the support for different R_s and t_s

Consistent with the decision to stay in the lower left-hand side of the graph, the radius R_s and thickness t_s values selected to proceed to the next steps of the analysis are:

$$R_s = 3 \cdot 10^{-3} m \qquad t_s = 1 \cdot 10^{-3} m \tag{5.49}$$

The associated values of area A_s and maximum number of supports allowed $N_{s,max}$ are:

$$A_s = 1.57 \cdot 10^{-5} m^2 \qquad N_{s,max} = 1390 \tag{5.50}$$

This results in the following axial stiffness k_{ax} and flexural stiffness k_{flex} values for the support:

$$k_{ax} = 7.33 \cdot 10^6 N/m \qquad k_{flex} = 1.98 \cdot 10^4 N/m \tag{5.51}$$

5.8.2. Deformation of the inner vessel due to ΔT and Δp

Evaluating the deformation of the inner vessel in response to significant variations in temperature and pressure during the transition from the manufacturing phase to the operational phase is critical for determining the design requirements for the support system. The support system must be able to accommodate the vessel's displacements while minimizing the risk of inducing excessive stresses that could lead to plastic deformation or even structural failure. The design challenge involves balancing the use of more flexible designs, which can better accommodate displacements, against stiffer designs, which offer greater support but restrict flexibility. Given the stringent requirements for emergency landing loads, the support system cannot be overly flexible, as it must provide adequate structural integrity during such events. Therefore, the optimal solution is a support structure sufficiently compliant to absorb the inner vessel's displacements without generating high stress concentrations, yet robust enough to ensure the vessel's stability and support under emergency conditions.

Using the methodology presented in section 5.4.1, various studies can be conducted to identify acceptable and compatible values for the analysis variables, in line with the design requirements.

Given the conditions the tank will face in this specific phase, the positioning of the supports is not the main concern, as the system's equivalent stiffness does not significantly impact the tank's deformation, which is primarily driven by the temperature differential (ΔT). The key objective here is to analyze how each individual support can accommodate the tank's displacement at the point of contact between the two, regardless of its location. To focus therefore mainly on the properties of the individual support, the simple support system configuration (Figure 5.9) can be assumed.

The values assumed for supports' characteristics directly reflect what was discussed in the previous section. The circular-ring cross-section geometry is then defined by R_s = $3 \cdot 10^{-3}$ m and t_s = $1 \cdot 10^{-3}$ m. The length of the single support is equal to the thickness of the insulation layer t_{vacuum} = 0.006 m and the selected material is G-10 CR, a high-pressure glass-reinforced epoxy laminate. The corresponding axial stiffness k_{ax} and flexural stiffness k_{flex} values for the individual support are k_{ax} = $7.33 \cdot 10^6 N/m$ N/m and k_{flex} = $1.98 \cdot 10^4$ N/m.

The solutions obtained for the displacement functions (previously presented in Equations 5.25, 5.26, and 5.27) are presented in the Equations 5.52, 5.53, and 5.54. Some of the unknown coefficients assume very small values (e^{-21}, e^{-22}, e^{-23}) which could be removed as they represent rounding effects.

$$\begin{aligned} u &= \left(7.2868e^{-4}x^5 - 0.0051x^4 + 0.0144x^3 - 0.0200x^2 + 0.0065x + 0.0066\right) + \\ &\quad x\left(1.3524e^{-07}\cos(\phi) - 5.7038e^{-22}\sin(\phi) - 1.3720e^{-08}\cos(2\phi) - 8.0162e^{-23}\sin(2\phi)\right) \\ &= \left(7.2868e^{-4}x^5 - 0.0051x^4 + 0.0144x^3 - 0.0200x^2 + 0.0065x + 0.0066\right) + \\ &\quad x\left(1.3524e^{-07}\cos(\phi) - 1.3720e^{-08}\cos(2\phi)\right) \end{aligned} \tag{5.52}$$

$$\begin{aligned} v &= \left(-1.1025e^{-23}x^5 + 6.4188e^{-23}x^4 - 1.2293e^{-23}x^3 + 7.8071e^{-23}x^2 + 4.0187e^{-24}x + 4.2867e^{-22}\right) + \\ &\quad x\left(-1.9247e^{-21}\cos(\phi) + 6.8605e^{-07}\sin(\phi) - 2.3921e^{-22}\cos(2\phi) + 1.4766e^{-07}\sin(2\phi)\right) \\ &= x\left(6.8605e^{-07}\sin(\phi) + 1.4766e^{-07}\sin(2\phi)\right) \end{aligned} \tag{5.53}$$

$$\begin{aligned} w &= \left(-3.1922e^{-08}x^5 - 7.4332e^{-04}x^4 + 0.0042x^3 - 0.0076x^2 + 0.0049x - 0.0028\right) + \\ &\quad x\left(-1.4318e^{-06}\cos(\phi) - 3.4712e^{-21}\sin(\phi) - 6.1538e^{-07}\cos(2\phi) - 7.3761e^{-22}\sin(2\phi)\right) \\ &= \left(-3.1922e^{-08}x^5 - 7.4332e^{-04}x^4 + 0.0042x^3 - 0.0076x^2 + 0.0049x - 0.0028\right) + \\ &\quad x\left(-1.4318e^{-06}\cos(\phi) - 6.1538e^{-07}\cos(2\phi)\right) \end{aligned} \tag{5.54}$$

The curves for u, v, w are visualised in Figure 5.14a for ϕ = 0 rad over x, and in Figure 5.14b for x = 1.4052 m (location that corresponds to the centre location of the inner vessel) over ϕ. Furthermore, the surface plots of the u, v, w displacements over both x and ϕ are presented in Figure 5.15.

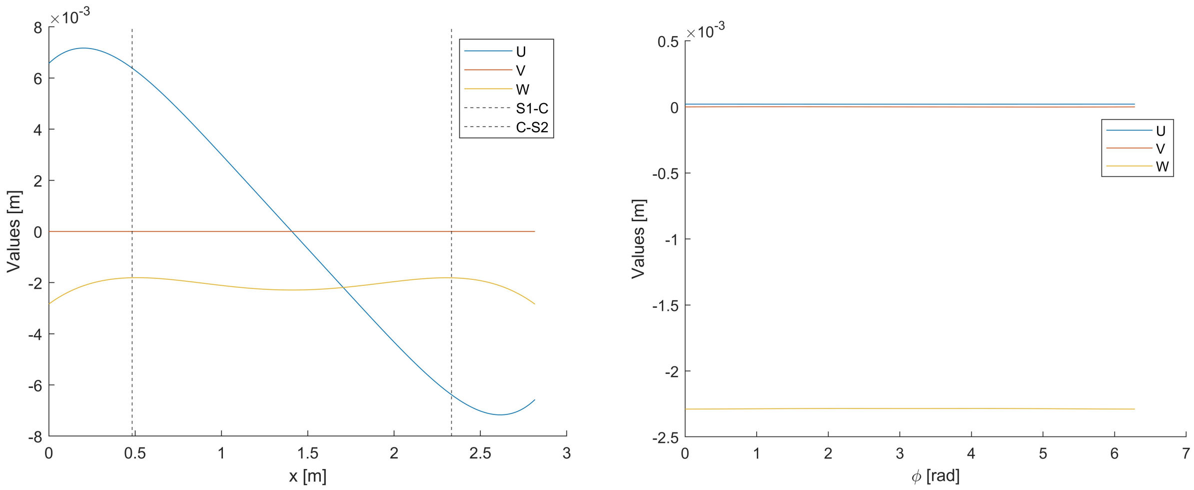

(a) U, V, W plots over x for $\phi = 0$ rad

(b) U, V, W plots over ϕ for $x = 1.4052$ m

Figure 5.14: U, V, W plots

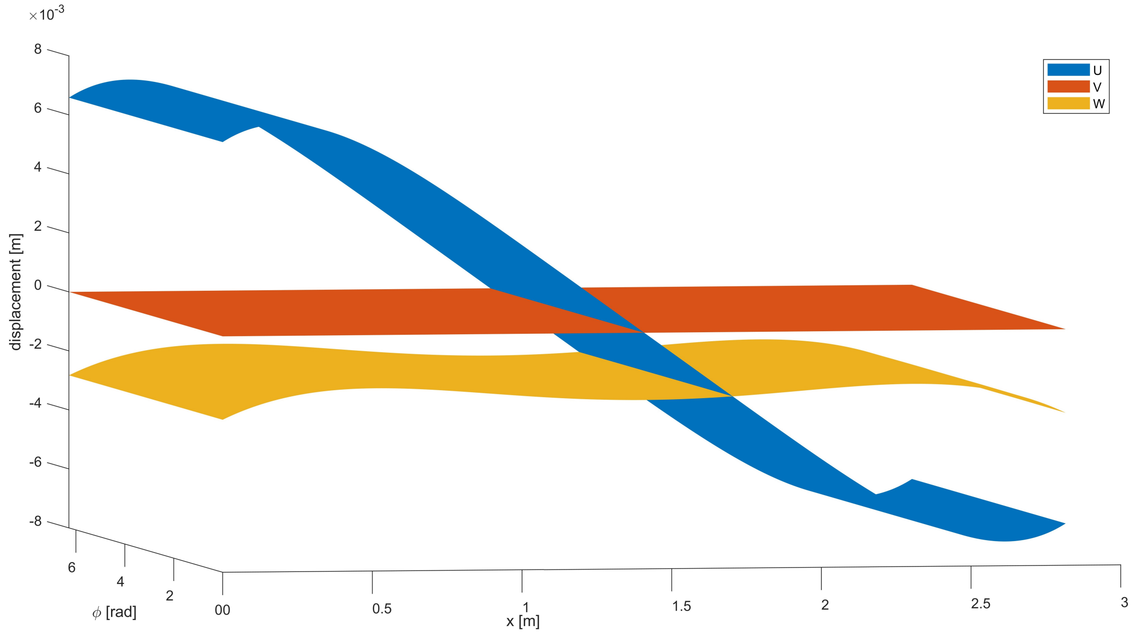

Figure 5.15: U, V, W plots over ϕ and x

The effect of the u, v, w displacements on the shape of the inner vessel is presented in Figure 5.16 for the transversal cross-section and Figure 5.17 for the longitudinal cross-section. In both graphs, the values of the displacements u, v, w have been scaled by a factor of 5 to enhance the visibility of the deformations experienced by the inner vessel, thereby facilitating the comparison between the configurations before and after the first filling and pressurization.

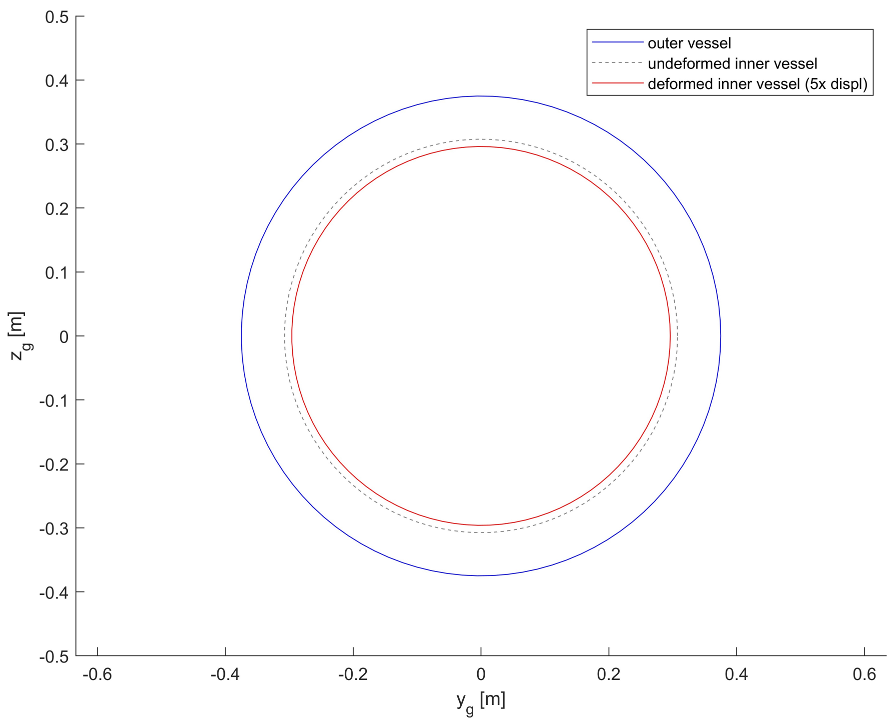

Figure 5.16: Deformed VS Undeformed shape of the tank, transversal cross-section

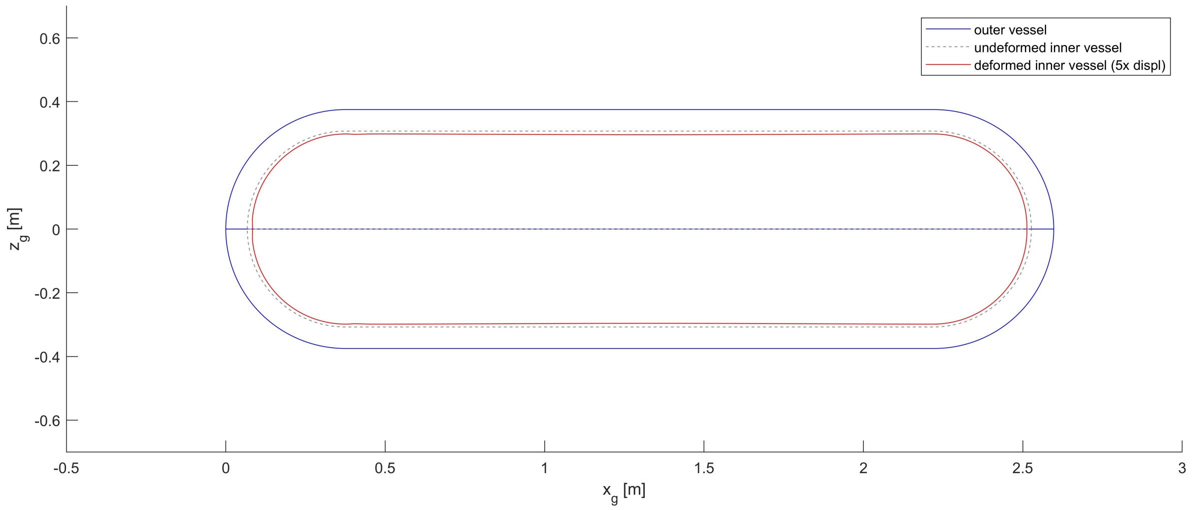

Figure 5.17: Deformed VS Undeformed shape of the tank, longitudinal cross-section

The stresses σ_{xx}, σ_{yy}, and σ_{xy} evaluated at the inner vessel shell's mid-surface are presented in Figure 5.18a for ϕ = 0 rad over x, and in Figure 5.18b for x = 1.4052 m (approximately in correspondence with the centre location of inner vessel) over ϕ.

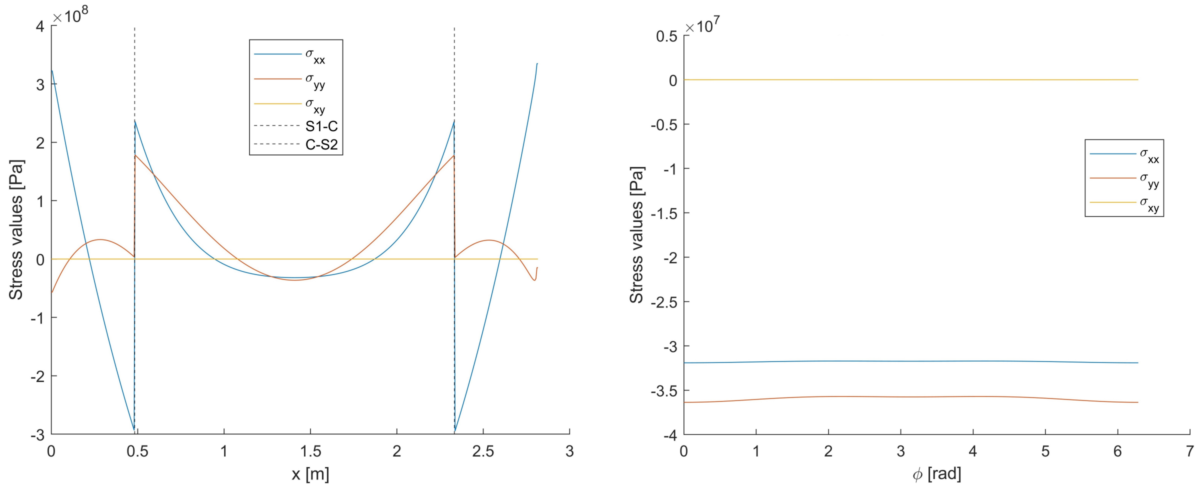

(a) σ_{xx}, σ_{yy}, σ_{xy} plots over x for $\phi = 0 rad$

(b) σ_{xx}, σ_{yy}, σ_{xy} plots over ϕ for $x = 1.4052m$

Figure 5.18: σ_{xx}, σ_{yy}, σ_{xy} plots

In analyzing Figure 5.14a, several symmetries are noticeable, particularly with respect to the center of the vessel. The plot of u exhibits a sinusoidal pattern that starts positive, decreases, crosses zero at the center point (at x = 1.4080 m), and then becomes negative. This behavior indicates that the u function has reflective symmetry around the midpoint of the x-axis. Similarly, the w displacement curve shows a slight undulation that is mirrored on either side of the midpoint of the x-axis. The plot for v is relatively flat: the values of v over x are between a maximum of $4.39 \cdot 10^{-22}$ m and a minimum of $-5.70 \cdot 10^{-21}$ m, which corresponds to a maximum difference of $6.12 \cdot 10^{-21}$ m (negligible if compared to the values assumed by displacement functions u and w, which are in the order of 10^{-3} m, not meaningful as the values of these coefficients represent numerical rounding errors).

The points along x undergo a displacement u in the x direction such that the points at the midpoint of the x-axis remain stationary, while the others undergo a shift towards the center. Radial displacements w are negative over the whole vessel. These considerations indicate that the inner tank is shrinking when exposed to the difference in temperature ΔT and pressure Δp. This is further testified by the representation of the deformed shape of the tank in the figures 5.17 and 5.16.

From Figure 5.14b, it is possible to note that the displacement functions u, v, and w for a certain x value are almost constant over ϕ. For x = 1.4052 m, the maximum deviation from the average u value is $1.90 \cdot 10^{-7}$ m, the maximum deviation from the average v value is $1.04 \cdot 10^{-6}$ m, and the maximum deviation from the average w value is $2.16 \cdot 10^{-6}$ m. By analysing Figure 5.15, similar considerations can be made for all the other points over x.

A comparison of the coefficients of the displacement functions reveals that the largest contribution comes from the axisymmetric portion of the solution, i.e. the part that depends solely on x and not on ϕ. The predominance of x as the determining variable for the displacement functions, coupled with the observation that v assumes almost zero values across the whole range of x and ϕ, confirms that the solution obtained is very close to a purely axisymmetric one.

Similar considerations can be made for the symmetries in the stress functions over x and ϕ in Figure 5.18a. All curves are in fact symmetrical with respect to the center point of the vessel (x = 1.4080 m). From Figure 5.18b, it is possible to note that the stress functions σ_{xx}, σ_{yy}, and σ_{xy} for a certain x value are almost constant over ϕ.

Furthermore, high stress values are reported at the ends of the domes and at the connection points between domes and cylinder, where a step in stress values is clearly visible. The high stress values in these areas are justified by the fact that these are the points at which the greatest displacements occur. The step in stress values between domes and cylinder can be justified by the fact that the definition of the strain components for cylindrical shell and for spherical shell is different (reference to subsection 5.4.1). In fact, comparing the definition of the strain ϵ_{xx0} for the spherical shell and for the cylindrical shell, it can be seen that ϵ_{xx0_s} contains an additional term (w/R). Furthermore, in the definitions of ϵ_{yy} and ϵ_{xy}, for the cylinder the only value of radius is the geometry's own radius R, while for the sphere the term local radius r_s appears, which is not constant but varies according to the section of the sphere considered. Stresses are directly calculated from the strains and, as a result, steps in stress values may occur in proximity of the connection points between domes and cylinder.

If the stress values are compared with the ultimate stress of the inner vessel material (S_u = $4.21 \cdot 10^8$ Pa), it can be noticed that the stress values found are particularly high. The maximum stress encountered is in fact equal to 79.5 $\%$ of the ultimate stress of the material.

Evaluation of stresses in the supports

Having now determined the actual displacements of the inner vessel, a detailed evaluation of the stresses in the various supports can be carried out.

As mentioned above, at this stage we assume the simple support arrangement presented in the Figure 5.9. The position of each support can be expressed in terms of x and ϕ. Two different types of support can also be differentiated according to their position: horizontal support H and support positioned in the plane in which the cross-section lies CS (vertical or lateral). The simple support configuration is axysimmetric and symmetric around the midpoint of the x-axis, while the displacement functions u, v, w are symmetric around the midpoint of the x-axis and almost constant over ϕ. This means that all the supports positioned at the same x location are going to be subjected to the same displacements and will develop the same normal stress distribution. Also, all the supports positioned symmetrically with respect to the midpoint of the x-axis are going to be subjected to the same displacements and will develop the same normal stress distribution. It is then possible to attribute the 14 supports to three types of normal stress distribution: type 1, type 2 and type 3. While type 1 refers to the horizontal supports, type 2 and 3 are defined based on the position of vertical and lateral supports with respect to the midpoint of the x-axis. The relevant data is summarised in table 5.8.

The geometry of the cross-section considered is a circular ring and the respective stress recovery points are presented in Figure 5.19. The (x_s, y_s) coordinates of the 16 stress recovery points are summarised in Table 5.9, where d_s is the inner diameter and $d_s = D_s - 2t_s$.

Table 5.8: Supports location and characteristics

Support n.	x [m]	ϕ [rad]	Position	Type
1	0	0	H	1
2	2.8160	0	H	1
3	0.9455	0	CS	2
4	0.9455	π	CS	2
5	0.9455	π/2	CS	2
6	0.9455	(3/2)π	CS	2
7	1.8705	0	CS	2
8	1.8705	π	CS	2
9	1.8705	π/2	CS	2
10	1.8705	(3/2)π	CS	2
11	1.4080	0	CS	3
12	1.4080	π	CS	3
13	1.4080	π/2	CS	3
14	1.4080	(3/2)π	CS	3

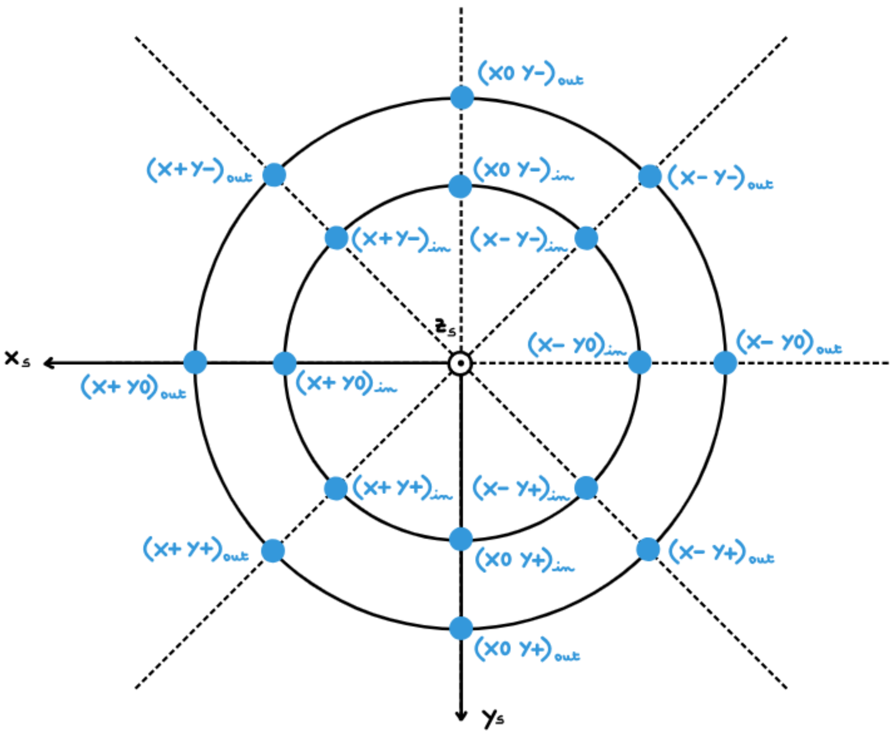

Figure 5.19: Stress recovery points for circular ring cross-section

Table 5.9: Coordinates of stress recovery points for circular ring cross-section

Coordinate	X0 Y+		X+ Y+		X+ Y0		X+ Y-	
in/out	in	out	in	out	in	out	in	out
x_s	0	0	$\sqrt{2}d_s$/4	$\sqrt{2}D_s$/4	d_s/2	D_s/2	$\sqrt{2}d_s$/4	$\sqrt{2}D_s$/4
y_s	d_s/2	D_s/2	$\sqrt{2}d_s$/4	$\sqrt{2}D_s$/4	0	0	-$\sqrt{2}d_s$/4	-$\sqrt{2}D_s$/4
Coordinate	**X0 Y-**		**X- Y-**		**X- Y0**		**X- Y+**	
in/out	in	out	in	out	in	out	in	out
x_s	0	0	-$\sqrt{2}d_s$/4	-$\sqrt{2}D_s$/4	-d_s/2	-D_s/2	-$\sqrt{2}d_s$/4	-$\sqrt{2}D_s$/4
y_s	-d_s/2	-D_s/2	-$\sqrt{2}d_s$/4	-$\sqrt{2}D_s$/4	0	0	$\sqrt{2}d_s$/4	$\sqrt{2}D_s$/4

The most critical normal stress distributions for each type of support are presented in Figure 5.20.

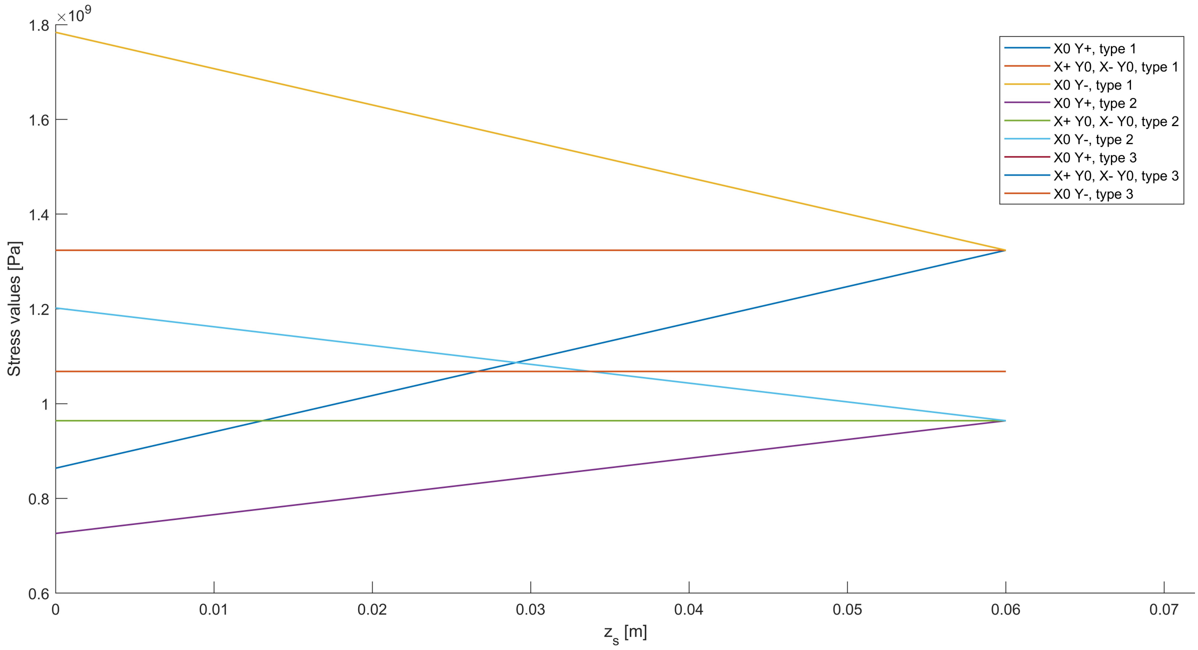

Figure 5.20: Evaluation of stresses in the supports

The first observation is that all the stress values presented exceed the ultimate strength of the material selected for the supports (S_u = $4.7 \cdot 10^8$ Pa). The stress values experienced by the supports range between approximately $7.5 \cdot 10^8$ Pa to $1.8 \cdot 10^9$ Pa, which means that the stress values exceed by at least 1.6 times the material's ultimate stress limit. The most critical stress value, reaching around $1.8 \cdot 10^9$ Pa, is nearly 3.8 times greater than the ultimate strength of the material.

This clearly highlights that the support designs, as currently configured, is inadequate in providing the necessary flexibility to accommodate the displacements imposed by the inner vessel. However, it must be emphasised that the imposed displacements are significant, particularly when compared to the length of the supports. Therefore, it can be concluded that there is a need to explore materials that are capable of withstanding substantial displacements, even under extremely low temperatures. Moreover, the simple tubular shape selected for the supports is insufficient for the intended application. There is considerable potential for optimizing the support's shape to reduce the stiffness values, thereby enhancing its ability to accommodate the imposed displacements.

Further analysis of the figures reveals that, for Type 1 and Type 2 supports, the upper surface (Y+) is subjected to compression while the lower surface (Y-) experiences tension. This phenomenon is attributed to the bending moments introduced by the displacements in the u and v directions. In contrast, Type 3 supports are primarily subjected to stress components arising from axial loading. The only displacement experienced by the Type 3 support is w, which is aligned with the z-axis of the support z_s, as the displacements u and v are negligible at the central position of the inner vessel (see Figure 5.14a).

In summary, the analysis highlights two key areas for improvement: the need for flexible materials and the potential for geometric optimization of the supports in order to obtain a support design able to accommodate large displacements at low temperatures. Specifically, the current tubular design should be reconsidered, as optimizing the shape could significantly reduce the stiffness values and improve the overall performance of the support system in terms of flexibility.

Fatigue considerations

As previously discussed in section 5.5, it is important to assess the fatigue life of both inner vessel and supports, i.e. the number of loading cycles that inner vessel and supports can sustains before failure occurs. The load cycles considered are characterised by a stress amplitude S_a equal to half of the maximum stress encountered. For the inner vessel the maximum stress value considered is $S_{a,i}$ = $3.21 \cdot 10^8$ Pa, while for the supports $S_{a,s}$ = $1.78 \cdot 10^9$ Pa.

For the **metal inner vessel**, the S-N fatigue curve in Figure 5.21 is directly obtained following the methodology presented in section 5.5 for metal components. The S-N curve obtained is presented in Figure 5.21 and the fatigue life calculated for the inner vessel corresponds to approximately $8 \cdot 10^3$ cycles. Assuming that the tank is emptied and refilled every 6 months and thus each cycle corresponds to 6 months, the fatigue life of the inner vessel could then be expressed as $4 \cdot 10^3$ years, which far exceeds the life span of the airplane (around 25-30 years [71]).

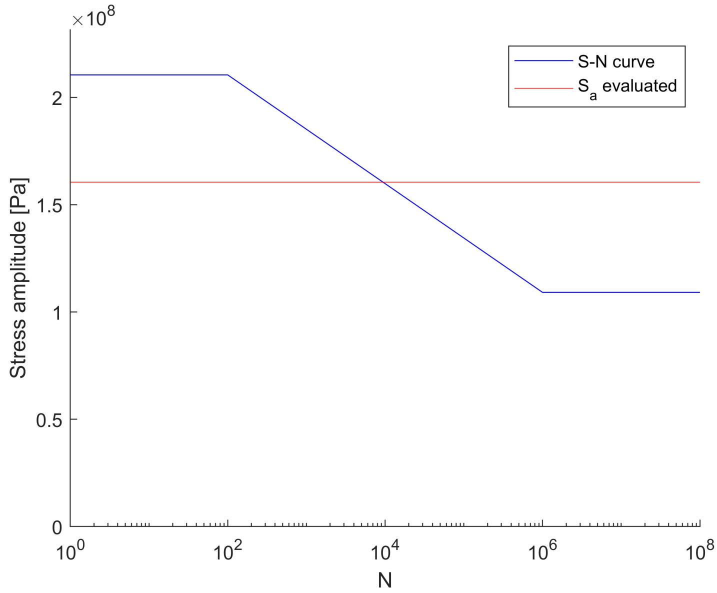

Figure 5.21: S-N curve for the inner vessel

Regarding the **composite support structure**, it has already been established that the stresses developed due to the displacements of the inner vessel exceed the ultimate strength of the selected material (S_u = $4.7 \cdot 10^8$ Pa). However, it is crucial to note that the design requirements for the support structure should not primarily focus on the ultimate strength but rather on the fatigue properties of the material. Fatigue life is a critical factor because, under the repeated loading cycles experienced by the tank during its operational life, supports may be subjected to stresses that are well below their ultimate strength but could still accumulate damage over time. For the specific material selected (G-10 CR), the fatigue properties at cryogenic conditions are currently unknown.

The general final remark is that the existing design is insufficient to handle the full range of displacements without compromising the structural integrity and lifespan of the supports. Therefore, substantial modifications to the support structure are needed, either by selecting more suitable materials with known fatigue properties, higher fatigue resistance, and flexibility, or by redesigning the support geometry to better distribute and manage the imposed loads and displacements. This is necessary to ensure that the supports can endure the operational stresses over the intended service life without failure. Additionally, this evaluation highlights the importance of aligning the fatigue life of the supports with that of the inner vessel to avoid premature failure and ensure reliable long-term performance of the overall system.

Following the established design methodology (reference to section 5.7), the logical next step would be to either adjust the material properties or safety factors of the inner vessel, or alternatively, modify the material properties and/or section geometry of the supports. However, as previously stated, the challenges encountered thus far are of such magnitude that they necessitate substantial changes in the design (search for more appropriate materials, especially those with better fatigue resistance at cryogenic conditions, and a comprehensive topology optimization to refine the geometry of the supports), which lie outside the scope of the current design methodology and would require a separate and focused study. Once support characteristics that can withstand the first filling of the tank are successfully identified, the design process can proceed with the subsequent steps of the analysis, continuing to evaluate the emergency landing load cases.

In the interest of presenting the rest of the design methodology, these modifications will not be implemented at this stage. Instead, the focus will remain on illustrating the design process and evaluating the current configuration against the emergency landing scenario. This will allow for a clear understanding of how different aspects of the methodology apply, while keeping in mind that future iterations should incorporate material or geometric changes to fully address the identified challenges.

5.8.3. Emergency landing scenario - static conditions

The parameters of the performed analyses are in line with what is presented in table 5.5. The values assumed for supports' characteristics directly reflect what was discussed in section 5.8.1. The circular-ring cross-section geometry is defined by $R_s = 3 \cdot 10^{-3}$ m and $t_s = 1 \cdot 10^{-3}$ m. The length of the single support is equal to the thickness of the insulation layer t_{vacuum} = 0.006 m and the selected material is G-10 CR, a high-pressure glass-reinforced epoxy laminate. The corresponding axial stiffness k_{ax} and flexural stiffness k_{flex} values for the individual support are $k_{ax} = 7.33 \cdot 10^6$ N/m and $k_{flex} = 1.98 \cdot 10^4$ N/m.

An important parameter in this analysis is the mass value of the inner vessel m_i. This is calculated by summing the contributes of the aluminum inner vessel, the hydrogen mass contained in it, and the piping system connected to it. Assuming a fill rate $FR = 0.95$, the m_i value can be calculated for the LCP retrofit design. Based on the mass of the inner vessel, it is then possible to define the values of the ultimate forces considered in the analysis. These values are summarised in table 5.10.

Table 5.10: Inner vessel mass and ultimate forces values for LCP retrofit design

m_i LCP [kg]	F_{upward} [N]	$F_{forward}$ [N]	$F_{sideward}$ [N]	$F_{downward}$ [N]	$F_{rearward}$ [N]
17.81	524.15	1572.45	698.86	1048.3	262.07

Subsequently, for a certain support structure configuration, the equivalent stiffness of the whole support system in each of the three global coordinate directions (k_{eq,x_g}, k_{eq,y_g}, and k_{eq,z_g}) must be calculated (global coordinates system: x_g, y_g, and z_g). This calculation involves summing the equivalent stiffness values of the individual supports based on their orientation and characteristics, as outlined in section 5.6. The specific support structure configuration that lead to acceptable levels of total displacement in the direction of the applied force and maximum stress within safe limits is not known beforehand. A practical approach is to first evaluate the simple configuration (Figure 5.9) to establish baseline stiffness values. Subsequently, multiples of these baseline values are evaluated in order to observe and analyse their effect on the structural response under ultimate applied forces. The results of this analysis for total displacement in the direction of force application and for maximum stress in the support structure are presented in Figure 5.22.

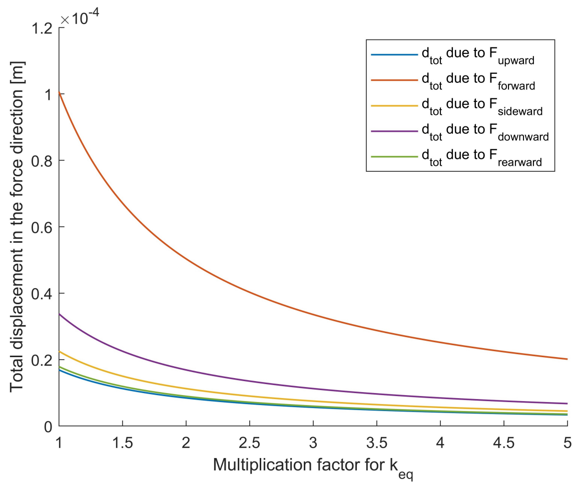

(a) Total displacement in the force direction over increasing k_{eq}

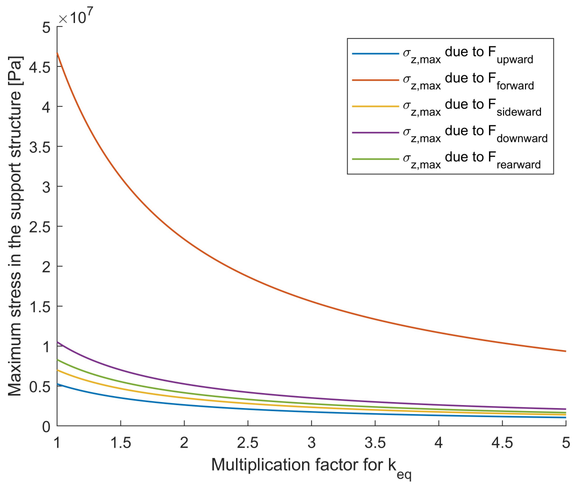

(b) Maximum stress in the support structure over increasing k_{eq}

Figure 5.22: Evaluation of appropriate equivalent stiffness values

The figures 5.22a and 5.22b indicate that, for the selected baseline configuration, the most critical ultimate load case is undoubtedly $F_{forward}$. The total displacements in the force direction introduced by $F_{forward}$ are up to 6 times greater than those introduced by the other ultimate forces, while the maximum stresses induced in the support structure are up to 6 times greater than those introduced by the other ultimate forces. By comparing the values presented in table 5.10, it becomes evident that the magnitude of the $F_{forward}$ force is significantly higher than that of the other ultimate loads (at least 50$\%$ higher). Additionally, this force is applied in a horizontal direction and, in the baseline support structure configuration, only two supports are positioned in this direction. While the axial stiffness of the two horizontally positioned supports plays a major role in resisting $F_{forward}$, it is important to note that the flexural stiffness properties of the vertically and laterally positioned supports also contributes to the overall equivalent stiffness. However, it should be emphasized that the axial stiffness of the supports is significantly higher than their flexural stiffness (more than two orders of magnitude difference). In fact, this is confirmed by the comparison of the equivalent flexural stiffness values of the baseline support structure in the vertical, horizontal and lateral directions: $k_{eq,vertical}$ = $4.41 \cdot 10^7$ N/m, $k_{eq,horizontal}$ = $1.49 \cdot 10^7$ N/m, $k_{eq,lateral}$ = $4.41 \cdot 10^7$ N/m. The equivalent stiffness values in the vertical and lateral direction are, in fact, almost 3 times greater than the equivalent stiffness value in the horizontal direction.

Despite these considerations, the baseline configuration is capable of providing a satisfactory response to all ultimate load cases. The maximum stresses encountered are approximately an order of magnitude lower than the ultimate load capacity of the material: the maximum stress in the support structure found is in fact equal to $4.70 \cdot 10^7$ Pa, while the ultimate stress for the support material is $4.7 \cdot 10^8$ Pa. This margin of safety allows us to conclude that the baseline configuration is sufficient to ensure adequate support when evaluating static conditions under an emergency landing scenario.

While further optimization may enhance performance, would also result in an increase of added material implying both a greater mass and a greater heat inflow from the external environment through the supports.

5.8.4. Emergency landing scenario - dynamic conditions

Consistent with the methodology presented in subsection 5.6.2, the system consisting of external vessel, inner vessel and respective support system can be represented by a simplified model characterised by:

- *Mass properties:* m_i is the mass value of the mass point representing the inner vessel. For the LCP retrofit design, m_i = 17.81 kg (reference to section 5.8.3).
- *Stiffness properties:* k is the equivalent stiffness value of the support system in the direction of the input acceleration (vertical). Its value depends on the stiffness properties of the individual support (axial stiffness k_{ax} = k_{ax} = $7.33 \cdot 10^6 N/m$ and flexural stiffness k_{flex} = $1.98 \cdot 10^4$ N/m) and how the various supports have been positioned around the inner vessel.
- *Damping properties:* it is possible to assume standard values for the damping factor ζ depending on the type of structure. For a metal structure, it is usually assumed $\zeta = 0.02$.

The specific support structure configuration that results in acceptable levels of vertical displacement over time and ensures that maximum stress remains within safe limits is not known in advance. A practical approach begins by evaluating the simple support structure configuration (Figure 5.9) to establish a baseline stiffness value in the vertical direction. Once this baseline is determined, the next step involves evaluating multiples of this baseline stiffness to observe and analyze how changes in stiffness affect the structural response to the applied acceleration spectrum. To facilitate this analysis, M is introduced as a multiplication factor applied to the baseline stiffness value in the vertical direction.

First of all, the total displacement imposed on the support structure over time $\delta(t)$ must be evaluated. Secondly, the corresponding maximum stress in the supports over time must be calculated. In this case, it is possible to define two different types of axial stresses distribution in the supports. For the vertically oriented supports, δ corresponds to an axial displacement (w) and the response will be governed by the axial stiffness of the supports (type 1). In contrast, for the horizontally and laterally positioned supports, δ corresponds to a lateral displacement (u or v), and the response will be determined by the flexural stiffness of these supports (type 2).

The results of this analysis are presented in figures 5.23 and 5.24.

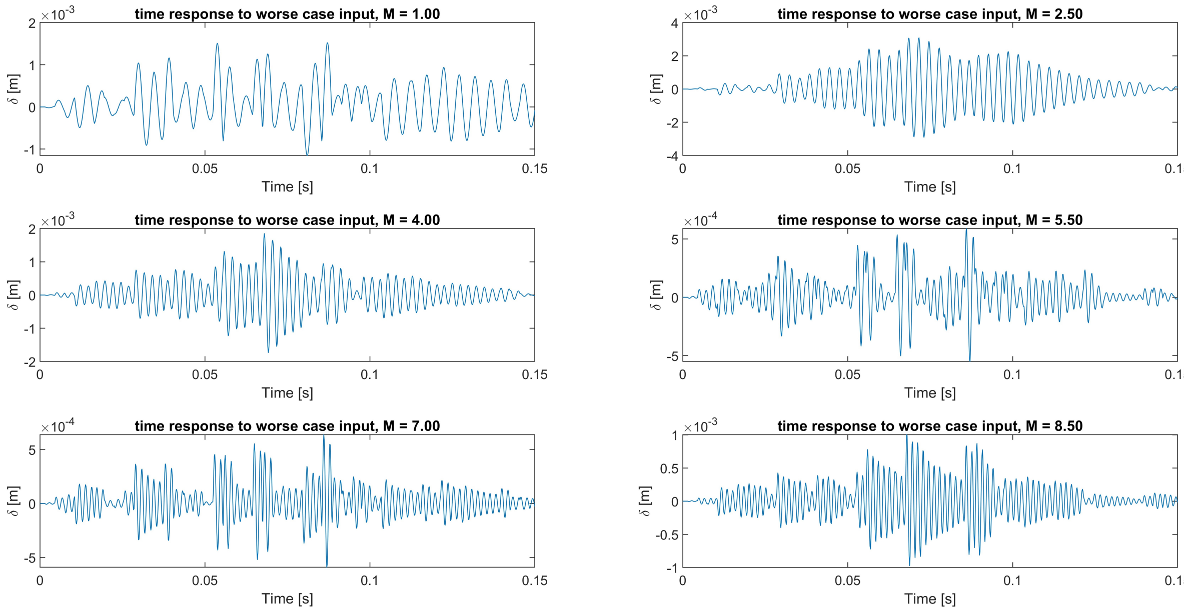

Figure 5.23: Evaluation of the displacement imposed on the support structure over time $\delta(t)$

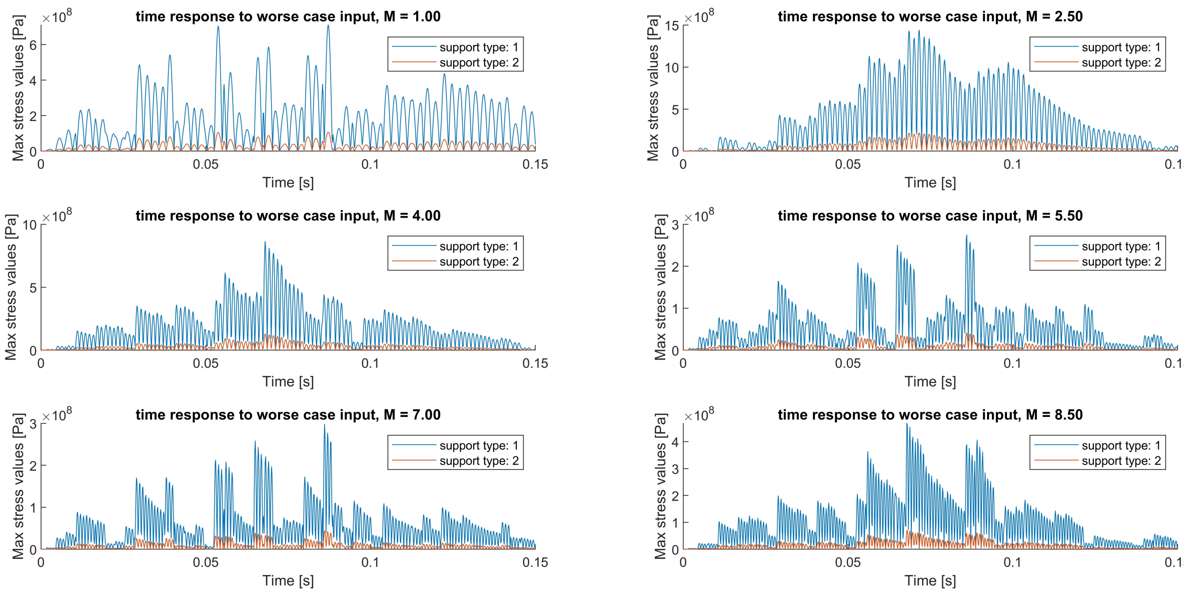

Figure 5.24: Evaluation of the maximum stress in the supports over time

In contrast to the conclusions drawn for the static conditions, the baseline support structure configuration is inadequate in this case. From figures 5.23 and 5.24, it is possible to notice how the time response analysis for the baseline configuration (M = 1, k = $4.41 \cdot 10^7$ N/m) reveals displacements that result in maximum peak stresses exceeding the ultimate stress of the material, which is $4.7 \cdot 10^8$ Pa. The baseline configuration's inability to withstand dynamic loading conditions without exceeding material limits highlights the need for a more robust support system that can provide the necessary equivalent stiffness to reduce the total displacement imposed on the support structure and maintain stress levels within safe limits during an emergency landing scenario.

From Figure 5.24, it can be noted that when the multiplication factor M is increased to 5.5, the resulting peak stresses fall below $3 \cdot 10^8$ Pa. This indicates the necessity of developing an alternative support structure configuration that can achieve an equivalent stiffness in the vertical direction k approximately 5.5 times greater than that of the baseline configuration, which corresponds to a stiffness value of $2.42 \cdot 10^8$ N/m.

To achieve a higher equivalent stiffness, it is clear that additional supports must be introduced. However, since adding supports increases both the overall mass and the heat inflow from the external environment through the support structure, it is crucial to strategically place these supports where they will have the greatest impact. Given that the emergency landing dynamic conditions consist in an acceleration spectrum applied in the vertical direction to the outer vessel of the tank, the key stiffness value influencing the system's response is the equivalent stiffness in the vertical direction. Furthermore, considering that the axial stiffness of the supports is significantly greater than their flexural stiffness, it can be concluded that the most effective strategy is to add vertical supports to the configuration. This approach ensures that the additional supports contribute directly to enhancing the system's ability to resist vertical loads, thereby improving the overall performance under dynamic loading conditions while minimizing unnecessary increases in mass and heat leakage through the support system.

After performing the necessary calculations, it has been determined that 26 additional vertical supports need to be added to the baseline configuration. Specifically, 13 supports should be positioned at ϕ = 0 and another 13 at $\phi = \pi/2$. These supports will be strategically located in the cylindrical region of the inner vessel.

6 Conclusion

The present thesis examined the **retrofit of a regional airliner with non-integral metal liquid hydrogen tanks**, aiming to accelerate hydrogen propulsion adoption. Retrofitting existing aircraft is crucial for quickly advancing hydrogen propulsion, reducing emissions, and enabling more sustainable air travel by leveraging current infrastructure. The study focuses on performance requirements like cruise and dormancy times, favoring metal over composites for the tank due to reliability and predictability under cryogenic conditions. Both single-wall and double-wall tank designs are considered, with a focus on balancing structural integrity, thermal insulation, and weight, especially for the inner vessel's support system.

The first architecture to be analysed was the **single-wall tank**. This design approach, while simpler and potentially more cost-effective, has been found to be primarily feasible for larger tank dimensions. The ratio of surface area to volume is a key determinant: low values minimise the heat transfer into the fuel, limiting hydrogen boil-off, and could be obtained by choosing spherical geometries and increasing the tank's size. The designs considered for the retrofit are characterized by relatively small dimensions: this is because the retrofit requirements (such as ease of installation, the need for tanks to fit through existing aircraft doors, and the requirement to avoid modifications to the aircraft's primary structures) necessitate the use of multiple smaller tanks rather than a single large one. This implies a higher surface area relative to the tank's volume, which results in increased thermal losses, reducing efficiency and preventing the design from meeting performance requirements.

In conclusion, while the single-wall LH_2 tank design has potential, its application is limited by the need for larger dimensions to offset thermal inefficiencies inherent in its architecture. This makes it suitable primarily for larger-scale applications where the surface area-to-volume ratio can be minimized.

The analysis of the **double-wall tank** architecture reveals its potential feasibility for the current case study, being able to meet the requirements of cruise time and dormancy time for the retrofit designs considered. The double-wall architecture, with its insulation system based on vacuum and MLI, demonstrates a superior thermal performance, which significantly reduces heat transfer and boil-off rates compared to the single-wall architecture.

Moreover, the analysis of the heat leakage budget through the support structure reveals that the maximum allowable heat leakage is higher than the originally assumed heat leakage value relative to two cylindrical composite supports developing longitudinally through the thickness of the insulation layer. This offers additional thermal margin, providing flexibility to introduce alternative support structures or optimize the existing ones without compromising the overall thermal performance. The design's strong thermal efficiency enables the exploration and optimization of different support strategies and materials, offering the flexibility to tailor geometric configurations to meet specific structural and operational needs while maintaining overall thermal performance.

In order to ascertain the actual feasibility of the double-wall architecture, however, it is necessary to evaluate possible designs for the **support structure**. Among the retrofit designs proposed by Yi-Hsiu in his thesis project [82], the Longitudinal Circle Packing design is considered to have the greatest potential for retrofitting the baseline aircraft, due to its superior crashworthiness and extended range, and was taken as reference to continue the analysis and focus on the support structure.

The heat leakage budget through the supports associated with the specific design considered (characteristics presented at the beginning of section 5.8) imposes a **thermal requirement for the support structure**, as any introduced design must stay within the allowable heat inflow limit while meeting structural and operational demands. As already mentioned in section 2.5, the material selected for the support structure should be characterised by low thermal conductivity. This is further supported by the observation that, within the entire range of possible thermal conductivity values (range between 0.01 W/mK to 1000 W/mK), only those below 109 W/mK fall within the feasibility zone imposed by the heat leakage budget. Generally, materials with lower thermal conductivity allow for larger cross-sectional areas and a higher maximum number of supports without exceeding the heat leakage budget. Consequently, these materials offer greater flexibility in designing both the geometry of individual supports and the overall configuration of the support structure. It is also for these reasons that the *material G-10 CR*, a high-pressure glass-reinforced epoxy laminate, was selected for further analysis.

The primary function of the support structure is to prevent any contact between outer vessel and inner vessel. The two most **critical events** in the operational life of a tank are the filling of the empty tank initially at ambient temperature and pressure, and the static and dynamic conditions associated with the emergency landing. As presented in section 5.1, the ability of the tank to remain functional in these events results in the following requirements for the support structure: be compliant enough to withstand the large thermal deformation of the inner vessel without plastic deformation, while being stiff enough to withstand the crash loads without failing or causing damage to other components. The two scenarios described place conflicting demands on the support system and one way to simplify the problem is by decoupling them. Specifically, the flexibility of individual supports should be prioritized to accommodate the thermal displacements during the tank's initial filling process, ensuring the inner vessel can expand and contract without issues. In contrast, the overall stiffness of the support structure is key to withstanding the inertial forces and accelerations experienced during an emergency landing static and dynamic conditions.

The key factors for ensuring the flexibility of the individual support is its stiffness properties (axial stiffness k_{ax} and flexural stiffness k_{flex}), which depend on the geometry and material properties of the support and determine how compliant the supports will be against deformations and displacements that the inner tank experiences during the various phases of its operational life. Assuming a *circular-ring cross section* characterised by the parameters radius R_s and thickness t_s, it is possible to analyse the feasibility area in terms of these parameters and determine the possible associated stiffness characteristics. In order to avoid the development of excessive stresses in the supports during the **first filling of the tank**, the choice for the cross-section geometry must be directed towards values of radius and thickness associated with relatively low stiffness. To proceed with the analysis, the following values were assumed: R_s = $3 \cdot 10^{-3}$ m and t_s = $1 \cdot 10^{-3}$ m.

When evaluating the inner tank's response to temperature and pressure differences experienced during the first filling, the analysis found that the locations of tank's center remained almost constant, with minimal displacement, and, in general, the observed phenomenon is shrinking of the tank. This confirms that between the decrease in temperature and the increase in pressure, the most decisive phenomenon is the decrease in temperature. Moreover, the deformation undergone is almost comparable to the axisymmetric solution. This makes sense as the entire structure (inner vessel, outer vessel, support structure) is axisymmetric, as well as the applied temperature and pressure loads.

The **stress analysis** further confirmed that the tank's structural integrity was intact, with a satisfactory fatigue life, indicating that the design is robust enough to withstand the operational stresses over its intended lifespan. However, the study also highlighted significant challenges in the design of the support structure. The stresses within the supports were found to be over the ultimate strength of the supports' material, signaling the need for further optimization. Key areas for improvement include the selection of more flexible materials and the geometric optimization of the supports to better accommodate large displacements, particularly at low temperatures. The current straight tubular design, while functional, should be replaced in order to reduce stiffness and improve flexibility to better handle displacements from thermal contraction and expansion.

The study also examined the tank's performance under **emergency landing conditions**, both static and dynamic. In *static conditions*, the basic support structure configuration was sufficient to maintain the tank's integrity, ensuring that it could withstand the ultimate inertial loads encountered during an emergency landing. However, under *dynamic conditions*, the basic configuration proved inadequate. Its inability to withstand dynamic loading conditions without exceeding material limits highlights the need for a more robust support system that can provide the necessary equivalent stiffness to reduce the total displacement imposed on the support structure and maintain stress levels within safe limits during an emergency landing scenario. Achieving higher stiffness requires adding more supports, but since this also increases the overall mass and heat inflow, it's essential to place these supports strategically for maximum effect. Since emergency landing conditions primarily involve vertical acceleration, the focus should be on enhancing vertical stiffness. Given that the supports' axial stiffness is much higher than their flexural stiffness, the most effective solution is to add vertical supports. This approach boosts the system's ability to withstand vertical loads, improving performance under dynamic conditions while minimizing the additional mass and heat leakage.

The most significant challenge identified was then ensuring that the support structure could accommodate the displacements of the inner tank caused by the substantial temperature differential applied during the first filling. To address this issue, two potential solutions could be proposed. The first involves replacing the inner vessel material with one that has a significantly lower coefficient of thermal expansion in order to drastically reduce the magnitude of the inner tank's displacements. The second solution focuses on developing a support structure capable of accommodating larger displacements without undergoing plastic deformation or failure, employing advanced design techniques such as topology optimization. Both approaches require careful consideration of material properties and structural design to ensure that the system can maintain its integrity and performance under the demanding thermal conditions typical of cryogenic hydrogen storage. The choice between these two solutions will depend on a variety of factors, including material availability, cost, and the specific operational requirements of the tank system. Both options require further research and development to fully realize their potential in creating a reliable and efficient liquid hydrogen storage system.

Overall, the methodology employed to evaluate various tank design solutions for retrofit case studies yielded significant and insightful results. Among the options considered, only the double-wall design proved to be feasible. However, this configuration introduces a considerable level of complexity due to the necessity of a support structure for the inner vessel. The methodology proved to be capable of effectively analysing the performance of a hypothetical support structure under operating conditions. Consequently, this study establishes a solid foundation for future research, providing clear and actionable directions for addressing the remaining challenges associated with advanced hydrogen storage technologies.

7 Recommendation for future work

The present study has laid a strong foundation for understanding the challenges and limitations of designing cryogenic liquid hydrogen storage systems for aircraft retrofits. However, several aspects remain unexplored or require further refinement to achieve a fully optimized and reliable design. The following recommendations outline areas where additional research and analysis are necessary to address the limitations identified in this work, improve design robustness, and ensure long-term operational safety. These future efforts will contribute to the development of more advanced, resilient tank systems, capable of withstanding the critical conditions of aerospace operations.

Research effort in the development of design solutions for flexible supports

Future research should focus on the development of flexible support structures that are capable of accommodating relatively large displacements without undergoing plastic deformation or failure as well as the complex loading scenarios encountered by the tank system. Advanced design techniques such as topology optimization could be employed to create supports that flex and adapt under different loads, while maintaining structural integrity. Additionally, the development and investigation of materials with superior fatigue resistance and flexibility, especially at cryogenic temperatures, is critical. These materials should be able to withstand repeated loading and thermal cycling without experiencing degradation, ensuring the supports remain functional over the tank's operational life.

Analyze more complex support designs such as ring-like supports

Future work should also investigate more complex support geometries, such as ring-like supports. These designs may offer advantages in load distribution and structural stability. Ring supports could better distribute loads across a larger surface area, reducing localized stress concentrations and enhancing the overall durability of the tank-support system.

Include flexible-body modes of the vessels in the emergency landing dynamic analysis

In the current dynamic analysis, the inner and outer vessels are modeled as rigid bodies during emergency landing scenarios. However, in reality, the vessels exhibit flexible-body behavior that could significantly affect the response of the whole system. Future work should incorporate flexible-body dynamics into the emergency landing simulations to capture the real-world behavior of the tank structure under high-impact conditions.

Consider sloshing loads

Another area for future improvement involves accounting for sloshing loads in the tank's design. Liquid sloshing inside partially filled tanks can introduce significant dynamic forces during sudden maneuvers, takeoff, or emergency landings.

Recommendations for aircraft designers

From the conclusions presented in chapter 6, general recommendations for aircraft designers can be drawn, particularly concerning the design of cryogenic hydrogen storage tanks. The key points are outlined below:

- *Single-wall tank architecture*: This design is primarily feasible for larger tanks, where the surface area-to-volume ratio is inherently lower. This reduces heat transfer and makes the architecture more suitable for retaining thermal performance.
- *Double-wall tank architecture*: With superior thermal performance due to the vacuum layer and multi-layer insulation, this design is highly effective when the surface area-to-volume ratio cannot be minimized enough, such as in smaller tanks.
- *Support structure flexibility*: To accommodate the large thermal deformations of the inner vessel without causing plastic deformation, it's recommended to use a greater number of smaller, more flexible supports rather than fewer large, stiff supports. This approach facilitates the decoupling of the conflicting requirements for flexibility (to manage thermal expansion and contraction) and stiffness (to withstand mechanical and crash loads). Furthermore, advanced design techniques, such as topology optimization, should be employed in the design of the support structures, allowing for the fine-tuning of geometric features, while also minimizing material use and enhancing thermal efficiency.
- *Material selection for supports*: Materials with low thermal conductivity are critical for minimizing heat leakage. Metals, due to their high thermal conductivity, should be avoided, and instead, composite materials or advanced polymers with low thermal conductivity should be favored for the support structure.

References

[1] Air Transport Action Group (ATAG). “Waypoint 2050”. In: *Aviation Benefits Downloads* (2021). URL: https://aviationbenefits.org/downloads/waypoint-2050/.

[2] International Air Transport Association (IATA). *Global Outlook for Air Transport — A local sweet spot*. 2023. URL: https://www.iata.org/en/iata-repository/publications/economic-reports/global-outlook-for-air-transport---december-2023---report/ (visited on 02/21/2024).

[3] International Air Transport Association (IATA). *Global Outlook for Air Transport — Highly Resilient, Less Robust*. 2023. URL: https://www.iata.org/en/iata-repository/publications/economic-reports/global-outlook-for-air-transport----june-2023/ (visited on 02/21/2024).

[4] P. Adam and J. Leachman. “Design of a reconfigurable liquid hydrogen fuel tank for use in the Genii unmanned aerial vehicle”. In: *AIP Conference Proceedings* 1573.1 (Jan. 2014), pp. 1299–1304. ISSN: 0094-243X. DOI: 10.1063/1.4860856. eprint: https://pubs.aip.org/aip/acp/article-pdf/1573/1/1299/12110978/1299_1_online.pdf.

[5] R.K. Ahluwalia and J.K. Peng. “Dynamics of cryogenic hydrogen storage in insulated pressure vessels for automotive applications”. In: *International Journal of Hydrogen Energy* 33.17 (2008), pp. 4622–4633. ISSN: 0360-3199. DOI: https://doi.org/10.1016/j.ijhydene.2008.05.090.

[6] Institute of Air Handling and Refrigeration (ILK): Dresden Germany. *Storage Density of Hydrogen*. 2015. URL: https://commons.wikimedia.org/wiki/File:Storage_Density_of_Hydrogen.jpg (visited on 02/23/2024).

[7] National Research Council (US) Committee on Air Quality in Passenger Cabins of Commercial Aircraft. *The Airliner Cabin Environment and the Health of Passengers and Crew*. National Academies Press (US), 2002.

[8] AIRBUS. *Hydrogen combustion, explained*. 2020. URL: https://www.airbus.com/en/newsroom/stories/2020-11-hydrogen-combustion-explained (visited on 02/23/2024).

[9] AIRBUS. *Hydrogen fuel cells, explained*. 2020. URL: https://www.airbus.com/en/newsroom/news/2020-10-hydrogen-fuel-cells-explained (visited on 02/23/2024).

[10] AircraftMaterialsUK.com. *Aluminium Alloy 2219*. URL: https://www.aircraftmaterials.com/data/aluminium/2219.html#:~:text=Aluminium%20Alloy%202219%20is%20a,resistant%20to%20stress%20corrosion%20cracking. (visited on 02/28/2024).

[11] R.C. Alderliesten and J.A. Pascoe. *Learning unit: Fatigue Life Analyses*. Course: Fatigue of Structures and Material, Department of Aerospace Structures and Materials, Delft University of Technology. 2022.

[12] G. AlZohbi, A. Almoaikel, and L. AlShuhail. “An overview on the technologies used to store hydrogen”. In: *Energy Reports* 9 (2023). Proceedings of 2022 7th International Conference on Renewable Energy and Conservation, pp. 28–34. ISSN: 2352-4847. DOI: https://doi.org/10.1016/j.egyr.2023.08.072.

[13] *ASME, Boiler and Pressure Vessel Code, Division 1, Section VIII, Rules for Construction of Pressure Vessels*. 2019.

[14] *Combined Hazard Analyses to Explore the Impact of Liquid Hydrogen Fuel on the Civil Aviation Industry*. Vol. Volume 3: Ceramics; Coal, Biomass, Hydrogen, and Alternative Fuels. Turbo Expo: Power for Land, Sea, and Air. Sept. 2020, V003T03A009. DOI: 10.1115/GT2020-14977. eprint: https://asmedigitalcollection.asme.org/GT/proceedings-pdf/GT2020/84119/V003T03A009/6614938/v003t03a009-gt2020-14977.pdf.

[15] L. Bjerregaard. *Aftermarket Builds Groundwork For Hydrogen-Electric Retrofits*. 2022. URL: https://aviationweek.com/mro/emerging-technologies/aftermarket-builds-groundwork-hydrogen-electric-retrofits (visited on 02/29/2024).

[16] B. Blunier and A. Miraoui. “Air management in PEM fuel cells: State-of-the-art and prospectives”. In: *2007 International Aegean Conference on Electrical Machines and Power Electronics*. 2007, pp. 245–254. DOI: 10.1109/ACEMP.2007.4510510.

[17] Boeing. *Commercial Market Outlook 2023–2042*. 2023. URL: https://cmo.boeing.com/ (visited on 02/21/2024).

[18] P. Boer, A. Wit, and R. Benthem. “Development of a Liquid Hydrogen-based Fuel Cell System for the HYDRA-2 Drone”. In: Jan. 2022. DOI: 10.2514/6.2022-0443.

[19] O. Anatol’evna Boeva et al. “Low-temperature ortho–para hydrogen conversion catalyzed by gold nanoparticles: Particle size does not affect the rate”. In: *International Journal of Hydrogen Energy* 42.36 (2017), pp. 22897–22902. ISSN: 0360-3199. DOI: https://doi.org/10.1016/j.ijhydene.2017.07.187.

[20] D.G. Brewer. *Hydrogen Aircraft Technology*. Springer Cham, 1991. DOI: https://doi.org/10.1201/9780203751480.

[21] S.G.P. Castro. *The CrashProof Knowledge Centre (CrashProofLab)*. en. 2022. DOI: 10.5281/ZENODO.11500722. URL: https://zenodo.org/doi/10.5281/zenodo.11500722.

[22] S.G.P. Castro and J. Sodja. *Supporting code for Stability and Analysis of Structures II*. Tech. rep. DOI: 10.5281/zenodo.2583004. Department of Aerospace Structures and Materials, Delft University of Technology, 2024.

[23] Fuel Cells and Hydrogen 2 Joint Undertaking (EU body or agency). *Hydrogen-powered aviation – A fact-based study of hydrogen technology, economics, and climate impact by 2050*. Publications Office, 2020. DOI: doi/10.2843/471510.

[24] Y.A. Cengel. *Heat Transfer - A practical approach, 3rd edition*. URL: https://www.academia.edu/38856854/Heat_and_Mass_Transfer_A_Practical_Approach_3rd_Edition_by_Cengel20190418_8592_13b2vml.

[25] V. Cipolla et al. “A Parametric Approach for Conceptual Integration and Performance Studies of Liquid Hydrogen Short-Medium Range Aircraft”. In: *Applied Sciences* 12.14 (2022). ISSN: 2076-3417. DOI: 10.3390/app12146857.

[26] C.O. Colpan and A. Kovač. *Fuel Cell and Hydrogen Technologies in Aviation*. Springer Cham, 2022. DOI: https://doi.org/10.1007/978-3-030-99018-3.

[27] Energy Supply Device Aviation Rulemaking Committee. “Energy Supply Device Aviation Rulemaking Committee Final Report, Technical Report DOT/FAA/TC-19/16”. In: Apr. 2019.

[28] D.A. Crowl and Y. Jo. “The hazards and risks of hydrogen”. In: *Journal of Loss Prevention in the Process Industries* 20.2 (2007), pp. 158–164. ISSN: 0950-4230. DOI: https://doi.org/10.1016/j.jlp.2007.02.002.

[29] MatWeb - material property data. *Aluminum 5083-O*. 2024. URL: https://www.matweb.com/search/DataSheet.aspx?MatGUID=d105c2a24d6942cdad79259f770fb806 (visited on 07/31/2024).

[30] Council of the European Union. *European Green Deal*. 2023. URL: https://www.consilium.europa.eu/en/policies/green-deal/ (visited on 02/21/2024).

[31] A.J. Eytan and J.R.R.A. Martins. “Hydrogen-powered aircraft: Fundamental concepts, key technologies, and environmental impacts”. In: *Progress in Aerospace Sciences* 141 (2023). Special Issue on Green Aviation, p. 100922. ISSN: 0376-0421. DOI: https://doi.org/10.1016/j.paerosci.2023.100922.

[32] M.F.M. Hoogreef G. Onorato P. Proesmans. “Assessment of hydrogen transport aircraft”. In: *CEAS Aeronautical Journal* 13 (2022). DOI: 10.1007/s13272-022-00601-6.

[33] N.M. Garceau et al. “Performance test of a 6 L liquid hydrogen fuel tank for unmanned aerial vehicles”. In: *IOP Conference Series: Materials Science and Engineering* 101.1 (Nov. 2015), p. 012130. DOI: 10.1088/1757-899X/101/1/012130.

[34] M. Ghadimi and M.M. Barzegari. “A numerical transient thermomechanical modeling of the metal-polyamide internal supports for cryogenic vessels”. In: *Journal of Thermal Analysis and Calorimetry* 148.21 (2023), pp. 11917–11927.

[35] V. Giurgiutiu. "Chapter 3 - Classical lamination theory". In: *Stress, Vibration, and Wave Analysis in Aerospace Composites*. Ed. by Victor Giurgiutiu. Academic Press, 2022, pp. 111–277. ISBN: 978-0-12-813308-8. DOI: https://doi.org/10.1016/B978-0-12-813308-8.00011-9.

[36] A. Gomez and H. Smith. "Liquid hydrogen fuel tanks for commercial aviation: Structural sizing and stress analysis". In: *Aerospace Science and Technology* 95 (2019), p. 105438. ISSN: 1270-9638. DOI: https://doi.org/10.1016/j.ast.2019.105438.

[37] I.A. Hassan et al. "Hydrogen storage technologies for stationary and mobile applications: Review, analysis and perspectives". In: *Renewable and Sustainable Energy Reviews* 149 (2021), p. 111311. ISSN: 1364-0321. DOI: https://doi.org/10.1016/j.rser.2021.111311.

[38] MKS Instruments. *Creating a Vacuum*. 2024. URL: https://www.mks.com/n/creating-a-vacuum (visited on 05/01/2024).

[39] E. Janicka et al. "Optimization of the Relative Humidity of Reactant Gases in Hydrogen Fuel Cells Using Dynamic Impedance Measurements". In: *Energies* 14.11 (2021). ISSN: 1996-1073. DOI: 10.3390/en14113038.

[40] W.B. Jiang et al. "Coupling optimization of composite insulation and vapor-cooled shield for on-orbit cryogenic storage tank". In: *Cryogenics* 96 (2018), pp. 90–98. ISSN: 0011-2275. DOI: https://doi.org/10.1016/j.cryogenics.2018.10.008.

[41] J. Jönsson. *Continuum Mechanics of Beam and Plate Flexure*. English. U : Institut for Bygningsteknik, Aalborg Universitet U9512. pdf. for print 232 pp. Department of Mechanical Engineering, Aalborg University, 1995.

[42] M.B. Kasen et al. "Mechanical, Electrical, and Thermal Characterization of G-10Cr and G-11Cr Glass-Cloth/Epoxy Laminates Between Room Temperature and 4 K". In: *Advances in Cryogenic Engineering Materials: Volume 26*. Ed. by A.F. Clark and R.P. Reed. Boston, MA: Springer US, 1980, pp. 235–244. DOI: 10.1007/978-1-4613-9859-2_24.

[43] H. Kim et al. "Effects of key operating parameters on the efficiency of two types of pem fuel cell systems (High-Pressure and Low-Pressure operating) for Automotive Applications". In: *Journal of Mechanical Science and Technology* 19 (2005), pp. 1018–1026. URL: https://doi.org/10.1007/BF02919185.

[44] Heinz G. Klug and R. Faass. "CRYOPLANE: hydrogen fuelled aircraft — status and challenges". In: *Air & Space Europe* 3.3 (2001), pp. 252–254. ISSN: 1290-0958. DOI: https://doi.org/10.1016/S1290-0958(01)90110-8.

[45] M. Koç and T. Altan. "Prediction of forming limits and parameter in the tube hydroforming process". In: *International Journal of Machine Tools and Manufacture* 42 (Jan. 2002), pp. 123–138. DOI: 10.1016/S0890-6955(01)00048-7.

[46] A. Kogan et al. "Cryogenic Vacuum Insulation for Vessels and Piping". In: *International Cryogenic Engineering Conference 23 - International Cryogenic Materials Conference 2010 (ICEC 23 - ICMC 2010)* (2010).

[47] G. Lampeas and G. Tzoumakis. "Thermo-mechanical numerical model of a small-scale liquid hydrogen aircraft fuel tank". In: *10th European conference for aeronautics and space sciences (EUCASS)* (2023). DOI: 10.13009/EUCASS2023-013.

[48] G. Lampeas and G. Tzoumakis. "Thermo-mechanical simulation of a small-scale liquid hydrogen fuel tank for aviation applications". In: *9th European conference for aeronautics and space sciences (EUCASS)* (2022). DOI: 10.13009/EUCASS2022-7281.

[49] E. Lisowski, W. Czyżycki, and K. Łazarczyk. "Simulation and experimental research of internal supports in mobile cryogenic tanks". In: (Jan. 2010).

[50] F. Lisowski and E. Lisowski. "Design of Internal Supports for Double-Walled Liquefied Natural Gas Road Tanker". In: *Heat Transfer Engineering* 43.3-5 (2022), pp. 238–247. DOI: 10.1080/01457632.2021.1874653. eprint: https://doi.org/10.1080/01457632.2021.1874653.

[51] G.R. Liu and S.S. Quek. "Chapter 3 - Fundamentals for Finite Element Method". In: *The Finite Element Method (Second Edition)*. Ed. by G.R. Liu and S.S. Quek. Second Edition. Oxford: Butterworth-Heinemann, 2014, pp. 43–79. ISBN: 978-0-08-098356-1. DOI: https://doi.org/10.1016/B978-0-08-098356-1.00003-5.

[52] Z. Liu et al. “Thermal performance of liquid hydrogen tank in reduced gravity”. In: *Advances in Space Research* 62.5 (2018), pp. 957–966. ISSN: 0273-1177. DOI: https://doi.org/10.1016/j.asr.2018.06.006.

[53] V.K. Mantzaroudis and E.E. Theotokoglou. “Computational Analysis of Liquid Hydrogen Storage Tanks for Aircraft Applications”. In: *Materials* 16.6 (2023). ISSN: 1996-1944. DOI: 10.3390/ma16062245.

[54] K. Mazloomi and C. Gomes. “Hydrogen as an energy carrier: Prospects and challenges”. In: *Renewable and Sustainable Energy Reviews* 16.5 (2012), pp. 3024–3033. ISSN: 1364-0321. DOI: https://doi.org/10.1016/j.rser.2012.02.028.

[55] G.E. McIntosh. “Layer by Layer MLI Calculation Using a Separated Mode Equation”. In: *Advances in Cryogenic Engineering*. Ed. by Peter Kittel. Boston, MA: Springer US, 1994, pp. 1683–1690. ISBN: 978-1-4615-2522-6. DOI: 10.1007/978-1-4615-2522-6_206.

[56] Dr. O. Memon. *What Is Fuel Sloshing How Is It Controlled In Aircraft Tanks?* 2023. URL: https://simpleflying.com/fuel-sloshing-guide/ (visited on 09/04/2024).

[57] M.G. Millis et al. “Hydrogen Fuel System Design Trades for High-Altitude Long-Endurance Remotely-Operated Aircraft”. In: *NASA Technical Reports Server* (2009).

[58] S.K. Mital et al. “Review of Current State of the Art and Key Design Issues with Potential Solutions for Liquid Hydrogen Cryogenic Storage Tank Structures for Aircraft Applications”. In: *NASA Technical Reports Server* (2006).

[59] R. Morales-Ospino, A. Celzard, and V. Fierro. “Strategies to recover and minimize boil-off losses during liquid hydrogen storage”. In: *Renewable and Sustainable Energy Reviews* 182 (2023), p. 113360. ISSN: 1364-0321. DOI: https://doi.org/10.1016/j.rser.2023.113360.

[60] Y.S.H. Najjar. “Hydrogen safety: The road toward green technology”. In: *International Journal of Hydrogen Energy* 38.25 (2013), pp. 10716–10728. ISSN: 0360-3199. DOI: https://doi.org/10.1016/j.ijhydene.2013.05.126.

[61] NIST. *Aluminum 5083-O (UNS A95083)*. 2021. URL: https://www.nist.gov/mml/acmd/aluminum-5083-o-uns-a95083 (visited on 07/31/2024).

[62] NIST. *Material Properties: G-10 CR (Fiberglass Epoxy)*. 2024. URL: https://trc.nist.gov/cryogenics/materials/G-10%20CR%20Fiberglass%20Epoxy/G10CRFiberglassEpoxy_rev.htm (visited on 08/16/2024).

[63] P.C. Okonkwo et al. “A focused review of the hydrogen storage tank embrittlement mechanism process”. In: *International Journal of Hydrogen Energy* 48.35 (2023), pp. 12935–12948. ISSN: 0360-3199. DOI: https://doi.org/10.1016/j.ijhydene.2022.12.252.

[64] E.C. Preissner and J.R. Vinson. “Application of theorem of minimum potential energy to a complex structure Part I: two-dimensional analysis”. In: *International Journal of Solids and Structures* 40.5 (2003), pp. 1089–1108. ISSN: 0020-7683. DOI: https://doi.org/10.1016/S0020-7683(02)00654-6.

[65] R.R. Ratnakar, Z. Sun, and V. Balakotaiah. “Effective thermal conductivity of insulation materials for cryogenic LH2 storage tanks: A review”. In: *International Journal of Hydrogen Energy* 48.21 (2023), pp. 7770–7793. ISSN: 0360-3199. DOI: https://doi.org/10.1016/j.ijhydene.2022.11.130.

[66] F. Salucci et al. “Retrofit of hydrogen-powered helicopters: a sizing approach”. In: June 2022. DOI: 10.2514/6.2022-3206.

[67] M. Schröder et al. “Optimal operating conditions of PEM fuel cells in commercial aircraft”. In: *International Journal of Hydrogen Energy* 46.66 (2021), pp. 33218–33240. ISSN: 0360-3199. DOI: https://doi.org/10.1016/j.ijhydene.2021.07.099.

[68] Indian Institute of Science. *The Principle of Minimum Potential Energy*. 2017. URL: https://mecheng.iisc.ac.in/suresh/me237/feaNotes/Chapter2.pdf (visited on 07/25/2024).

[69] D.F. Shanahan. “Basic Principles of Crashworthiness”. In: 2005. URL: https://api.semanticscholar.org/CorpusID:10388142.

[70] S.A. Sherif, N. Zeytinoglu, and T.N. Veziroglu. "Liquid hydrogen: Potential, problems, and a proposed research program". In: *International Journal of Hydrogen Energy* 22.7 (1997), pp. 683–688. ISSN: 0360-3199. DOI: https://doi.org/10.1016/S0360-3199(96)00201-7.

[71] JETechnology Staff. *What Determines the Life Span of an Airplane?* 2021. URL: https://aircraftmaintenancestands.com/blog/life-span-of-an-airplane/ (visited on 09/06/2024).

[72] P.J. Sun et al. "Experimental study of the influences of degraded vacuum on multilayer insulation blankets". In: *Cryogenics* 49.12 (2009), pp. 719–726. ISSN: 0011-2275. DOI: https://doi.org/10.1016/j.cryogenics.2009.09.003.

[73] R. Thomson and U. Weichenhain. "Hydrogen | A future fuel for aviation?" In: *Techical report Roland Berger* (2020).

[74] N.S. Trahair. et al. *The Behaviour and Design of Steel Structures to EC3*. 4th. CRC Press, 2008. DOI: 10.1201/9781315273518.

[75] G. Tzoumakis, K. Fotopoulos, and G. Lampeas. "Multi-Physics Digital Model of an Aluminum 2219 Liquid Hydrogen Aircraft Tank". In: *Aerospace* 11.2 (2024). ISSN: 2226-4310. DOI: 10.3390/aerospace11020161.

[76] E. Ventsel, T. Krauthammer, and E. Carrera. *Thin Plates and Shells: Theory, Analysis, and Applications*. Applied Mechanics Reviews, 55(4), B72–B73, 2002.

[77] D. Verstraete. "The Potential of Liquid Hydrogen for long range aircraft propulsion". Ph. D. Thesis. Cranfield University - School of Engineering, 2008-2009.

[78] B. Wang et al. "Characterization and monitoring of vacuum pressure of tank containers with multilayer insulation for cryogenic clean fuels storage and transportation". In: *Applied Thermal Engineering* 187 (2021), p. 116569. ISSN: 1359-4311. DOI: https://doi.org/10.1016/j.applthermaleng.2021.116569.

[79] P. Wang. "Chapter 5 - Preliminary System Safety Assessment". In: *Civil Aircraft Electrical Power System Safety Assessment*. Ed. by P. Wang. Butterworth-Heinemann, 2017, pp. 101–156. ISBN: 978-0-08-100721-1. DOI: https://doi.org/10.1016/B978-0-08-100721-1.00005-4.

[80] D.W.J. Willems. *Cryostat thermal model 3, calorimetric measurements and analysis on a full-scale model of the LHC arc dipole cryostat*. Master's thesis. Available at https://research.tue.nl/en/studentTheses/cryostat-thermal-model-3-calorimetric-measurements-and-analysis-o. Aug. 1999.

[81] C. Winnefeld et al. "Modelling and Designing Cryogenic Hydrogen Tanks for Future Aircraft Applications". In: *Energies* 11 (Jan. 2018), p. 105. DOI: 10.3390/en11010105.

[82] Y. Wu. "Crashworthy Hydrogen-Powered Aircraft, Retrofit Preliminary Design". Master's thesis. Delft, Netherlands: Delft University of Technology, 2024.

[83] W. Xu, Q. Li, and M. Huang. "Design and analysis of liquid hydrogen storage tank for high-altitude long-endurance remotely-operated aircraft". In: *International Journal of Hydrogen Energy* 40.46 (2015), pp. 16578–16586. ISSN: 0360-3199. DOI: https://doi.org/10.1016/j.ijhydene.2015.09.028.

[84] L. Yin, H. Yang, and Y. Ju. "Review on the key technologies and future development of insulation structure for liquid hydrogen storage tanks". In: *International Journal of Hydrogen Energy* 57 (2024), pp. 1302–1315. ISSN: 0360-3199. DOI: https://doi.org/10.1016/j.ijhydene.2024.01.093.

[85] Y. Yu et al. "Design and Optimization of the Insulation Performance of a 4000 m3 Liquid Hydrogen Spherical Tank". In: *Processes* 11 (June 2023), p. 1778. DOI: 10.3390/pr11061778.

[86] J. Zheng et al. "A novel insulation system based on active cooling without power input for liquid hydrogen storage". In: *Energy* 182 (2019), pp. 1–10. ISSN: 0360-5442. DOI: https://doi.org/10.1016/j.energy.2019.06.050.